Pericentric heterochromatin specificity, propagation and memory effect in mouse fibroblast

Anna Matveeva

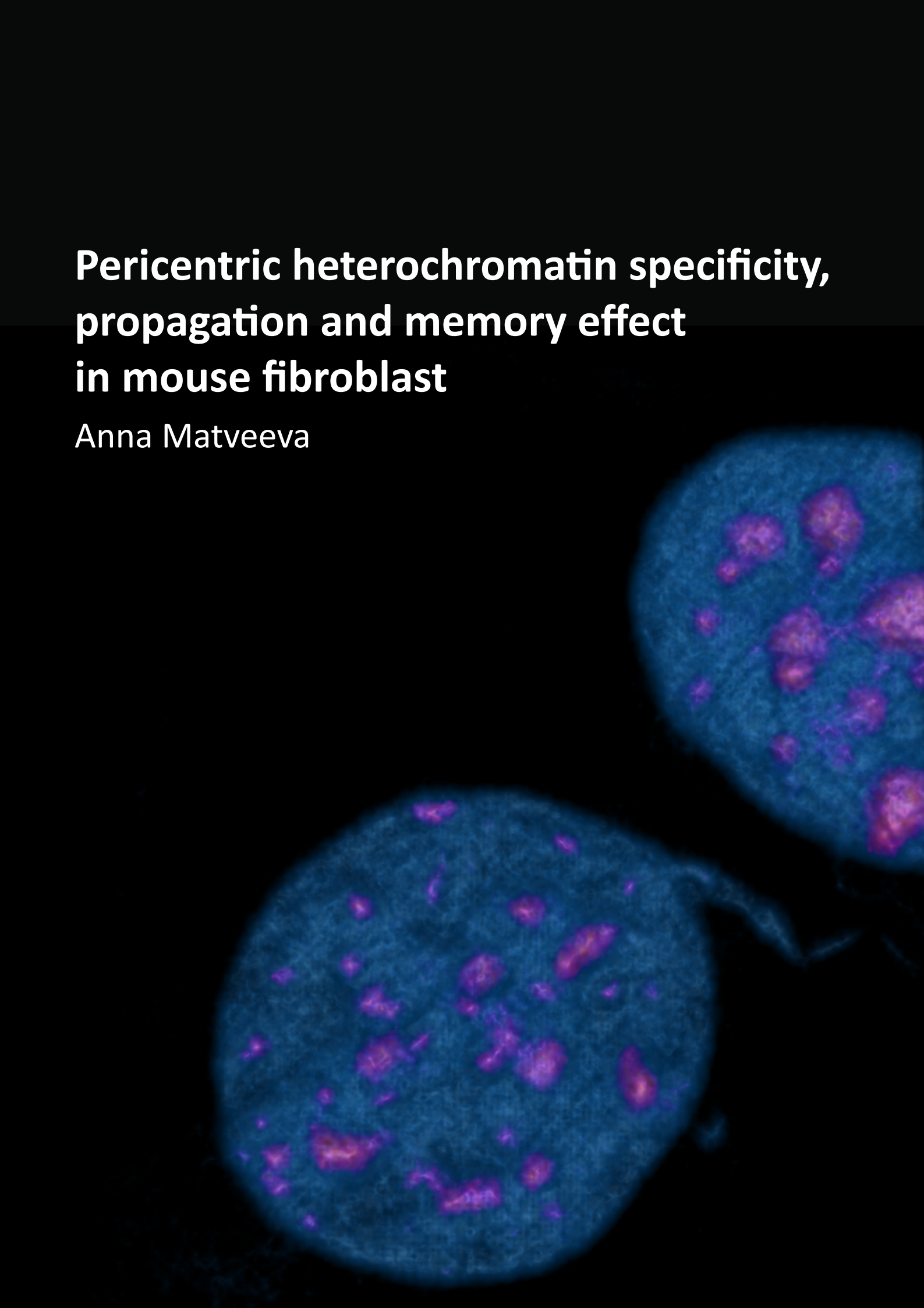

DISSERTATION

Submitted to the
Combined Faculties for the Natural Sciences and for Mathematics
of the Ruperto-Carola University of Heidelberg, Germany
for the degree of
Doctor of Natural Sciences

Presented by
M. Sc. (Physics) Anna Matveeva
Born in Sankt-Petersburg, Russia

Oral examination: 20.03.2014

PERICENTRIC HETEROCHROMATIN SPECIFICITY, PROPAGATION AND MEMORY EFFECT IN MOUSE FIBROBLAST

Referees: Prof. Dr. Ursula Kummer

Prof. Dr. Thomas Höfer

Declaration

I hereby declare that I have written the submitted dissertation “Pericentric heterochromatin specificity, propagation and memory effect in mouse fibroblast” myself and in this process have used no other sources or materials than those explicitly indicated. I hereby declare that I have not applied to be examined at any other institution, nor have I used the dissertation in this or any other form at any other institution as an examination paper, nor submitted it to any other faculty as a dissertation.

(Place, date) Anna Matveeva

Summary

The transcriptional activity of genes as well as the conformation of transcriptionally silenced genomic regions is defined by the epigenetic state of the associated chromatin fragment. Chromatin is composed of repetitive units called nucleosomes. Each nucleosome consists of a core complex of four histones and the fragment of DNA that is wrapped around it. The distinct residues of N-terminal tails of the histones that extend out from the nucleosomal core are subject to post-translational epigenetic modifications. The composition of these modifications defines the electric charge of the histone tails and, therefore, its coupling strength with DNA. Thus, the epigenetic mark composition of each individual nucleosome governs the overall conformation of the chromatin filament.

In mammals, the tight conformation of chromatin in pericentric genomic regions, called pericentric heterochromatin (PCH), is important for the stability and the proper segregation of chromosomes. The epigenetic hallmark signature of PCH is di- or trimethylation of histone H3 at lysine 9 (H3K9me2/3) enriched over the entire centromere region. This epigenetic state is constitutively maintened through cell cycle progression and throughout multiple cell generations thereby preventing chromosomal breakages, missegregation and perturbed chromosomal interactions.

This work investigates the specificity, propagation and the long-term autonomous memory effect for H3K9me2/3 silencing marker in PCH in mouse fibroblasts on the single cell level. We apply fluorescent microscopy techniques, high-throughput image-processing method and mathematical modeling to test the stability of the system upon changes in the expression of the chromatin-modifying enzymes. The network operating H3K9me2/3 in PCH was constructed and translated into a deterministic system of ordinary differential equations as well as

formulated stochastically using the Gillespie simulation algorithm. The model incorporates the contribution of H3K9me2/3 binding protein HP1 together with H3K9 specific methyltransferase Suv39h, the H3K9 specific demethylase JMJD2 and cell cycle dependent kinase Aurora B as well as nucleosome collision processes via DNA looping. The realization that most of these chromatin-modifying processes depend on each other and also appear to be regulated by multiple positive and negative feedback loops has lead to the proposal of nonlinear stationary and dynamical features of PCH network function.

The modeling simulations have revealed an increased variability in methylation degree upon increases in JMJD2 expression in the cell. This prediction was qualitatively supported by the heterogeneity observed experimentally on the single PCH foci level. However, in the experiment the response of the whole cell population remains monostable, in spite of the presence of a bistable memory element in the network. The model explains this property confirming the significant impact of the persistent silencing origins organized by the high residence time binding of HP1-Suv39h complexes that initiate the spread of the H3K9me2/3 mark. Therefore, on the population level the bistable mechanism of silencing propagation in PCH is hidden, appearing only as severe fluctuations in the H3K9me2/3 level.

In summary, a consistent model of the silencing propagation in PCH was developed. Based on that model a scenario of PCH epigenetic state maintenance and robustness towards transient perturbation and intrinsic noise is established.

Zusammenfassung

Die transkriptionelle Aktivität von Genen sowie die Konformation von transkriptionell stillgelegten genomischen Regionen wird durch den epigenetischen Zustand des entsprechenden Chromatinfragmentes definiert. Chromatin besteht aus wiederkehrenden Einheiten, den Nukleosomen. Jedes Nukleosom ist aus einem Komplex von vier Histonen und einem DNA-Fragment, das um die Histone gewickelt ist, aufgebaut. Bestimmte Reste der N-terminalen Histonstränge, die aus dem Zentrum der Nukleosomen herausragen, unterliegen posttranslationalen epigenetischen Modifikationen. Die Zusammensetzung dieser Modifikationen bestimmt die elektrische Ladung der Histon-Enden und damit ihre Bindungsstärke mit der DNA. Somit reguliert die Komposition der epigenetischen Marker der individuellen Nukleosomen die übergeordnete Konformation der Chromatinfasern.

Bei Säugetieren ist die dichte Chromatin-Konformation in den perizentrischen Regionen des Genoms, perizentrisches Heterochromatin (PCH) genannt, wichtig für die Stabilität und die ordnungsgemäße Segregation der Chromosomen. Epigenetisches Kennzeichen des PCH ist die Di- oder Trimethylierung des Histones H3 am Lysin 9 (H3K9me2/3), angereichert entlang der gesamten Centromer-Region. Dieser epigenetische Zustand wird während Zellzyklusprogression und zahlreichen Zellgenerationen konstitutiv aufrechterhalten, wodurch Chromosomenbrüche, fehlerhafte Chromosomensegregation und Störungen der Chromosomeninteraktion verhindert werden.

Die vorliegende Arbeit untersucht auf Einzelzellebene die Spezifität, Verbreitung und den langfristigen autonomen Gedächtniseffekt des Stilllegungs-Markers H3K9me2/3 im PCH von murinen Fibroblasten. Wir wenden Fluoreszenzmikroskopie, Verfahren der Hochdurchsatz-Bildverarbeitung und

mathematische Modellierung an, um die Stabilität des Systems bei Änderungen in der Expression der Chromatin-modifizierenden Enzyme zu prüfen. Es wurde ein Reaktions-Netzwerk, welches H3K9me2/3 im PCH reguliert, erstellt und in ein deterministisches System von gewöhnlichen Differenzialgleichungen übertragen, sowie unter Verwendung des Gillespie-Algorhitmus stochastisch formuliert.
Das Modell berücksichtigt die Interaktion des H3K9me2/3-bindenden Proteins HP1 mit der H3K9-spezifischen Methyltransferase Suv39h, der H3K9-spezifischen Demethylase JMJD2 und der Zellzyklus-abhängigen Aurorakinase B sowie die Zusammenführung der Nukleosomen durch DNA-Schleifenbildung. Die Erkenntnis, dass die meisten dieser Chromatin-modifizierenden Prozesse voneinander abhängen und von zahlreichen positiven und negativen Rückkopplungsschleifen reguliert zu sein scheinen, hat zu dem Ansatz der nichtlinearen stationären, und dynamischen Eigenschaften der PCH-Netzwerkfuntkion geführt.

Die Modellsimulationen haben eine zunehmende Variabilität des Methylierungs-Grades bei gesteigerter JMJD2-Expression in der Zelle offengelegt. Diese Prognose wurde qualitativ dahingehend unterstützt, dass auf der Ebene der einzelnen PCH-Bereiche auch experimentell Heterogenität, beobachtet wurde. Jedoch bleibt im Experiment die Reaktion der Gesamt-Zellpopulation monostabil, trotz des Vorhandenseins eines bistabilen Gedächtniselementes in dem Netzwerk. Das Modell erklärt diese Eigenschaft und bestätigt so den signifikanten Einfluss des persistenten Ursprung der Stilllegung, reguliert durch die lange Verweildauer des HP1-Suv39h Komplexes, wodurch die Verbreitung des Markers H3K9me2/3 ausgelöst wird. Daher ist auf der Populationsebene der bistabile Mechanismus der Ausbreitung der Stillegung im PCH verborgen und erscheint nur als grobe Fluktuationen auf der Ebene von H3K9me2/3.

Zusammenfassend, wurde ein konsistentes Modell der Verbreitung der Stillegung im PCH entwickelt. Basierend auf diesem Modell ist ein Szenario zur Aufrechterhaltung des epigenetischen Zustandes des PCH und zur Stabilität in Bezug auf vorübergehende Perturbationen und intrinsisches Rauschen begründet.

Contents

Chapter 1

Introduction

1.1 Epigenetic networks regulate the proper genome organization and function

Aberrant gene expression and epigenetic abnormalities have been found to be causative factors for a number of diseases such as cancer (Bender et al., 2013; Young et al., 2013; Pujadas et al., 2012; Slee et al., 2012; Hoffmann et al., 2012; Varier et al., 2011), neurodegenerative (Peleg et al., 2010; Chouliaras et al., 2010; Ryu et al., 2008), autoimmune (Yang et al., 2013;) disorders and pediatric syndromes (Allis et al., 2007). Therefore, therapeutic drugs that induce epigenetic changes have emerged as potential treatment strategies. There are several chromatin targeting inhibitors that suppress histone-modifying enzymes responsible for different posttranslational histone modifications: acetylation, methylation, phosphorylation and DNA methylation. The acetylation is controlled by the histone acetyltransferases (HATs) and histone deacetylases (HDACs). HATs promote gene expression by transferring an acetyl group to lysine and HDACs promote gene repression by removing an acetyl group from the lysine of the histone tail. The methylation driven by histone methyltransferases (HMTs), the writers responsible for adding a distinct number of methyl marks (mono-, di- or trimethylation) to the distinct residue of histone (Bannister et al., 2005) and also highly selective for the position and methylation level of histone demethylases (JmjC) (Whetstine et al, 2006). The histone phosphorylation is induced by Aurora B kinase and antagonized by phosphatase PP1A (Fischle, 2008). Finally, the DNA methyltransferases (DNMTs)

are responsible for methylation of cytosine bases (meC) in DNA. Some of the inhibitors of these enzymes have already demonstrated good prognosis for disease regression in clinical studies (Lehrman et al., 2005; Kantarjian et al., 2006; Oki et al., 2006; Raval et. al., 2007). Hence, characterization of the epigenetic changes and molecular mechanisms that lead to disease is critical for maximizing the potential of the therapeutic approaches.

The mechanism to maintain stable and heritable epigenetic states is of special interest, in particular the genome loci that require epigenetic memory. Constitutive heterochromatin domains are among them. There the heterochromatin formation and consequent epigenetic silencing is mediated by multiple pathways, which trigger DNA methylation, covalent modifications of the histone tails and protein-protein/DNA interactions, altering the fixed position and tight integrity of the nucleosomes within the chromatin fiber. One of the dynamic features of heterochromatin formation is the ability to propagate in a region-specific manner. Such spreading across domains causes epigenetic silencing of nearby genomic regions. Once established, the heterochromatic state is maintained by binding of a highly conserved family of heterochromatin proteins, homologues of which were found in numerous organisms from fission yeast (Swi6) to humans (HP1). Heterochromatin proteins are able to recruit histone-modifying enzymes resulting in correspondent progressive histone mark addition or removal from the nucleosomes. The realization that many chromatin-modifying processes depend on each other, and also appear to be regulated by positive and negative feedback loops (Sneppen et al., 2012) has led to the proposal of a signaling network model for heterochromatin regulation.

1.2 Silencing network in pericentric heterochromatin of the mammalian genome

The largest constitutively heterochromatic domain in the mammalian genome is pericentric heterochromatin (PCH) that is flanking the centromeric region of every chromosome. The DNA of PCH is composed of pericentric major satellite repeats flanking the centromeric minor repeats. The PCH from individual chromosomes form clusters, distinct highly condensed chromatin foci (Guenatri et al., 2004), that can be easily visualized under the microscope by fluorescence staining with DAPI (4',6-diamidino-2-phenylindole) (Fig 1.2.1).

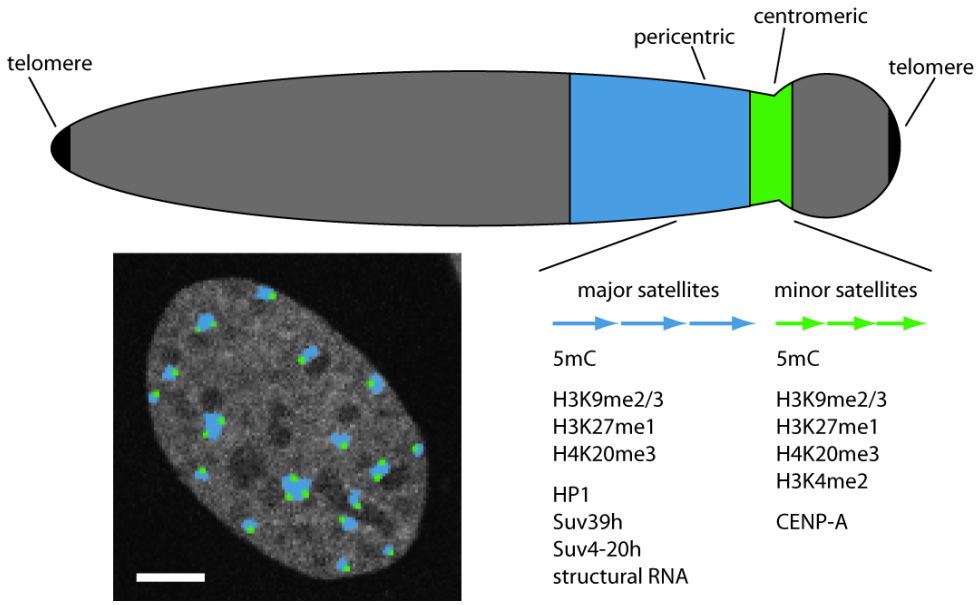

Figure 1.2.1 Pericentric heterochromatin foci in mouse fibroblast cells are clusters of pericentric chromatin from individual chromosomes. Whereas major satellites of different chromosomes cluster and form so-called chromocenters, the minor satellite repeats locate individually at the periphery. These condensed foci are enriched in DNA methylation and the following histone modifications: H3K9me2/3, H3K27me1 and H4K20me3. Pericentric chromatin is also marked by HP1, Suv39h and Suv4-20h co-localization and possibly a structural RNA component. Specific for (centromeric) minor satellites is the assembly of CENP-A and an additional H3K4me2 modification. Scalebar, 10 µm. Figure is recreated by Katharina Müller-Ott from (Probst and Almouzni, 2008).

The epigenetic state of PCH is of particular interest because it controls the chromosomal stability preventing perturbed chromosome interactions, breakages and missegregation (Slee et al., 2012; Peters et al., 2001). The hallmark signature of PCH is histone-H3 lysine-9 methylation (H3K9me2/3) enriched over the entire centromere region (Fig 1.2.1). It plays a crucial role in the constitutive maintenance of PCH through cell cycle progression and throughout multiple cell generations resulting in a long-term autonomous memory effect.

Single PCH domains are recognizable on the microscopy images due to their high chromatin content density (Grewal et al., 2007), the enrichment of particular epigenetic markers can be measured by immunofluorescence microscopy imaging techniques together with an image quantification procedure. These measurements provide the information on the evolution of the posttranslational

histone modifications in PCH with respect to cell cycle progression and the change of other environmental conditions.

The evolution of H3K9me2/3 in PCH as the key silencing marker was studied in many experimental systems (Barski et al., 2007; Peters et al., 2001; Schotta et al., 2004; Rea et al., 2000; Hathaway et al, 2012). The propagation of this residue specific methylation is dependent on the synergistic function of HP1 together with Suv39h methyltransferase (Fig 1.2.2).

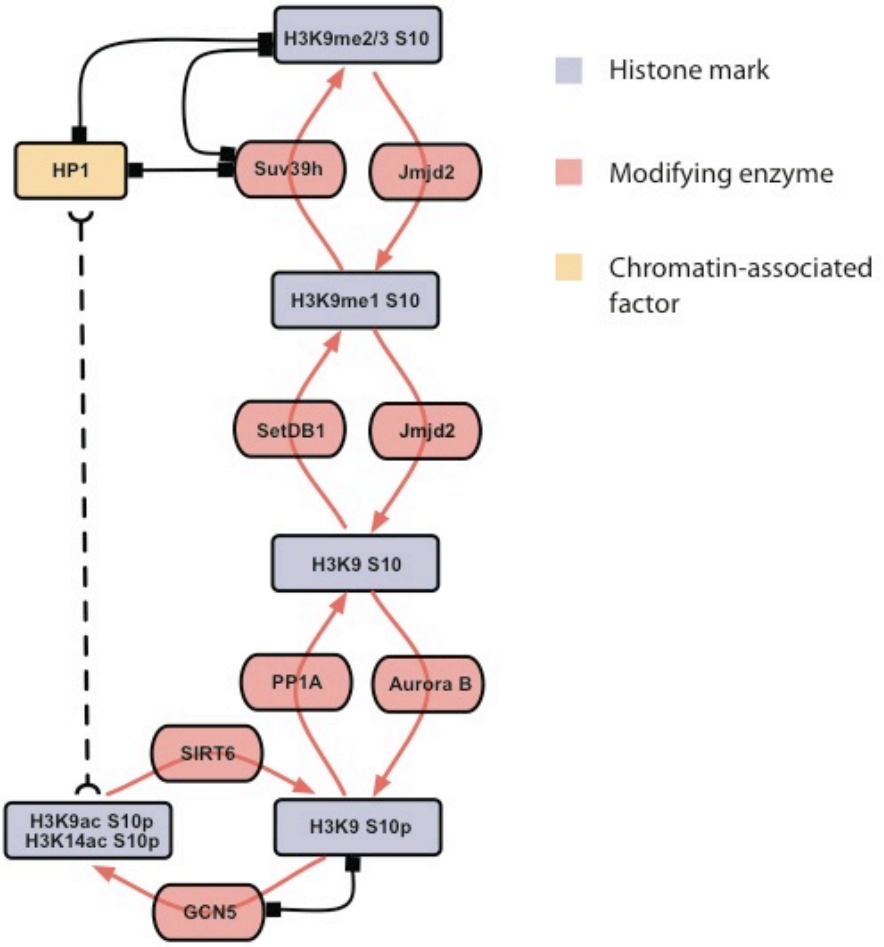

Figure 1.2.2 Silencing network in pericentric heterochromatin. H3K9me2/3 is bound and maintain by the heterochromatin protein 1 (HP1) in the complex with Suv39h histone methyltransferase. Repressive di- and tri- methylation and neutral mono- methylation can be removed by group of Jmjd2 demethylases in the processive manner. The mono- methylation can be reestablished by methyltransferase SetDB1. The cell cycle dependent kinase Aurora B in G2 phase triggers the massive H3S10 phosphorylation. This histone mark able to bind the GCN5 acetyltransferase that acetylates the H3K9 and H3K14 residues that are free of methyl mark and consequently causes the HP1 eviction from the pericentric heterochromatin.

Their complex binds to the H3K9me2/3 histone tail and propagates methylation on neighboring nucleosomes (Schotta et al., 2002; Grewal et al., 2007).

The small fraction of tightly bound HP1-Suv39h complex in PCH is considered to represent the silencing origins (Müller-Ott et al., submitted) whose constant persistence was questioned in earlier experimental and theoretical studies (Dood et al., 2007; Hathaway et al, 2012). The role of the CpG dinucleotides content in the DNA major satellite repeats in PCH is discussed in the context of origin existence. For instance, DNA methylation at CpG was found to enhance recruitment affinity of the HP1-Suv39h complex to the PCH via methyl-CpG-associated chromatin complexes like MeCP2 (Müller-Ott et al., submitted), Mi-2/NuRD (Sims et al., 2011) and NoRC (Postepska-Igielska et al., 2013) that facilitate the triggering of epigenetic silencing propagation over large chromosomal regions. Moreover, the repetitive DNA content was found to be associated with genomic boundary elements in PCH that can spatially limit the propagation of H3K9me2/3. The boundary elements organized by identical inverted repeats on DNA have been suggested to mark the borders between adjacent chromatin domains and to act as barriers against the effects of enhancer and silencer elements from neighbouring regions (Noma et al., 2001).

Other aspect that must be considered in epigenetic system are a spatial conformation and stiffness of the chromatin fiber that might facilitate or block the spontaneous or directed contacts between the distant nucleosomes that would support or suppress the spreading mechanism. Consequently, the ranges of inter-nucleosomal contacts defined by the flexibility of the chromatin fiber (Rippe, 2001; Rosa et al., 2010; Becker et al., 2010) will play a significant role in the methyl mark propagation process.

Finally, the uncertainty evolved with the stochastic nature of the PCH epigenetic network would contribute to the variability of the single PCH silencing level giving the rise to the heterogenic system response (Jeong et al., 2011).

1.3 Related mathematical models

Mathematical modeling can be usedis one of the advanced approaches one could employ to effectively dissect common definitive feautures of the epigenetic state inheritance as well as evolution of epigenetic modifications through cell cycle progression. Modeling procedures can also be utilized to characterize the linkage between binding of chromatin proteins and enzymes activity. The signaling network of chromatin is complex. Many chromatin-modifying processes depend on each other and appear to be organized in positive and negative feedback loops (Schreiber et al., 2002). Nevertheless, the study of simplified mathematical models that incorporate a number of the basic underlying features of the proposed system can already lead to nontrivial insights about the dynamical behavior (Micheelsen et al., 2010; David-Rus et al., 2003).

Recently developed models of posttranslational histone modification crosstalk focus on the epigenetic silencing propagation within distinct chromatin regions and explain the long-term memory effect of the epigenetic silencing for different biological systems. Some examples are the yeast mating type locus silencing system (Dodd et al., 2007), the polycomb-based silencing in plants (Angel et al., 2011) and H3K9me3-dependent gene silencing in mice (Hathaway et al., 2012; Hodges et al., 2012). All models are maximally simplified utilizing only two mutually exclusive histone marks, silencing markers (H3K9me for yeast, H3K27me3 in plants and H3K9me3 in mouse) and its opposing competitor mark (H3K4me for yeast, optional for plants and H3K4me3 or H3K27ac in mice). In these models, silencing and active histone marks antagonistically promote the transition of other nucleosomes towards the same modification leading to positive feedback.

For yeast and plant systems the presence of bistability was assumed to be the basis of the memory potential and long-range nucleosomal interactions were postulated as a crucial factor to robustly maintain the active and silenced state. The simulations of these two systems with only short-range effective nucleosomal interactions reveal a high level of noise that is dramatically destabilizing the two opposing states. The bistable regime of the network allow for parameter controlled switching between silencing propagational regimes in case of the presence of nucleation origins. Therefore, propagation can be limited by distance, causing local enrichment of the silencing marker around the origin and unlimited where it needs

the boundary elements for termination of front propagation process. Without nucleation origins, bistability allows the spontaneous transition between states.

On the contrary, the epigenetic network of Oct4 gene silencing in mice is interpreted as a monostable system that handles the silencing propagation on the origin dependent manner. In addition, the long-range interactions along the chromatin fiber that tend to average out the spontaneous fluctuations are forbidden. This results in a system with a persistent nucleation origin where local propagation is well controlled by the balance of the histone modifiers concentration due to the long-term memory absence. Consequently, a certain size of the silencing domain is defined according to the sigmoidal response of the system on the change of balance.

1.4 Research objectives

In this report, we present mathematical deterministic and equivalent stochastic model of PCH epigenetic system to study the mechanisms of PCH silencing specificity, propagation and memory effect in mouse fibroblasts. Contrary to the previously published simplified models of epigenetic networks, our models take into account all possible compositions of posttranslational modifications of histone H3 that were found to be associated with PCH in large number of experimental studies. In the model, the interplay between silencing modification, H3K9 methylation, and opposite modifications of transcriptional activity, H3K9 and H3K14 acetylation, assumes the synergistic and antagonistic feedback loops. These loops are explained by the progressive recruitment of modification associated enzymes HP1-Suv39h complex and GCN5 acetyltransferase as well as dependent on the product of their activity - a function of JMJD2 demethylase and Aurora B kinase. To elucidate the strength of the stochastic noise in the assembly of nucleosomes composing the chromatin filament that represents the unified independent fragment of PCH, our stochastic model simulated by use of Gillespie stochastic simulation algorithm (SSA). That allows us to predict the ranges of variability of silencing degree for the individual PCH within the deterministically driven stimulus response. Thus, we study the impact of persistent silencing origins and influence of JMJD2 demethylase and Aurora B kinase dosages on the H3K9me2/3 propagation and heterogeneity. In the last part of this work, we successfully performed the experimental validation of our theoretical predictions in the transgenic mouse embryonic fibroblast (MEF) cell line wherein the high-resolution measurement

technique at the level of individual foci enabled proper segmentation of PCH foci and quantification of the silencing marker enrichment in these foci with following proper statistical data analysis.

Chapter 2

Epigenetic Silencing as a Model System

In this chapter, a molecular pericentric heterochromatin (PCH) epigenetic network of silencing propagation is constructed and translated into a mathematical model. The silencing bifurcation analysis was performed based on numerically approximated solutions of deterministic model. Based on this analysis, the prediction of phenomenological functionality of the PCH epigenetic silenced mark is discussed. An additional stability analysis was also performed.

2.1 Epigenetic network defining the specificity, propagation and memory of silencing in pericentric heterochromatin

Pericentric heterochromatin (PCH) in mice contains, as a hallmark signature, di- and thrimethylated lysine 9 of histone H3 (H3K9me2/3). This histone modification associated with global epigenetic silencing in PCH causes chromatin compaction as well as transcriptional repression of the genes by repressing the gene promoter function (Barski et al., 2007; Peters et al., 2001; Schotta et al., 2004; Rea et al., 2000). H3K9me2/3 mark is bound and maintained by heterochromatin protein 1 (HP1) together with Suv39h methyltransferase. HP1 in the complex with Suv39h binds to H3K9me2/3 via N-terminal chromo domain (CHD) and promotes methylation of adjacent nucleosomes, progressive binding of HP1-Suv39h and consequently heterochromatin spreading (Schotta et al., 2002; Grewal et al., 2007). Additionally, C-terminal chromo shadow domain (CSD) of HP1 mediates dimerization of HP1 that is found to be crucial for the recruitment of Suv39h onto the nucleosomes (Yamamoto et al., 2003). Furthermore, CSD provides

internucleosomal binding modes that could crosslink two nucleosomes that are either adjacent or discontinuous in DNA sequence (Ruthenburg et al., 2007). It has been proposed that HP1-binding itself could stabilize a pattern of nucleosomal array that confers transcriptional repression. Moreover, Suv39h was found be bound to the H3K9me2/3 directly without any contribution of HP1 (Chin et al., 2006).

However, binding property of H3K9me2/3 can be disrupted by the phosphorylation of neighboring amino acid residue, serine 10 (H3S10ph). H3S10 phosphorylation is catalyzed by cycle dependent kinase Aurora B that is expressed from the middle of the S phase of the cell cycle progression triggering phospho-methyl switch in PCH (Fischle et al., 2005). According to the experimental results of our collaborators, HP1 binding to H3K9me2/3 is significantly disrupted with the increase of H3S10 phosphorylation in G2-M phase. HP1 is evicted from heterochromatin even though H3K9me2/3 marks are relatively preserved. One another study has reported about reduced methylation activity of Suv39h for H3K9 when H3S10 is phosphorylated (Rea et al., 2000). They found the underlying reason for that to be acetyltransferase GCN5. GCN5 efficiently recognizes H3S10ph modification initiating the acetylation K9 and K14 lysines on H3 histone tail (H3K9ac and H3K14ac) (Mateescu et al., 2004). The acetylation may occur on the targeted by GCN5 nucleosome as well as on histone tails of the nearest neighboring nucleosomes. The modification H3K14ac as well as the dual H3K14ac with H3S10ph blocks the binding of HP1 to H3K9me2/3 (Fischle et al., 2005; Mateescu et al., 2004). Consequently, Aurora B initialization drives the antagonistic crosstalk between H3K9me2/3 silencing marker and active H3K9ac and H3K14ac modifications from the late S phase, progressing to the following G2-M phase.

Both combinatorial synergistic and antagonistic crosstalks depend on another important component of the present epigenetic network, JMJD2 histone demethylase. This enzyme represented by few isoforms (Jmjd2a, Jmjd2b, Jmjd2c and Jmjd2d) was identified as trimethylation-specific demethylases containing the highly conserved JmjC-domain that catalyzes demethylation via an oxidative reaction (hydroxylation) (Fodor et al., 2006; Whetstine et al., 2006). All JMJD2 proteins contain besides the JmjC domain, a JmjN domain at the N-terminus. Jmjd2a/b/c also have PHD-fingers and tudor domains, which link them to chromatin and transcriptional regulation (Whetstine et al., 2006). All members of JMJD2 family catalyze demethylation of H3K9me3 and its reduction to different methylation levels. While Jmjd2b and Jmjd2c convert H3K9me3 to me2 the isoform Jmjd2d reduces

methylation to me2 or me1. The enzymatic demethylation power strictly depends on efficiency of JMJD2 chromatin accessibility. Thus, the fusion of the demethylase with HP1 greatly increases demethylation rate in the PCH as compared to the control. JMJD2 alone having lower affinity to the PCH drives the limited full-scale demethylation. Moreover the over expression of JMJD2 leads to the heterogeneous course of H3K9me2/3 redaction in PCH foci distinguishing the cells with severe, moderate and weak response (Jeong et al., 2011).

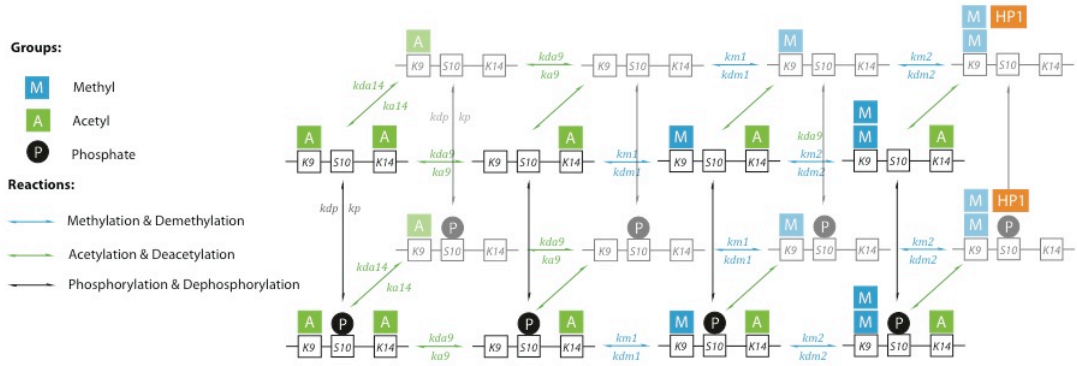

Figure 2.1.1 Schematic outline of the model. The model is a simplification of the nucleosome modification processes that are believed to control silencing at the mouse pericentric heterohromatin (PCH). Reaction scheme for transition between 16 types of the H3 histone tail modifications is presented here.

The biological context of the epigenetic network was translated into a mathematical model that utilizes a set of possible H3 histone modifications shown on Fig 2.1.1. For simplification, only one histone H3 tail is considered as subunit of the nucleosome core. Silenced or heterochromatic state of the particular nucleosome was split up into four H3K9 associated epigenetic groups representing possible repressed nucleosomal states. Thus, H3K9me2, H3K9me2S10ph and its HP1 bound variants characterize the silenced conformation of the nucleosome composing the heterochromatin. The HP1 bound repressive modifications promote the transition towards the same modification of other surrounding histones in a distance dependent manner (Fig 2.1.2). Moreover, implementing the dimerization property of HP1-binding, model assumption is that only a couple of repressive histones, dinucleosomes, could trigger this positive silencing feedback.

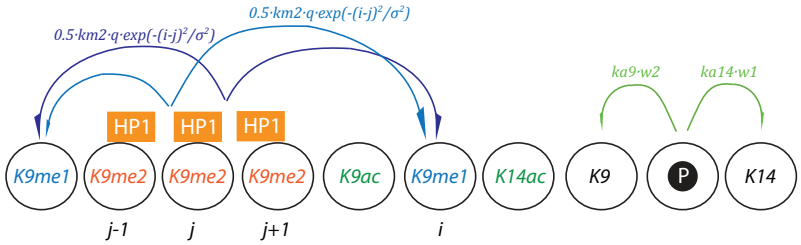

Figure 2.1.2 Distance dependent front propagation of H3K9me2 and H3K9/K14ac. The fragment of linearized fiber of the nucleosomes represents the individual fragment of PCH locus. A silenced chromatin region mostly consists of the H3K9me2 type nucleosomes (orange). In the form of dimer this type feedbacks to the dimethylation rate of the neighbors lacking the dimethyl group (blue) in the distance dependent manner expressed within exponential decay function (formula in blue). The H3S10ph type of nucleosomes (P) feedback into the acetylating rate of the free K14 and K9 types (green arrows) with linear enhancement formula (in green).

Furthermore, all combinatorial phosphorylated states over the fiber feedback onto its local neighbor's acetylation capacity acting in a short-range interaction manner (Fig 2.1.2) by the recruitment of GCN5 acetyltransferace. GCN5 catalyzing acetylation of the neighboring histones at the residues K9 and K14 gives a negative feedback directly into K9 methylation and abundance of HP1 in PCH. This process is initiated in the middle S phase of the cell cycle and progresses into G2 phase with the increase of Aurora B expression in the cell.

2.2 Deterministic model description

The mathematical model of epigenetic marks propagation is formulated as a system of ordinary differential equations (ODEs). The core variables constituting the network are the local probabilities of mono-, di-/trimethylation at K9, probability of acetylation at H3K9 and H3K14, probability of phosphorylation at H3S10 and the probabilitiy of the superposition of those marks possible on one single H3 tail. All probabilities depend on time and the position of nucleosome on DNA composing the chromatin fiber. The fiber is represented as one-dimensional lattice and varies in size corresponding to the total number of the nucleosomes (*N*) it consists of. The index *i* denotes the position of individual nucleosome on the fiber. Symbols used for the probability terms as the model variables in the differential equations are shown in the following table (Table 1).

States of H3 tail	Probability terms
K9***ac***S10K14	Ya
K9S10K14	Yb
K9***me1***S10K14	Yc
HP1-bound K9***me2***S10K14	Yd
K9***ac***S10***ph***K14	Ye
K9S10***ph***K14	Yf
K9***me1***S10***ph***K14	Yg
HP1-bound K9***me2***S10***ph***K14	Yh
K9***ac***S10K14***ac***	Yj
K9S10K14***ac***	Yk
K9***me1***S10K14***ac***	Yl
K9***me2***S10K14***ac***	Ym
K9***ac***S10***ph***K14***ac***	Yo
K9S10***ph***K14***ac***	Yp
K9***me1***S10***ph***K14***ac***	Yq
K9***me2***S10***ph***K14***ac***	Yr

Table 1 Variables of the model.

The ODEs system representing the time evolution of the probabilities to utilize each particular state for each nucleosome is indexed by i where $i \in [1;N]$ set as

$$
\begin{cases}
\frac{dYa_i}{dt} = kda_{14}Yj_i + kdpYe_i + ka_9Yb_i(1 + w_1Phos[i]) - Ya_i(ka_{14}(1 + w_2Phos[i]) + kda_9 + kp) \\
\frac{dYb_i}{dt} = kda_{14}Yk_i + kdpYf_i + kda_9Ya_i + kdm_1Yc_i - Yb_i(ka_{14}(1 + w_2Phos[i]) + ka_9(1 + w_1Phos[i]) + km_1 + kp) \\
\frac{dYc_i}{dt} = kda_{14}Yl_i + kdpYg_i + km_1Yb_i + kdm_2Yd_i - Yc_i(ka_{14}(1 + w_2Phos[i]) + kdm_1 + kp + km_2(1 + qMeth[i])) \\
\frac{dYd_i}{dt} = kda_{14}Ym_i + kdpYh_i + km_2Yc_i(1 + qMeth[i]) - Yd_i(ka_{14}(1 + w_2Phos[i]) + kdm_2 + kp) \\
\frac{dYe_i}{dt} = kda_{14}Yo_i + kpYa_i + ka_9Yf_i(1 + w_1Phos[i]) - Ye_i(ka_{14}(1 + w_2Phos[i]) + kda_9 + kdp) \\
\frac{dYf_i}{dt} = kda_{14}Yp_i + kpYb_i + kda_9Ye_i + kdm_1Yg_i - Yf_i(ka_{14}(1 + w_2Phos[i]) + ka_9(1 + w_1Phos[i]) + km_1 + kdp) \\
\frac{dYg_i}{dt} = kda_{14}Yq_i + kpYc_i + km_1Yf_i + kdm_2Yh_i - Yg_i(ka_{14}(1 + w_2Phos[i]) + kdm_1 + kdp + km_2(1 + qMeth[i])) \\
\frac{dYh_i}{dt} = kda_{14}Yr_i + kpYd_i + km_2Yg_i(1 + qMeth[i]) - Yh_i(ka_{14}(1 + w_2Phos[i]) + kdm_2 + kdp) \\
\frac{dYj_i}{dt} = ka_{14}Ya_i(1 + w_2Phos[i]) + kdpYo_i + ka_9Yk_i(1 + w_1Phos[i]) - Yj_i(kda_{14} + kda_9 + kp) \\
\frac{dYk_i}{dt} = ka_{14}Yb_i(1 + w_2Phos[i]) + kdpYp_i + kda_9Yj_i + kdm_1Yl_i - Yk_i(kda_{14} + ka_9(1 + w_1Phos[i]) + km_1 + kp) \\
\frac{dYl_i}{dt} = ka_{14}Yc_i(1 + w_2Phos[i]) + kdpYq_i + km_1Yk_i + kdm_2Ym_i - Yl_i(kda_{14} + kdm_1 + kp + km_2(1 + qMeth[i])) \\
\frac{dYm_i}{dt} = ka_{14}Yd_i(1 + w_2Phos[i]) + kdpYr_i + km_2Yl_i(1 + qMeth[i]) - Ym_i(kda_{14} + kdm_2 + kp) \\
\frac{dYo_i}{dt} = ka_{14}Ye_i(1 + w_2Phos[i]) + kpYj_i + ka_9Yp_i(1 + w_1Phos[i]) - Yo_i(kda_{14} + kda_9 + kdp) \\
\frac{dYp_i}{dt} = ka_{14}Yf_i(1 + w_2Phos[i]) + kpYk_i + kda_9Yo_i + kdm_1Yq_i - Yp_i(kda_{14} + ka_9(1 + w_1Phos[i]) + km_1 + kdp) \\
\frac{dYq_i}{dt} = ka_{14}Yg_i(1 + w_2Phos[i]) + kpYl_i + km_1Yp_i + kdm_2Yr_i - Yq_i(kda_{14} + kdm_1 + kdp + km_2(1 + qMeth[i]))
\end{cases}
$$

Where function $Phos[i]$ represents the enhancement of the H3K9 and H3K14 acetylation rates by factors of w_1 and w_2 correspondingly due to the presents of the phosphate group on the nearest neighboring nucleosomes

$$
\begin{aligned}
&Phos[i] = Ye_{i-1} + Yf_{i-1} + Yg_{i-1} + Yh_{i-1} + Yo_{i-1} + Yp_{i-1} + Yq_{i-1} + Yr_{i-1} \\
&+Ye_{i+1} + Yf_{i+1} + Yg_{i+1} + Yh_{i+1} + Yo_{i+1} + Yp_{i+1} + Yq_{i+1} + Yr_{i+1}
\end{aligned}
$$

The $Meth[i]$ function expresses the enhancement of the local dimethylation rate for the H3K9 by factor of q for nucleosome i via presence of the HP1-bound nucleosomes in the nearest or distant proximity. Parameter σ defines the strength of enchantment through the exponential distance function implemented as following

$$Meth[i] = \frac{1}{2}\sum_{j=2}^{N}(Yd_j + Yh_j)(Yd_{j-1} + Yh_{j-1})\exp(\frac{-(i-j)^2}{\sigma^2}) + \frac{1}{2}\sum_{j=1}^{N-1}(Yd_j + Yh_j)(Yd_{j+1} + Yh_{j+1})\exp(\frac{-(i-j)^2}{\sigma^2})$$

For the complete mathematical model the following conservation law is considered

$$Yr_i = 1 - (Ya_i + Yb_i + Yc_i + Yd_i + Ye_i + Yf_i + Yg_i + Yh_i + Yj_i + Yk_i + Yl_i + Ym_i + Yo_i + Yp_i + Yq_i)$$

together with the first-type (Dirichlet) boundary conditions at both the ends of the fiber

$$\begin{cases} Ya_l = 1 \\ \begin{pmatrix} Yb_l & \dots & Yr_l \end{pmatrix}^T = \begin{pmatrix} 0 & \dots & 0 \end{pmatrix}^T \end{cases} \quad \text{for } l = 0 \text{ and } l = N+1$$

Thus, the complete set of these equations together with the conservation condition and the boundary settings has been used in analyses of the uniform static solutions and to study its stability. The main focus is on the total dimethylation signature over the entire fiber that sums up the contribution of all four dimethylated (H3K9me2) states of the model constraints. This signature is expressed in terms of fractional dimethylation of the whole fiber and can be derived with the following formula

$$ME2 = \frac{1}{N}\sum_{i=1}^{N}(Yd_i + Yh_i + Ym_i + Yr_i)$$

2.3 Parameterization of the mathematical model

Phenomenological kinetic constants composing the initial parameter set of the model were chosen in accordance with biologically realistic kinetic parameter ranges. Most of them were specified based on recent experimental studies described in the literature.

The kinetic parameters of the different types of reactions composing the network, that are mono- and di- methylation, mono- di- demethylation, K14 and K9 acetylation and deacetylation, are biochemically defined in the *in vivo* experiments. One can determine the rate of turnover of a compound by measuring its exponential

increase in specific labeling provided that a steady state condition is reached.

Histone H3 acetylation half-life ($t_{1/2}$) time measured in yeast cells was approximately 10 minutes (Waterborg et al., 2001). In the pulse-chase labeling experiments for mammalian cells, the acetylation dynamic differentiated into classes of rapid and slow acetylation/deacetylation rates. As such, H3.2 histone had two acetylation rates: a fast rate with $t_{1/2}$ of 8 min and slow rate with a $t_{1/2}$ of 400 min (Sun et al., 2001). The fast slope reconstituted in short acetate pulse characterizes the rapid acetylation dynamics of newly synthesized DNA incorporated histones. The slow dynamics reviled in the long pulse assign for the bulk histones (Covault et al., 1980). Therefore, only a fast kinetics of acetyl turnover was taken into account in the model under the assumption of the naivety of histone subunits composing the chromatin fiber. Thus the ka_9 and ka_{14} parameters were both approximated by 0.01 min^{-1} rate value.

Relatively higher histone deacetylase (HDAC) activity has been observed as compared to the histone acetylase (HAC) activity in the bulk histone population, $t_{1/2}$ estimated by 30-150 min and 200-400 min respectively, give the relative score of acetylation/deacetylation rate ratio. Therefore, the demethylation rate kda_9 and kda_{14} in the model have been set to the 0.1 min^{-1} which is a fold higher than spontaneous acetylation.

Exchange of the histone methylation groups occurs in the range of hours and days (Zee et al., 2010). Demethylation activity reconstituted from *in vivo* SILAC experiment determined that the averaged kinetics was estimated by 2.4×10^{-4} min^{-1} summing up theoretically fitted rates of mono and dimethyl removal from H3K9 tail (Zee et al., 2010). This rate value is assigned to the kdm_1 modeling parameter. However, the enzymatic activity of JMJD2A demethylase, that have the strongest preference for the repressive epigenetic marker trimethyllysine of H3K9 tail (Wilson 2007), have been measured *in vitro* in much higher ranges. Thus, the JMJD2A catalytic rate for the H3K9me3 substrate was 0.015 min^{-1} (Couture et al., 2007). Consequently, initial rate for the repressive mark removal in the model, kdm_2, was roughly estimated by three fold higher value as compared to the kdm_1 and set to 10^{-1} min^{-1}.

Basal methylation rate constant km_2 was roughly estimated from the *in vivo* SILAC experiment and set to be equal to 10^{-3} min^{-1} (Zee et al., 2010). The basal rate of monomethylation, km_1, was chosen in accordance with the *in vitro* measurments of the mammalian G9a methyltransferase activity and was measured to be 1.5 min^{-1}

(Patnaik et al., 2004).

The spontaneous phosphorylation and dephosphorylation rates were chosen within the biologically relevant constrains. Thus *kp* and *kdp* parameter values were fixed to 0.01 min^{-1} and 1 min^{-1} respectively. Complete initial parameter set with additional enhancement coefficients are summarized in the following table (Table 2).

Parameter	**Symbol**	**Value**	**Unit**
Methylation activity			
Spontaneous monomethylation rate	km_1	1.5	min^{-1}
Di/tri- methylation rate	km_2	0.001	min^{-1}
Demethylation rate of H3K9me1	kdm_1	0.00024	min^{-1}
Demethylation rate of H3K9me2	kdm_2	0.1	min^{-1}
Acetylation activity			
K9 and K14 acetylation rate	ka_9, ka_{14}	0.01	min^{-1}
K9 and K14 deacetylation rate	kda_9, kda_{14}	0.1	min^{-1}
Phosphorylation activity			
S10 phosphorylation rate	*kp*	0.01	min^{-1}
S10 dephosphorylation rate	*kdp*	1	min^{-1}
Enhancement coefficients			
H3K9 acetylation factor	w_1	1000	
H3K14 acetylation factor	w_2	100	
H3K9 methylation factor	*q*	3000	
Methylation spread factor	*sigma*	2	

Table 2 Parameters of the model

2.4 Stationary deterministic solution

The final high dimensional first order nonlinear autonomous system of ODEs that represents the dynamical behavior of the model is almost impossible for finding any explicit or implicit solutions. The qualitative approach as well as the numerical approach are only hints to make a prediction, regardless of the solution and its dynamic and stationary properties with respect to parameter change.

The system can be represented in the vector form as $\frac{d\vec{Y}}{dt} = F(\vec{Y})$

Where vector of the system state variable $\vec{Y} = \begin{pmatrix} Ya_1 \\ \vdots \\ Ya_i \\ Yb_i \\ \vdots \\ Yq_N \end{pmatrix}$ and function $F(\vec{Y}) = \begin{pmatrix} Fa_1(\vec{Y}) \\ \vdots \\ Fa_i(\vec{Y}) \\ Fb_i(\vec{Y}) \\ \vdots \\ Fq_N(\vec{Y}) \end{pmatrix}$

The system is said to be in its equilibrium condition when the derivatives of its state variables equal to zero, which means there is no variation of the state variables. For the modeling system, this condition is given as following:

$$0 = F(\vec{Y})$$

Solutions of above system are the set of equilibrium points, $\vec{Y}_j^*$.

Further, the numerical search of the stationary solutions was performed by use of the Newton's method (Kuznetsov, 2001). Nonlinear multidimensional systems tend to have few closely spaced fixed points (steady states) under the certain parameter conditions and a sufficiently good starting guess would require to find one of them. To find all the steady states for a give parameter space, the population of initial starting guess points was set up and used in each independent iterative search.

Newton's method

Suppose the system of nonlinear equations

$$F(\vec{Y}) = 0,\ F(\vec{Y}),\ \vec{Y} \in R^{15N} \tag{2.1}$$

has stable equilibrium solutions $\vec{Y}_j^*$. The Newton method for determining this solution is based on a linearization around a starting guess $\vec{Y_0}$

$$F(\vec{Y}) \approx F(\vec{Y_0}) + J_F(\vec{Y_0})(\vec{Y} - \vec{Y_0}) \tag{2.2}$$

where $J_F(\vec{Y_0})$ the Jacobian matrix of $F(\vec{Y})$ evaluated at the a starting point $\vec{Y_0}$

$$J_F(\vec{Y}) = \begin{pmatrix} \frac{\partial Fa_1}{\partial Ya_1} & \cdots & \frac{\partial Fa_1}{\partial Yq_N} \\ \vdots & \ddots & \vdots \\ \frac{\partial Fq_N}{\partial Ya_1} & \cdots & \frac{\partial Fq_N}{\partial Yq_N} \end{pmatrix} \tag{2.3}$$

Consequently the initial system of nonlinear equations (2.1) can be replaced by linear system (2.4)

$$F(\vec{Y_0}) + J_F(\vec{Y_0})(\vec{Y} - \vec{Y_0}) = 0 \tag{2.4}$$

If the Jacobian matrix $J_F(\vec{Y_0})$ invertible, this linear system will have the solution

$$\vec{Y_1} = \vec{Y_0} - J_F(\vec{Y_0})^{-1} F(\vec{Y_0}) \tag{2.5}$$

The approximate solution $\vec{Y_1}$ which we could expect to be closer to $\vec{Y}_j^*$ than $\vec{Y_0}$ can be used as a new starting guess in an iterative process. Following the

arguments above, we use the Newton iterations expressed by the recurrence relation

$$\vec{Y}_{k+1} = \vec{Y}_k - J_F(\vec{Y}_k)^{-1} F(\vec{Y}_k) \tag{2.6}$$

Until the $\vec{Y}_{k+1}$ does not satisfy the convergence criteria (2.7) with reasonable accuracy. Once a search is close enough to a local equilibrium point $\vec{Y}^*$, the convergence is said to be quadratic, which means

$$\left\|\vec{Y}_{k+1} - \vec{Y}^*\right\| \le \beta \left\|\vec{Y}_k - \vec{Y}^*\right\|^2 \tag{2.7}$$

for some constant $\beta > 0$

The Newton search was implemented in `Mathematica 9.0` (Wolfram Research, Inc.. 2013) using the function, `FindRoot`. The biochemically allowed ranges for the kinetic parameter values, the population of initial starting guess points as well as additional requirements to the system's functionality were integrated as constraints in the algorithm.

At first the Newton algorithm starts with the population of sequential initial starting guess points set as following

$$\vec{Y}_{init} = (0.1*k \ldots 0.1*k)^T,\ k = 0,1\ldots,10. \tag{2.8}$$

In each independent run for particular k, the algorithm ends up with one numerical equilibrium solution of the steady state system that satisfied convergence rate criteria (2.7) with the default `Mathematica 9.0` machine-precision number. For one particulate parameter set the population of eleven numerical solutions are generated.

The sequence of the equilibrium solutions with respect to the change of demethylation rate value, kdm_2 parameter, shows preliminary generic structure of bifurcational diagrams for the system of N=10, 30, 60, 100 nucleosomes depicted on Fig 2.4.1. Considering the high degree of system complexity such as the multi dimensionality and nonlinearity, the expected multistable nature of the whole process is revealinged. For instance, the bifurcation of fractional dimethylation of the whole nucleosomal fiber, *ME2*, for kdm_2 parameter value range from 0.1 to the 0.4 min^{-1}. can be translated into the classical bistability for the system of different size *N* (Fig 2.4.1), since the corresponding populations of the equilibrium solutions defined only tree equilibrium states where one can be interpreted as unstable steady-state

and two others as the stable attractors.

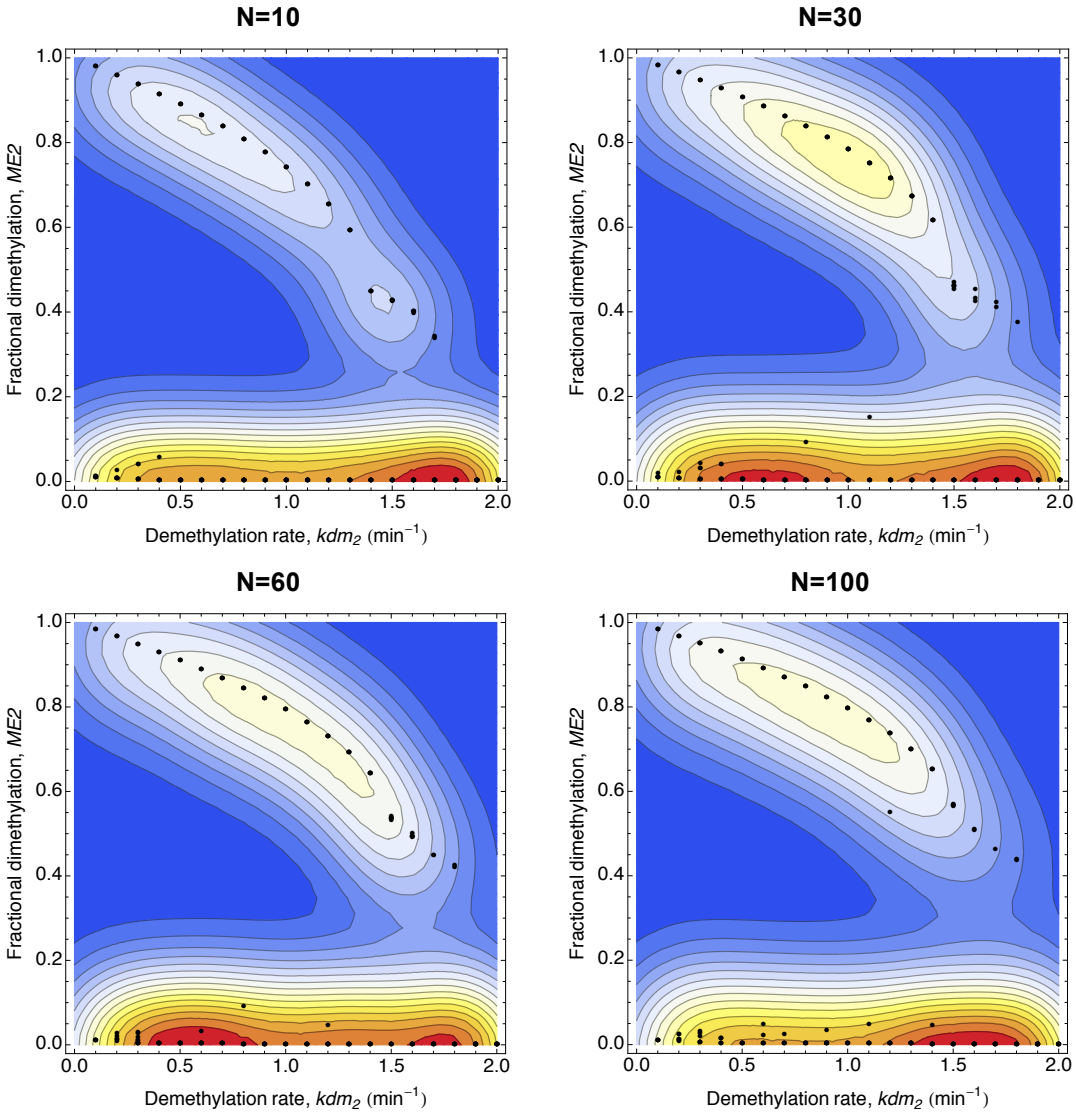

Figure 2.4.1 Rough bifurcation diagrams of the H3K9me2 enrichment as the function of the JMJD2 demethylation activity for system of different size. The temperature shades represent the frequency of Newton convergence from the fixed set of 11 initial guesses

2.5 Continuation on parameter

The above defined properties of rough steady-state bifurcations by initially applied random guess Newton search of parametric dependence leads to the discovery of the right initial guess points for the final Newton search with implementation of parameter continuation approach (Kubicek et al, 1976; Mittelmann et al, 1987).

Starting from kdm_2 parameter value of 0.2 min^{-1}, all tree steady-states solution branches can be continued with respect to kdm_2 for fixed values of others.

The algorithm starts with the Newton search of system roots for the kdm_2 equal to 0.3 min^{-1} and the initial guess points now are the three roots calculated at the previous step for parameter value 0.2 min^{-1}.

In each of the following iterations, the kdm_2 value increases stepwise by 0.1 min^{-1} and the Newton search initiated from the roots of the previous step value.

2.6 Deterministic system response upon the JMJD2 level perturbation

A few original theoretical studies of the inherence of the epigenetic state claim that the bistability is the most efficient and most reasonable explanation of the long term memory effect in the epigenetic systems (Dodd et al, 2007; Sedighi et al, 2007). Existence of the metastable state regime allows the preservence of silencing of the large chromosomal regions that tend to be a constitutively heterochromatic in the genome. On the other hand, its can cause a rapid change of the epigenetic state with the sudden external or internal stimuli appearance. This situation may be relevant for the conditionally expressed genes such as genes of the environmental response or developmental genes where the transcription factor activation, binding with following recruitment of the histone modifiers change the developmental or the evolutional program of the cell.

The bistable model type is presented in this study as the simplest representation of the silencing process in the pericentric heterochromatin (PCH). The presence and stability of two controversial heterochromatic states are assumed within the fixed conditional parameter space. Thus two independent, off-silenced, transcriptional active state with low H3K9me2 enrichment, and on-silenced, repressive state with the high H3K9me2 mark enrichment, coexist together and are regulated with respect to the environmental conditions such as the concentration of the histone modifying enzymes as well as the level of the chromatin associated proteins.

The nonlinear feedback loops and the nonlocal character of the interaction between the nucleosomes within the chromatin fiber were considered to be essential for the bistable type of response (Dodd et al, 2007). On the contrary, the mathematical model presented here determines the bistable response for the

system with almost local nucleosomal interaction capacity requiring only nonlinearity in the binding of the HP1-Suv39h complex that feedbacks to the methyl mark propagation.

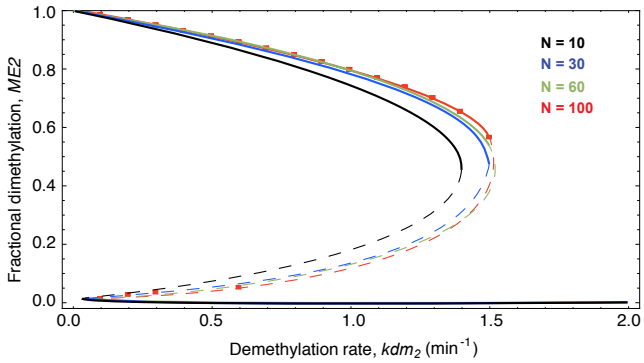

Figure 2.6.1 Deterministic bistable bifurcation diagrams of the H3K9me2 enrichment as the function of the JMJD2 demethylation activity for system of different sizes without persistent origin. The stationary fractional dimethylation against the *kmd2* rate values depicted for 10, 30, 60 and 100 nucleosomal fiber in black, blue, green and red correspondingly and represented the H3K9me2 enrichment with respect to the varying JMJD2 level for system of different size. The two contradictory stable states dependence on kdm2 shown in solid branches and unstable fixed point in between them in dashed lines.

Thus strong bistability have been revealed upon the perturbation of the JMJD2 level that characterized the demethylation activity shown in the bifurcation diagram (Fig. 2.6.1). The demethylation rate, kdm_2, enhancement from the wild-type (WT) level to the higher levels that correspond to the JMJD2 overexpression situation gives rise to the off-silenced state simultaneously with existing on-silenced state (Fig 2.6.2 A). With the further increase of the JMJD2 level, on-silenced state became weaker in terms of the H3K9me2 mark enrichment measured over the entire chromatin fragment and this trend differs only slightly for the fragments of different nucleosomal content (Fig. 2.6.1. N=10, 30, 60, 100 nucleosomes), although off-silenced state does not change the status by means of H3K9me2 enrichments and does not vary for systems of different size.

Consequently, two types of stable spatial distributions of H3K9me2 over the fiber can be observed with bistable regime. The first is the high H3K9me2 mark occupancy at almost every nucleosome that composed chromatin fiber as shown on the plot with high local H3K9me2 probability pattern (Fig 2.6.2 B red). The second is chromatin fiber that is free of repressive mark with the low local H3K9me2 probability pattern (Fig 2.6.2 B blue).

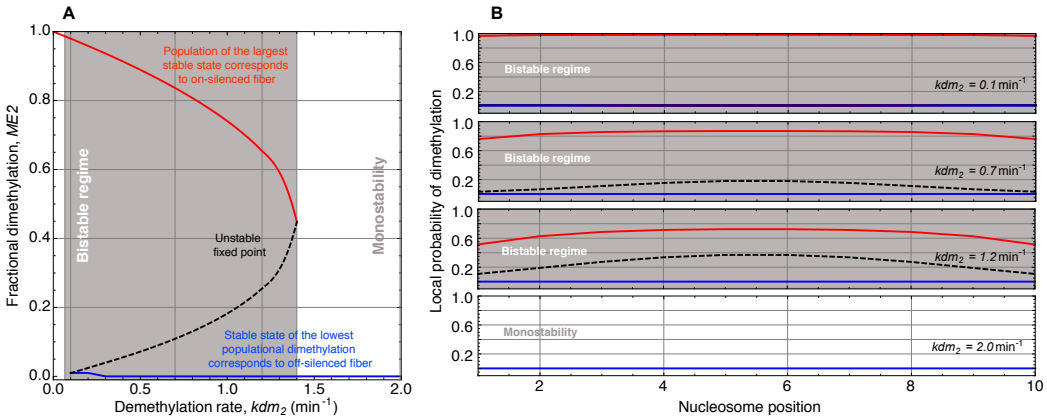

Figure 2.6.2 The stability representation for the system of 10 nucleosomes. (A) The bifurcation diagram of bistable response upon the rise of demethylation activity. The low H3K9me2 enrichment stable state depicted in blue represents the off-silenced situation. The red branch represents the stably high enrichment of H3K9me2 over the fiber meaning the on-silencing heterochromatic state. (B) The spatial steady state distribution of the methylation levels for the chromatin segment of 10 nucleosomes is shown. The distributions belonging to the on-silenced, off-silenced and unstable state depicted in red, blue and dashed black, respectively, for the different regimes driven by the different level of demethylase activity, kdm_2.

The decision about which of these two types of pattern is present at the particular region is made based on the initial constraints of the system. The system that started from the higher level of H3K9me2 is born to be silenced continuously and irresponsive to the change of the JMJD2 concentration within the bistable parameter space remembering the recent conformation. This memory can be broken only with the flux of demethylation rate that goes beyond the right boundary of the bistable kdm_2 space (Fig 2.6.2 A). In this case the system flips into the opposite state, turning silencing off by immediate removal of H3K9me2 mark. The back transition after all by slight suppression of demethylation is impossible since the memory component of the off-silenced state starts to play a role, making the state robust upon the reduction of JMJD2 level. Only the negative flux of kdm_2 going below the left boundary of the bistable space induces unlimited spreading of the H3K9me2 over the whole fiber causing total silencing.

The unstable steady state position in between the on- and off-silenced stable states is an alternative for the transient behavior of the system within the bistable regime. This state separates constraints of the initial H3K9me2 enrichment that lead to the establishment of one stable state over two possible ones on the long time scale. In addition, the system initiated in the closed parameter proximity to the unstable fixed point can rest in this unstable position for a short period of time.

2.7 Prediction of the silencing origins impact

The initiation of silencing in PCH is associated with highly specific PCH versus the surrounding euchromatin protein complexes that recognize a DNA target sequences in the major satellite repeats. All theses complexes are found to be associated with the Suv39h and HP1 proteins.

For example, a recent study reports on mutual function of the HP1, Suv39h1 and MeCP2 proteins in PCH (Müller-Ott et al., 2013). MeCP2 that binds to the methylated CpG islands on DNA has been found to be responsible for the global H3K9me3 enrichment in PCH of neuronal cells. The corresponding experiment for knockout of MeCP2 protein reveals the aberrantly low levels of H3K9me3 in PCH when, on the contrary, euchromatic level has been unperturbed (Thatcher et al., 2006).

One other experimental study has shown that Mi-2/NuRD complex containing several interaction partners of Suv39h and HP1, is necessary to maintain the H3K9me3 mark in heterochromatin and thus represents further protein factors for stabilization of the nucleation complex (Sims et al., 2011). Mi-2/NuRD complex, analogically to MeCP2, is targeted to the PCH in a sequence specific manner via the methyl-CpG-binding domain.

Furthermore, the association of HP1 with nucleation remodeling complex NoRC has been discovered. NoRC complex targeted to the centromere via non-coding RNA (ncRNA) and regulating the integrity of constitutive heterochromatin in general is responsible for the H3K9me3 propagation in PCH. Altering expression of TIP5 subunit of the NoRC that recruits NoRC to the DNA due to its association with the specific siRNA changes the epigenetic content in the PCH. Thus, overexpression and depletion of TIP5 leads to the increase and the lowering of the H3K9me2 occupancy in the PCH respectively (Postepska-Igielska et al., 2013).

Finally, major satellite repeats contain binding sites for Pax3 and Pax9 transcription factors that also interact with HP1 and can be considered as the potential centers of the nucleation of the silencing initiated in PCH (Bulut-Karslioglu et al., 2012).

Optionally, all these partners, acting upstream of the HP1 and Suv39h natural binding affinity to the H3K9me2/3 histone tail, contribute to the PCH specific persistence of the high-affinity HP1 and Suv39h binding sites. Relatively small fractions of the HP1 and Suv39h abundant in PCH occupy the high-affinity binding

sites organizing the silencing origins. Totally immobile HP1 and Suv39h fractions 1.4 μM and 0.7 μM out of total bound pool 40 μM and 4.4 μM, respectively, were detected *in vivo* by the FRAP measurement experiments for MEF cells (Müller-Ott et al., 2013). These concentrations are hardly comparable with the concentration 200-300 μM of nucleosomal cores in PCH (Wachsmuth et al., 2008). Thus, a very small amount of nucleosomes are associated with a stably bound HP1 and/or Suv39h complex.

Stimulation of the system by the local recruitment of the silencing origin complex gives rise to the few alternative modes of qualitative dynamic behavior of the epigenetic state of the chromatin fiber. Optional modes are distinguishable on the parameter space in accordance with the static bifurcation regimes appearing there.

The presence of the persistent origin in the chromatin fiber outside of the bistable space resolved it into the fiber with self-consistent degree of silencing. On the right hand side of the bistable space boundaries it would lead to the locally limited propagation of the H3K9me2 mark around the introduced origin. On the left from the bistable space, it will induce the unlimited spread of H3K9me2 modification over the entire chromatin fragment that assuming the short-range nucleosomal connectivity, can be terminated meeting the genomic boundaries elements such as CTCF binding sites.

Within the bistable parameter constrains, both scenarios of the H3K9me2 propagation is possible depending on the stability strength of each fixed point in correspondence to the current demethylation activity or JMJD2 expression level.
Moreover, the stochastic dynamics here would play the leading role since the random transient silencing appearance over chromatin fragment may give quick support to the main propagation course that is going out of the persistent origin. Therefore, beside the further presented stability analysis of deterministic solutions, the aspects of origin driven H3K9me2 propagation addressed to the equivalent stochastic model is discussed in Chapter 3.

2.8 Stability of stationary solutions

The stability of solutions of the modeling system near the equilibrium points that represent the stable steady states can be studied by use of the Lyapunov stability theory (Nicolis et al, 1989). Assuming that the dynamics of the nonlinear system

near to its equilibrium points are qualitatively similar to the dynamics of the same system represented in linearized form, the Jacobian matrixes (2.3) for all conditions of the demethylation activity at both the stable fixed points, on-silenced and off-silenced states, were calculated.

According to the *Poincare-Lyapunov* Theorem, if the eigenvalues $\lambda = [\lambda_1,...,\lambda_k]$ of the Jacobian matrix (2.3) evaluated at the equilibrium point $\vec{Y}_j^*$ are not equal to zero or are not pure imaginary numbers, then the trajectories of the system around the equilibrium point behave the same way as the trajectories of the associated linear system. Moreover, if the real components of all eigenvalues are negative ($\mathrm{Re}\,\lambda_k < 0$), then the correspondent equilibrium point is asymptotically stable and the more negative a value is, the greater is the stability.

Consequently, the weak and strong stable steady states are distinguishable in terms of the *Lyapunov* stability based on the theirs eigenvalues spectra.

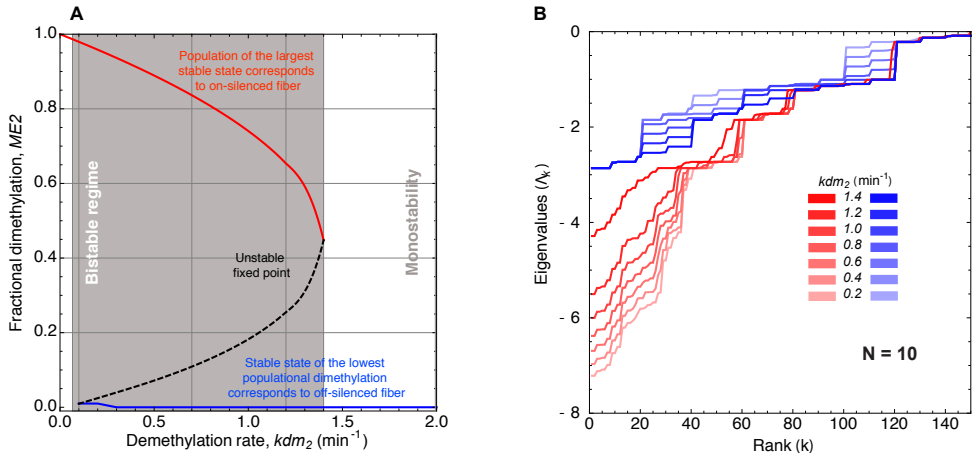

Figure 2.8.1 The stability representation for the system of 10 nucleosomes. (A) The bifurcation diagram of bistable response upon the rise of demethylation activity. The low H3K9me2 enrichment stable state depicted in blue represents the off-silenced situation. The red branch represents the stably high enrichment of H3K9me2 over the fiber meaning the on-silencing heterochromatic state. (B) The spectrum of eigenvalues for two steady states for varying values of demethylation rate depicted in colors correspondent to (A).

Figure 2.8.1 demonstrates that with the fiber *N=10* the stable branch corresponding to the silenced state caused by the high enrichment of the H3K9me2 mark (Fig 2.8.1 A red) is more stable since the whole spectra of eigenvalues (Fig 2.8.1 B in red) in this case is positioned lower than the spectra of the active state (Fig 2.8.1 B in blue). However, the step wise increase of the demethylation rate *kdm2* (Fig 2.8.1 B from 0.2 in the weakest red to 1.4 in the brightest red) is able to reduce the stability of the

on-silenced state and increase the off-silenced state stability (Fig 2.8.1 B from 0.2 in the weakest blue to 1.4 in the brightest blue).

The same trend is reproduced in the system of lager size. The off-silenced state spectra of eigenvalue for all conditions has higher than the on-silenced spectra (Fig 2.8.2).

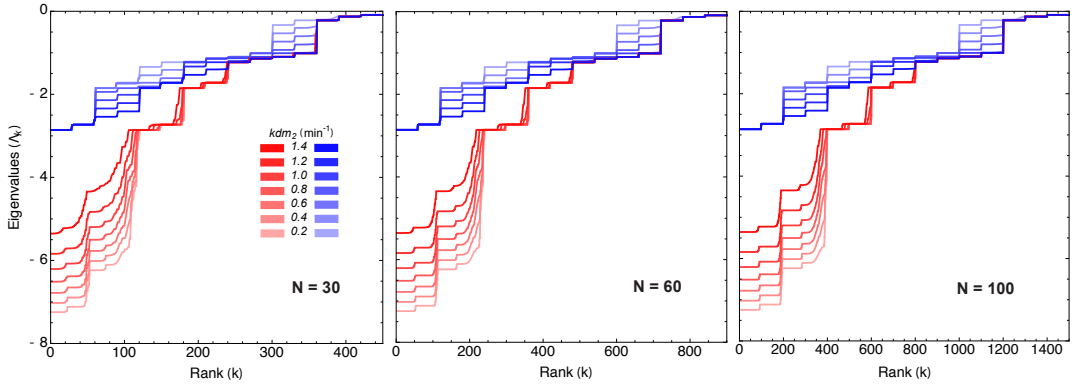

Figure 2.8.2 The eigenvalue spectra for on and off silenced states as a function of demethylation rate. The systems of size 30, 60 and 100 nucleosomes are analyzed. The on-silenced and off-silenced states depicted in red and blue respectively, the varying demethylation conditions represented in different color tones in correspondence to the legend.

The respective maximal eigenvalues across the spectra for all tested demethylation conditions and number of nucleosomes are very similar. Thus having them as the 'strongest' eigenvalue that corresponds to the most dominant eigenvectors and define the directions for the convergence of solutions at the infinite time scale is not precise measure of the conditional stability strength. Perturbation in different directions will lead to the dominance of different eigenvalues among all the distributions of the spread of solution convergence. Consequently, in the study of the system stability with respect to the conditional changes and the change of the system size, all eigenvalues must be considered, especially, if some of them are closed to each other within the particular spectra.

2.9 Estimated stability strength

The dynamics of the nonlinear system $\frac{d\vec{Y}}{dt} = F(\vec{Y})$ near its equilibrium point $\vec{Y}^*$ are qualitatively similar to the dynamics of linear system

$$\frac{d\vec{Y}(t)}{dt} = A\vec{Y}(t) \tag{2.9}$$

where $A = J_F(\vec{Y}^*)$ is Jacobian evaluated at the corresponding equilibrium point. The eigenvalues of the matrix A being Lyapunov characteristic exponents characterize the average rate of convergence of the time trajectories to the stable attractor $\vec{Y}^*$ on the large time scale (Nicolis et al, 1989). Thus the sum of all eigenvalues describe the mean rate of contraction of the phase space volume in a close proximity to the corresponding attractor and the absolute value of this sum can be used as the global "stability score" S for the given stable equilibrium point $\vec{Y}^*$

$$S(\vec{Y}^*) = \left| \sum_{i=1}^{n} \lambda_i \right| \tag{2.10}$$

The stability score S was calculated for the two coexisting stable equilibrium points, on-silenced and off-silenced, as the function of the control parameter demethylation rate, kdm_2. The increase of the demethylation rate value reduces the stability score of the on-silenced state, so the rate of the volume contraction from the small perturbation around on-silenced steady state decrease for the higher values of demethylation rate signifying the weaknesses of general stability strength for this point (Fig 2.9.1 A red) The decrease of the stability strength of the upper attractor explained by the change of global system balance that defined by the ensemble of the all-existing attractors for the given control parameter. For instance, with the increase of kdm_2 this attractor moves (Fig 2.6.2 A in red) towards to the lower stable attractor (Fig 2.6.2 A in blue) on the bifurcation diagram influencing the trajectory dynamics. The same trend is seen for the system of larger size. Thus the stability reduction follows the gradual increase of the demethylation rate value for the system of 100 nucleosomes (Fig. 2.9.1 B red).

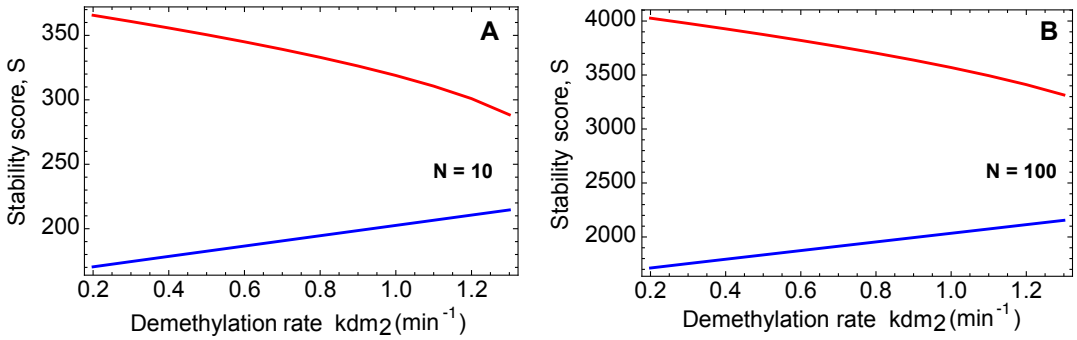

Figure 2.9.1 Stability score as the function of demethylation rate. The stability score for the system of 10 and 100 nucleosomes shown on (A) and (B), respectively, for on-silenced state in red and off-silenced state in blue.

The off-silenced state on the contrary becomes stronger in the stability terms with the rising demethylation activity (Fig 2.9.1 A-B blue). However, for all tested conditions and varying sizes of the system from 10 to the 100 nucleosomal units within the chromatin region, the on-silenced state is winning against the off-silenced state in stability strength since the mean rate of solution convergence is always higher.

Chapter 3

The Stochastic Formalism as the Tool for PCH Epigenetic Network Analysis

In this chapter, the dynamics of the PCH epigenetic silencing network are studied in terms of the stochastic formalization of the problem. The systematic bifurcation analysis was performed by use of the Gillespie stochastic simulation algorithm. This analysis covers the bistable property of the system, stochastic noise contribution and the influence of the possible support of the repressive state via the presence of persistent origins. In addition to it, the cell cycle dependent responses of the modeling network are explained together with the natural variability. Furthermore, the general stability of the repressive and the active epigenetic states is examined.

3.1 Bistability characterizes the PCH response to the perturbed demethylation activity.

In nonlinear epigenetic systems with long-range interaction constrains bistability within a broad range of the number of critical parameters is achieved (Dodd IB et al., 2007). Change in the number of nucleosomes in the modeling fragment of chromatin fiber, the spontaneous modifications appearing in a stochastic fashion, the strength of the positive and negative feedback loops, all these factors contribute in the broad well-distinguishable bistable response.

The short-range interaction between the nucleosomes within the PCH will not give such a degree of freedom for bistable regime, in spite of the nonlinearity of the feedback loop introduced via the nucleosome-mediated cooperativity in the methyl mark propagation. Moreover, considering the contribution of the stochastic

effects, bistability may become even more fragile to the extrinsic fluctuations, responding with respect to its own intrinsic fluctuations, consequently, appearing the ultrasensitivity.

In fact, the stochastic simulation experiment revealed ultrasensitive flipping-like behavior of epigenetic state of the chromatin fragment with respect to the change of the demethylation activity as will be shown in the following. This parameter, expressed in the transition rate from the dimethylated states (H3K9me2) to the monomethylated states (H3K9me1) of PCH network, signifies the spontaneous removal of the repressive modification by histone demethylase JMJD2. Following the gradual increase of the demethylation rate the system is switching from repressive, on-silenced, to the active, off-silenced, states of the chromatin fragment.

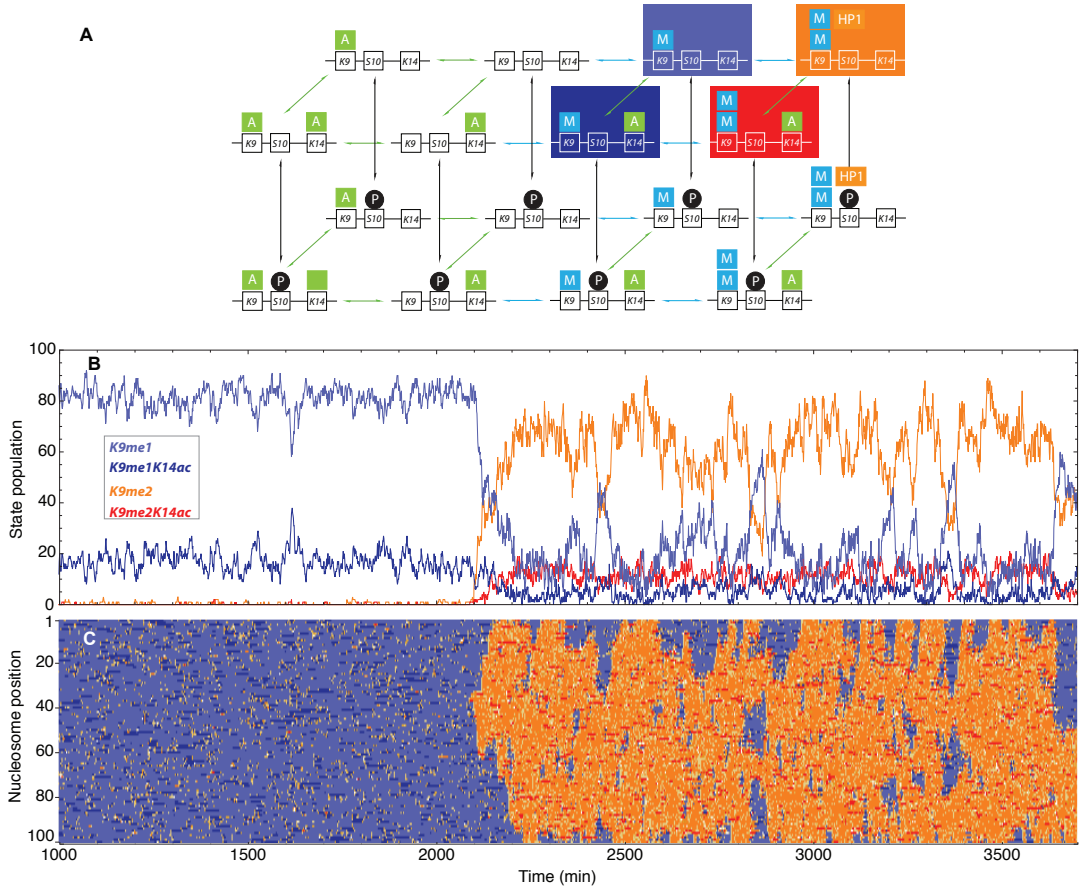

Figure 3.1.1 Spontaneous switch between competing meta-states for the kdm_2 = 0.25 min^{-1}. (A) Schema of the PCH epigenetic network with the assigned color code for the H3K9me2 and H3K9me1 controversial states. (B) Time evolution of H3K9me2 and H3K9me1 states population summarized over the modeling chromatin fragment composed of 100 nucleosomes. (C) The H3K9me2 and H3K9me1 states time evolution for every nucleosome with the chromatin fragment aligned vertically in the array plot.

Observing the system of 100 nucleosomes in the ultrasensitive regime a the long period of time the rare events of the spontaneous change of the chromatin status is perceived (Fig 3.1.1). The following figure demonstrates the single switch of the chromatin fragment from the active to the repressive epigenetic state.

Here the increased demethylation rate value (kdm_2=0.25 min^{-1}) resulted in the change of the repressive mark turnover allowing the meta-stable switches. The time track of the states evolution of each nucleosome (Fig 3.1.1 C) and the evolution of the states population over the whole 100 nucleosomal fiber (Fig 3.1.1 B) are depicted considering the states color code in the modeling schema (Fig 3.1.1 A). Thus, the system initially set to be off-silenced, is resting in the current state for the long time stably maintaining the high enrichment of H3K9me1 and H3K9me1K14ac mark in spite of the intrinsic fluctuations. In the shown stochastic system realization the stability is lasting for more that two cell cycles, around 2000 min. After that a massive spontaneous flip of the whole population of nucleosomes into the repressive state is realized. A dramatic shift of the balance between the active and repressive histone modifications is acquired. The system becomes silenced utilizing mostly the H3K9me2 nucleosomal states. The bistable mechanism allows, again, the stability of the silenced state for at least two cell cycles revealing the long-term epigenetic memory capacity. That results in the blocking of the region for the transcription initiation signals and the relevant for PCH high order structural compactization of the chromatin fiber inherited for many cell cycles.

The perturbing level of demethylase JMJD2 is the efficient way of shifting the balance between monomethylated/acetylated, off-silenced, state and the repressive dimethylated, on-silenced, state (Fig. 3.1.2). However, the bistability is possible only for the strict range of the demethylation rate values (Fig 3.1.3). This range is much smaller than the range predicted with deterministic formalization (Chapter 2). Thus the well distinguishable split of the H3K9me2 nucleosome population into two peaks is detected for 0.26-0.36 min^{-1} range of the demethylation rate. The main participants of the discovered bistable cross talk within this range are nonphosphorylated H3K9me1 and H3K9me2 states. Consequently, for the given conditions PCH epigenetic network can be reasonably reduced ignoring the acetylated and phosphorylated states because of its minimal contribution into the general balance. However, they cannot be neglected due to theirs crucial role in the cell cycle dependent dynamics that is going to be discussed in the text later.

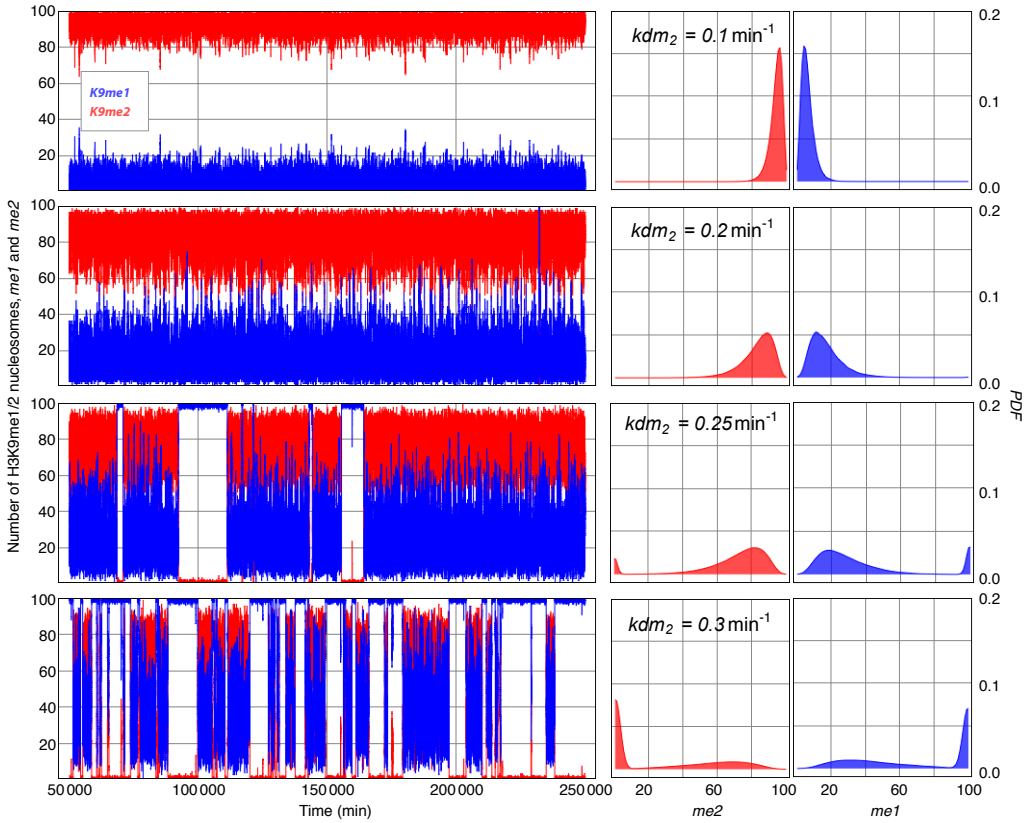

Figure 3.1.2 Bistability appearing as the function of the JMJD2 demethylation activity in the stochastic system. Time evolution of the stationary dynamic of the system 2 x 10^5 min with respect to the gradual increase of the demethylation rate value, kdm_2, shown on the left panel. The total amount of the H3K9me1 nucleosomes (*me1*) over the 100 nucleosomal fiber depicted in blue and the amount of the H3K9me2 nucleosomes (*me2*) in red. The left hand side plots represent the probability density function of populational enrichment of H3K9me1 and H3K9me2 in steady-state for increasing demethylation rate values, from the top to the bottom. Statistics collected over the 10^6 min long simulation runs.

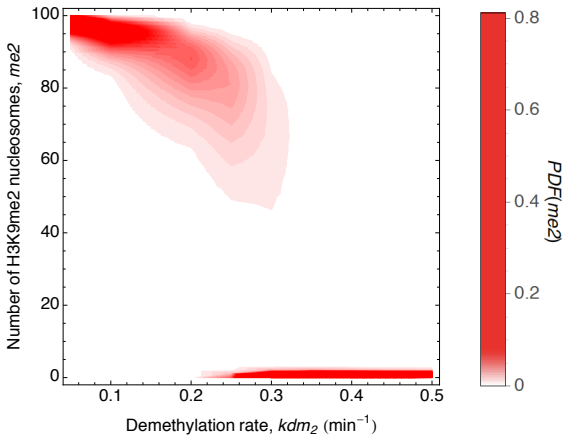

Figure 3.1.3 Stochastic bifurcation diagram of the H3K9me2 enrichment as the function of the JMJD2 demethylation activity. Probability distributions of the total amount of H3K9me2 nucleosomes over 100 nucleosomal fiber summarized for the different demethylation rates. The rate values vary from 0 to 0.5 min^{-1} using steps of size 0.05 min^{-1}. For each rate value the probability distribution of H3K9me2 with respect to the number of nucleosomes represented in the form of probability density function (PDF).

3.2 Active and repressive epigenetic state inheritance

During the bistable regime the meta-stable states flip from one into the opposite one in a spontaneous fashion. In fact, the life-time of each state and the transition rate between them are the functions of the demethylation rate.

To elucidate this dependence, we test a system of 100 nucleosomes. The study focused on the range of demethylation rate from 0.25 min^{-1} to 0.35 min^{-1} that characterizes the bistable regime. The stochastic H3K9me2 response was reconstituted with the small demethylation parameter step size 0.025 min^{-1}. The system dynamics were evaluated in the steady state for 3 x 10^6 min time interval for the good statistical average. The average length of time for which system remains continuously in one or the other state was calculated. In addition, the number of the transitions from one to another state within the simulation time was recorded.

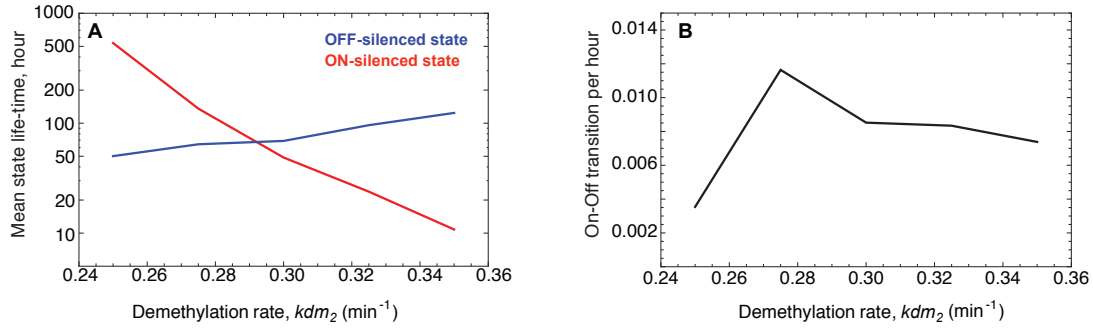

Figure 3.2.1 On-Off Silenced states life-times and transition probability as the function of the demethylation rate. (A) Mean life-times of the On-silenced (red) and Off-silenced (blue) states in the bistable regime for the given range of demethylation rate values. (B) The average number of the transitions from the on-silenced state to the off-silenced state (or vice versa) per hour interval.

3.2.1 Transition rate

The attempted switches between the states can happen much more frequently in our system simulated in comparison to the experimentally observed on-off silencing transition in the *S. pombe* (Grewal et al., 1998).

In *S.pombe* genome, the transition of *ura4*$^+$ reporter gene from the transcriptionally inactive to active form in the experiment of Grewal et al. happened in average 2.5 x 10^{-4} times per hour. The flipping behavior of the gene activity in this experiment was explained by its non-natural location. The gene inserted into the silent donor mating type locus replacing the natural origin of silencing called K-region. Thus the genomic fragment can be considered as the analogy to the PCH

lacking the nucleation origins and the *ura4*$^{+}$ gene transcription as the marker of spontaneous repression in there.

The simulation showed at least one fold higher rate of transition between competing repressive and active epigenetic states. Thus for the bistable regime the transition probability per hour does not drop less than 2.5 x 10^{-3} per hour reaching the maximum value, 1.15 x 10^{-2} per hour, at the demethylation rate equal 0.275 min^{-1} (Fig. 3.2.1 B).

3.2.2 States duration

There in an exponential decay of the life-time for on-silenced state and growth for the off-silenced state with respect to increasing doses of the JMJD2 overexpression, kdm_2, reflected on the semi-log plot (Fig. 3.2.1 A).

Stabilization of the both states duration is achieved at the demethylation rate value 0.2925 min^{-1}. The life-time of both states is roughly estimated at 65 hours, meaning the inheritance of each state for approximately 3 cell cycles in the mouse embryonic fibroblasts cell line (MEF). Taking into account the perturbance of the genome in the S phase during the replication with the partial dilution of the repressive epigenetic markers, the life-time of the on-silenced state in PCH can be reduced in the bistable mode (see 3.5.1).

3.3 Origin dependent dynamic

The bistable switch gives an opportunity for an immediate change in the transcriptional activity that might be relevant for the transcribed regions where a fast response to the internal stimuli is needed. However, this mechanism imperils the silenced epigenetic state of heterochromatic regions that handle the robust compact structural integrity of PCH consequently preventing chromosomal instability.

The PCH is the constitutive form of the heterochromatin and seems to maintain its silenced state as stably as possible. Epigenetic state of the PCH is in general clonally inherited and robust upon the cell cycle dependent epigenome transformations.

The origins would play a key role in this process preserving the silencing in the PCH region. Few experimental facts support this concept.

The sequence specific elements involve into initiation of the heterochromatin formation in *Drosophila* genome. The clustered transgene repeats have been found

responsible for the variegated expression of mini-*white* marker gene positioned in a closed proximity. Variegation is particularly strong for repeated transposons at the euchromatic site near heterochromatin, but also results from repeats at a site distant from heterochromatin (Dorer et al., 1994).

More concrete answer on the nature of the origins of silencing spread is found in the mating-type locus of the *S. pombe* genome, the simplest representatives of the eukaryotic organisms. Mating type locus being the analogy of the constitutive heterochromatin in the PCH and telomeres genomic regions of the mammals contains the nucleation origin. The origin is represented by 4.3 kb cenH sequence position in the middle of the isolated locus. This origin consists several clusters of short direct repeats that share strong homology with the centromeric repeats (elements dg and dh) (Noma et al., 2001). Deletion of the cenH sequence results in a meta-stable locus that displays alternative silenced and active epigenetic states (Hall et al., 2002). The mediation of the heterochromatin formation through the cenH initially requires the RNAi machinery. The RNAi mutants are dispensable for the maintaining of heterochromatin, although the suppression of the histone modifying enzymes such as the Clr4, homology of the Suv39h methyltransferase, and its binding partner Swi6, homology of the HP1 protein, causes less severe effect. Thus only the lowering of the H3K9me2 enrichment with the limiting of this mark spread across the entire silenced domain has been shown by the ChIP analysis (Hall et al., 2002).

Consequently, the origins are required at first for the PCH silencing and they related to the underlying DNA sequence content that persists constantly in the genome. One of them could be the repetitive AT-rich major satellites, MaSat, enriched in the PCH and represent 76% of the all tandem repeats in mouse whole genome assembly (Komissarov et al., 2011).

Another option for sequence specific nucleation of the repressive state is the CpG islands that are targets for DNA methylation. DNA methylated CpG (mCpG) are the repressive epigenetic marks that working together with the MBD and MeCP2 mCpG binding proteins (Baubec et al., 2013). In fact, the MeCP2 was found to be one of the most enriched and tightly bound histone associated protein in the PCH together with the HP1 and Suv39 (Müller-Ott et al., submitted). Such a mechanism of silencing would require the DNA methylation enzymes as like DNMT3 DNA methylases.

Finally, there is an evidence that these two mechanisms, RNAi and mCpG, could work together to secure each other. The RNA associated chromatin-remodeling complex NoRC is responsible for silencing ribosomal genes found to be bound with the DNMT3b DNA methylase (Schmitz et al., 2010).

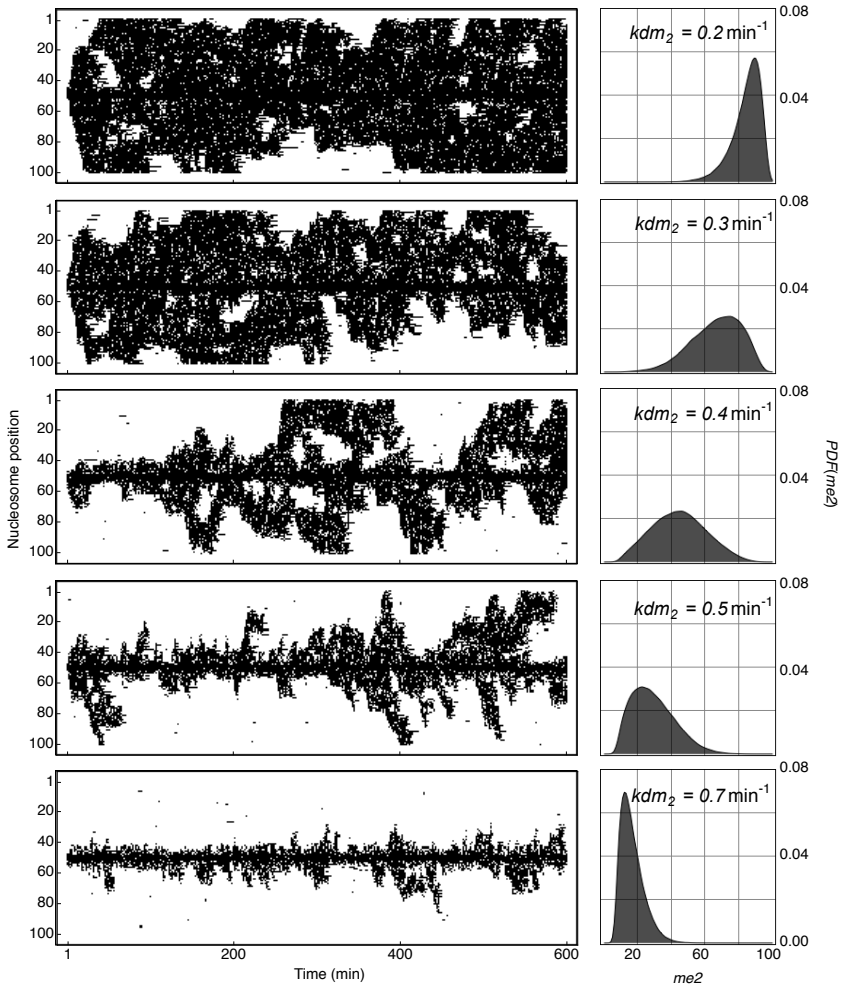

Figure 3.3.1 Origin driven propagation of the H3K9me2 modification over the fiber of 100 nucleosomes for different demethylation rate values. The H3K9me2 states time evolution over 600 min for every nucleosome within the chromatin fragment aligned vertically in the array plot depicted in black. The rest of the utilized states are depicted in white (left panel). For each correspondent demethylation rate value the probability distribution of H3K9me2 collected over 10^6 min with respect to the number of nucleosomes represented in the form of probability density function (PDF) (right panel).

Considering all these facts, the persistent origins were introduced for the modeling system of the 100 nucleosomes. Origins were represented as a patch of 4 nucleosomes in the middle of the fiber that are carrying on the H3K9me2 modification constantly during the simulation time. As in the bistable origin lacking case, the system with origins was evaluated for the rising doses of the JMJD2

demethylation activity. The steady state statistics for the H3K9me2 enrichment was collected from the long time simulation run lasting up to 10^6 minutes. The time dynamics of the H3K9me2 spread over the fiber for the 10 hours is recorded as well (Fig 3.3.1).

The response of the steady state level of H3K9me2 to the increasing demethylation rate is homogeneous (Fig 3.3.1, right panel). The origin in general secures the on-silenced state within the boundaries of the bistable regime. However, the high fluctuations of the H3K9me2 pattern size exist. These fluctuations can still give the significant impact into the general variability of the H3K9me2 in PCH (Fig 3.4.1 A). Positioning in the lower border of the kdm_2 parameter space assign for bistable mode, the origin initiates the propagation of the H3K9me2 over the entire region. Although, at the upper border of bistable parameter space characterized by high value of kdm_2, the system would give the stable but local distance limited propagation of the H3K9me2 around the origin position (Fig. 3.3.1).

According to the observed result, the next question to be answered is what is the size of the initial isolated fragments that would be recognizing these fragments as the repetitive units that consists the PCH. Other question is how the number of the nucleosomes within the single unit will correlate with the variability of the H3K9me2 pattern size with respect to varying doses of JMJD2?

3.4 Stochastic bistability is dependent on the number of the nucleosomes in the system

The insulator elements imply the local independency and isolation of the chromatin regions. The first, boundary elements organized by identical inverted repeats on DNA have been suggested to mark the borders between adjacent chromatin domains and to act as barriers against the effects of enhancer and silencer elements from neighbouring regions (Noma et al., 2001). The second, more recently discovered insulator protein CTCF binding sites have emerged as candidates to define the boundary elements that punctuate the genome to form higher-order chromatin domains (Shaw et al., 2010; Phillips et al., 2009; Labrador et al., 2002). The distribution of the boundary elements would dictate the size of the locally independent regions that compose the PCH and assuming the short-range

interaction constrain for the nucleosomes in PCH would give significant contribution to the system responses.

Therefore, the parameter space of bistable response strongly depends on the number of the nucleosomes in the system. The shift to the higher ranges of hyper demethylation activity of the bistable parameter space acquires for the system of lager size. Thus, the boundaries of the bistable mode for 100 nucleosomes include only a half of the bistable space for the 60 nucleosomes and do not overlap with bistable range for the fragment of 30 nucleosomes. This can be interpreted in the following way. For the system of larger size the stability of the on-silenced state and the beginning of the on-off switching with respect to the demethylation rate for system of smaller size translated as the end of the switching regime and the beginning of the off-silenced state stability (Fig 3.4.1 A-C).

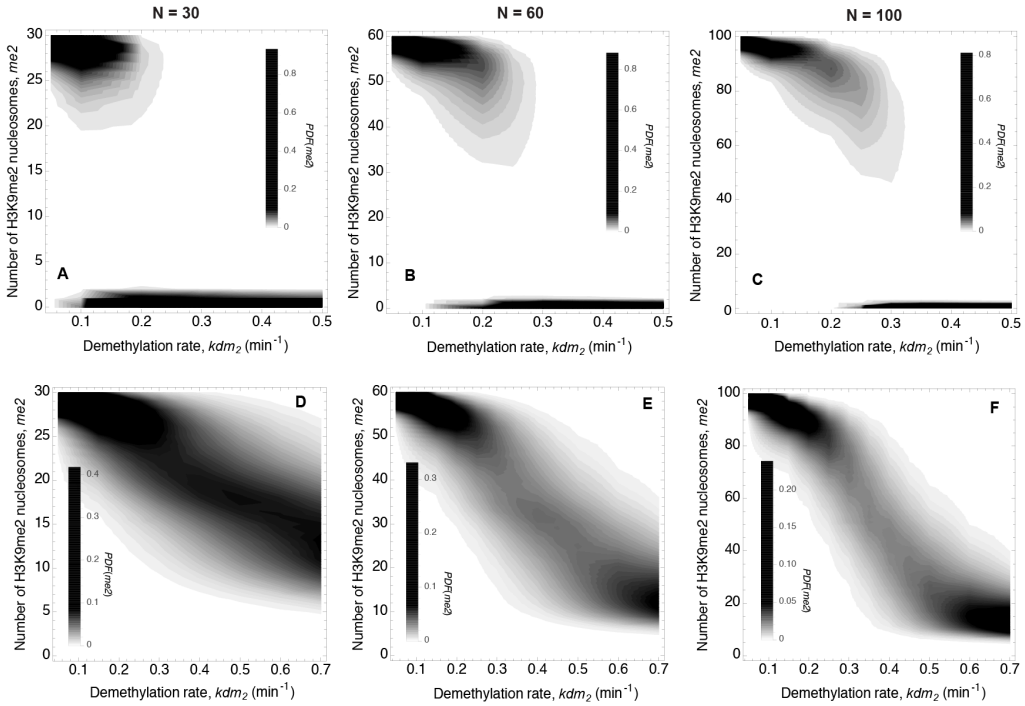

Figure 3.4.1 Stochastic bifurcation diagrams of the H3K9me2 enrichment as the function of the JMJD2 demethylation activity for system of different size with and without persistent origin. Probability distributions of the total amount of H3K9me2 nucleosomes over 30, 60 and 100 nucleosomal fiber summarized for the different demethylation rates. The rate values vary from 0 to 0.5 min^{-1} without origin and from 0 to 0.7 min^{-1} with persistent origin using steps of size 0.05 min^{-1}. For each rate value the probability distribution of H3K9me2 with respect to the number of nucleosomes represented in the form of probability density function (PDF).

The conditions of high variability of H3K9me2 over the fiber in the systems of different sizes follow the same trend (Fig 3.4.2 B). The degree of variability is estimated by the signal-to-noise ratio and is referred to the coefficient of variation

(CV=standard deviation over mean). A CV higher than one signifies high dispersion of the signal indicating the presence of the bistable response. In fact, in general the CV profile against kdm_2 for the system of smaller size is the highest. The increase in the system size lowers the CV. The amplification of CV raising the demethylation rate first appears for the system of smaller size (N=30) (Fig 3.4.2 B) reaching its maximum at the lower values of kdm_2. Consequently the strongest bistability is seen for the smaller system.

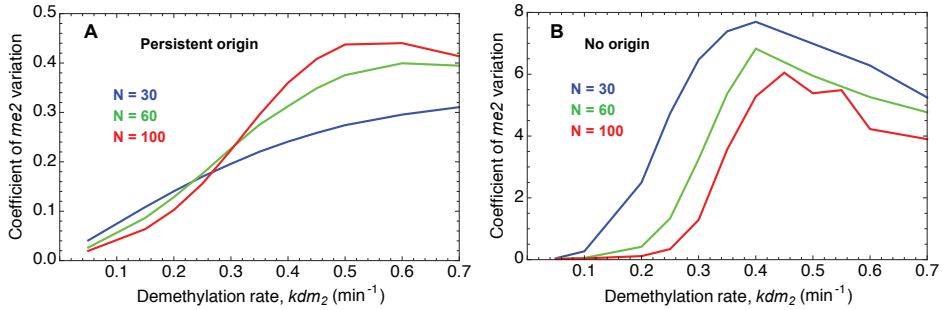

Figure 3.4.2 Variability of the silenced state as the function of demethylation rate and size of the system. Coefficient of H3K9me2 variation (CV) for the fiber of 30, 60 and 100 nucleosomes, blue, green and red correspondently, with persistent origins (A) and without (B). The CV calculated from the steady state system stochastic simulations for 10^6 min time frame and for the demethylation rate varies from 0 to 0.7 min^{-1} using 0.05 min^{-1} step sizes.

However, the opposite effect is observed with the presence of the persistent origins of H3K9me2. Overall the highest variability characterizes the system of 100 nucleosomes and increases for the lower nucleosomal numbers N=60 and N=30 (Fig 3.4.2 A). Although, at lower doses, the smaller size system still senses the change of the demethylation condition first.

3.5 Cell cycle control of silencing in PCH

3.5.1 Replication

The bistable system is susceptible to incorporation of the new nucleosomes while the replication process. These nucleosomes lack the repressive methyl modifications and have high acetylation content of the histone tails that enable theirs relaxed conformation needed for the nucleosome integration into the newly synthesized DNA. The speed of nucleosome incorporation can be compared to the DNA replication rate. A recently developed mathematical model of molecular network of DNA replication in *S. cerevisiae* predicts a progression rate of the

replication fork distribution between 0 and 11 kb/min with the mean value at 2.9 kb/min (Brümmer et al., 2010) that agreed with the experimentally measured rate 3.7 kb/min (Lengronne et al., 2001).

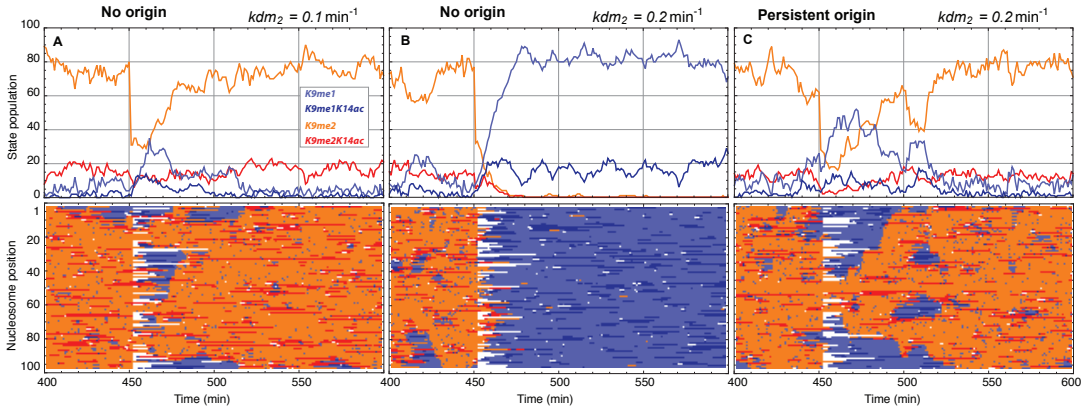

Figure 3.5.1 Different silenced state replication scenarios.
(A) Silencing in the origin lacking conditions for the monostable regime is not affected by the replication dependent nucleosomal exchange. (B) Silencing loss after the replication in the case of bistable regime without origins. (C) Silencing reconstitution after the replication in the case of bistable regime with origins. (Upper panel) Time evolution of H3K9me2 and H3K9me1 states population summarized over the modeling chromatin fragment composed of 100 nucleosomes. (Lower panel) The H3K9me2 and H3K9me1 states time evolution for every nucleosome with the chromatin fragment aligned vertically in the array plots. The rest of the utilized states are depicted in white.

The incorporation of the new histones was performed in the modeling system by exchanging a 50% of randomly chosen nucleosomes within the fiber for nucleosomes in the H3K9ac state. Taking into account the replication fork propagation rate, this exchange is very rapid event and assumes the immediate change of the state of all selected nucleosomes on the time scale of a minute. The origin missing system of 100 nucleosomes in the monostable regime characterized by the lower demethylation rate favors the immediate recover of the on-silenced state (Fig 3.5.1 A). The bistable regime, however, sensitive for the transient perturbations of the epigenetic pattern and the enhanced acetylation will initiate the metastable switch. Thus, it results in the loss of the H3K9me3 modification (Fig 3.5.1 B). Nevertheless, the presence of persistent origin of the H3K9me3 modification would ensure in this case the resistance of the on-silenced state (Fig 3.5.1 C)

3.5.2 G2 phase transition driven by Aurora B expression

Bistability of H3K9me2 in PCH against the Aurora B activity appears in origin free locus

The phosphorylation of Serine 10 of the H3 histone (H3S10ph) being the product of the enzymatic activity of Aurora B kinase are regulated according to the cell cycle. Thus dual epigenetic H3K9me2S10ph modification in the PCH shows a striking increase in the G2 phase following the increasing in Aurora B expression. The phosphate modification appearing next to the methylated K9 residue of the H3 tail disrupts the binding of the HP1 protein (Fischle et. al., 2005). Consequently, this would affect the HP1-Suv39h complex recruitment and Suv39h activity antagonizing H3K9me2 propagation over the related chromatin region.

Surprisingly, HP1 is released from the chromatin not due to H3S10ph alone because the phosphorylation by itself is not enough to reduce the binding of HP1 to the di-/tri-methylated H3 tail. The third concomitant modification, namely acetylation of H3 lysine 14 (H3K14ac), is required for delocalization of the protein. (Mateescu et al., 2004). In fact, S10 phosphorylation directly facilitates the H3K14 acetylation by the recruitment of histone acetyltransferase GCN5 (Cheung et. al., 2000).

The enlargement of the Aurora B kinase activity leading to the increase of the phosphorylation rate for the H3S10 residue was addressed in the stochastic model for the system with and without persistent origins.

The slight increase of the phosphorylation rate leads to the enhanced acetylation process that triggers HP1 eviction and slight reduction of the H3K9me2 enrichment as shown in the Figure 3.5.2.

The bistability of H3K9me2 state of the system without origins was appearing over the short range of the phosphorylation rate, *kp*. System was evaluated at the steady state for 10^6 min for the raised *kp* rate from 0.01 to the 0.08 min^{-1} with the step size 0.01 min^{-1}. The frequency of the H3K9me2 enrichment over 10^6 min and the time course of H3K9me2 dynamic for 2 x 10^5 min interval are depicted on the Figure 3.5.3.

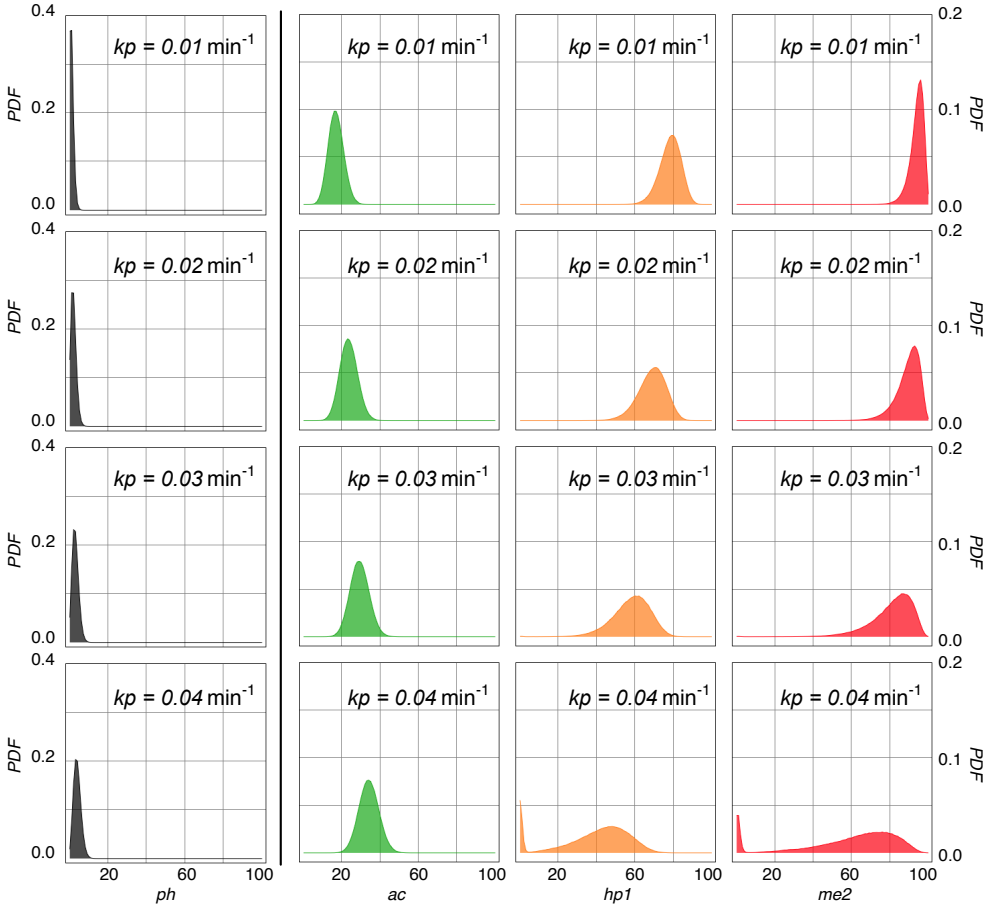

Figure 3.5.2 Cell cycle initiated change of H3 histone modifications. Plots represent the probability density functions of populational enrichment of H3K9me2HP1, H3K9me2, H3K6ac/K14ac and H3S10ph in steady-state for increasing phosphorylation rate values, from the top to the bottom. Statistics collected over the 10^6 min long simulation runs. The total amount of the HP1 bound nucleosomes (*hp1*) over the 100 nucleosomal fiber depicted in orange, amount of the H3K9me2 nucleosomes (*me2*) in red, acetylated nucleosomes (*ac*) in green and phosphorylated - in black.

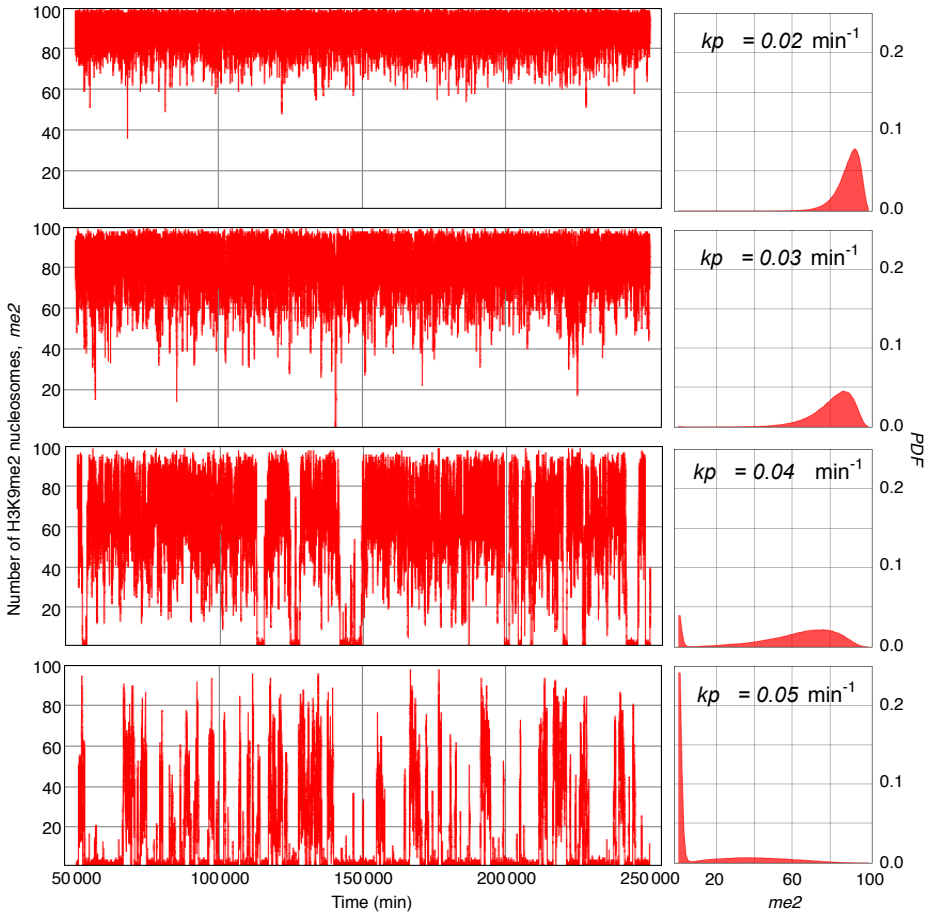

Figure 3.5.3 Bistability appearing as the function of the Aurora B activity in the stochastic system. Time evolution of the stationary dynamic of the system 2 x 10^5 min with respect to the gradual increase of the phosphorylation rate value, *kp*, shown on the left panel. The total amount of the H3K9me2 nucleosomes (*me2*) over the 100 nucleosomal fiber depicted in red. The left hand side plots represent the probability density function of populational enrichment of H3K9me2 in steady-state for increasing phosphorylation rate values, from the top to the bottom. Statistics collected over the 10^6 min long simulation runs.

Within the chosen *kp* steps, the bistable response of H3K9me2 is found only for the rate value 0.04 min^{-1}. The stationary frequencies are summarized for all *kp* conditions in the bifurcation diagram (Fig 3.5.4 A) in terms of the probability density function.

The origin driven scenario of PCH silencing explains the Aurora B kinase driven eviction of the HP1 without the significant H3K9me2 reduction in G2 phase.

Observed correlation of the HP1 and H3K9me2 state is stronger without persistent origins. This would mean better synchronization of the responses of these two variables on the perturbation of phosphorylation status in the nuclei (Fig. 3.5.5 A).

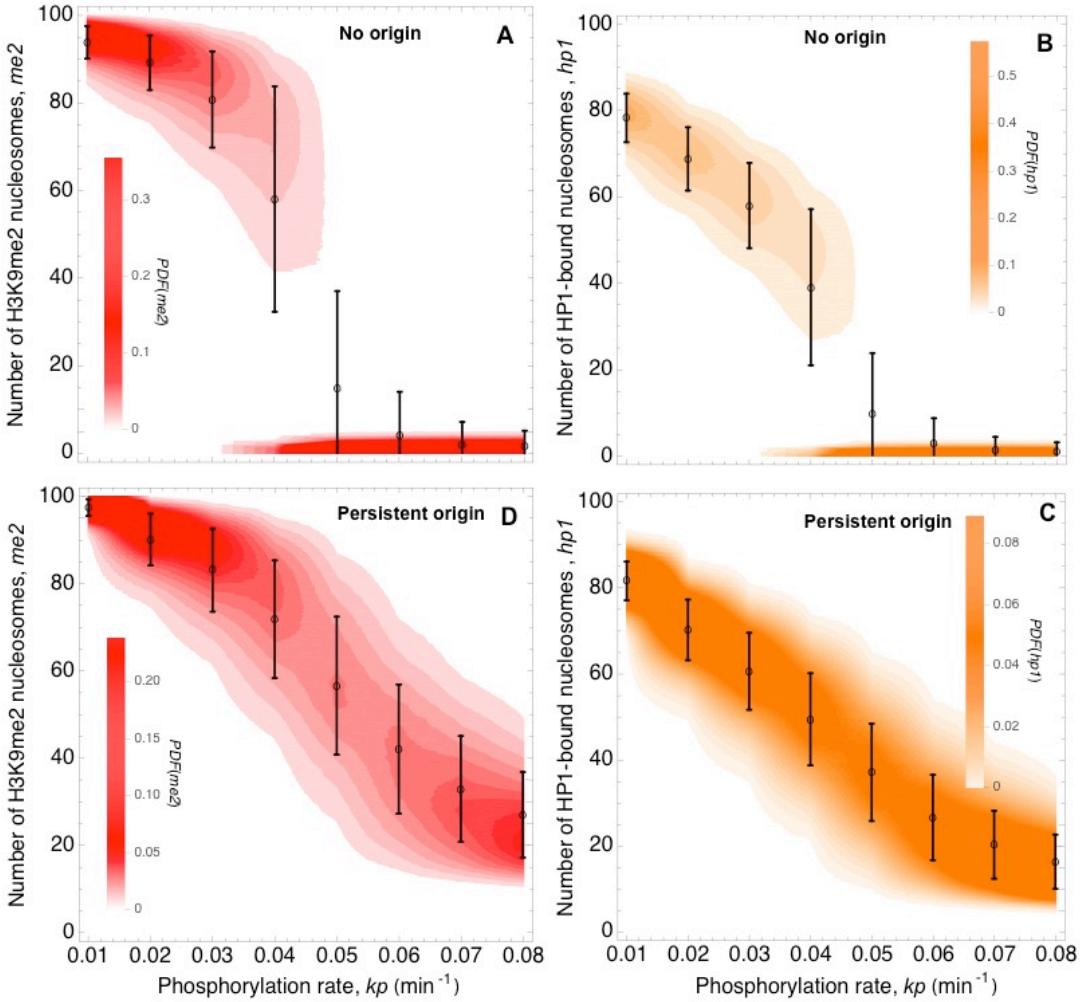

Figure 3.5.4 Stochastic bifurcation diagrams of the H3K9me2 and HP1 bound state enrichment as the function of the Aurora B activity for system with and without persistent origin. Probability distributions of the total amount of H3K9me2 nucleosomes over 100 nucleosomal fiber summarized for the different phosphorylation rate values. The values vary from 0.01 to 0.08 min^{-1} using steps of size 0.01 min^{-1}. For each rate value the probability distribution of H3K9me2 (red) and HP1-bound (orange) states with respect to the number of nucleosomes represented in the form of probability density function (PDF). The mean and standard deviation, black dots and black error bars correspondently, depicted for individually tested conditions.

The difference in variability of the HP1 state to the H3K9me2 total state is much higher in the case of the constant origin presence rather than in origin free regions. In both cases, the variability measured in standard deviation terms of the HP1 state is higher than for the H3K9me2 state (Fig. 3.5.5 B).

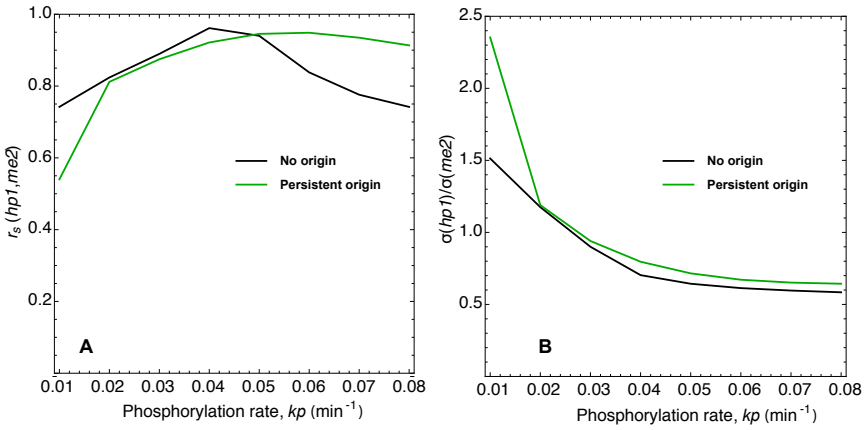

Figure 3.5.5 The state population of HP1-bound nucleosomes vs. H3K9me2 nucleosomes with respect to the increase of the Aurora B kinase. (A) Spearman's rank correlation coefficient (see Appendix A.2) used as the measure of the monotonic relationship between HP1-bound and H3K9me2 nucleosome states. (B) Ratio of the dispersion of HP1-bound to H3K9me2 state population.

In the case of origins, slight increase of the *kp* would lead to a stronger difference for stationary HP1 and H3K9me2 level. And the reason for that is the origin that in general constantly supports the H3K9me2 over the whole region, making this state more robust against *kp* change. While HP1 bound state gets reduced via phosphate modification that interrupts the HP1 binding.

The H3K9me2 pattern is much more robust rather than the HP1-bound state pattern, especially for the lower increase of *kp*. Thus, small increase of *kp* leads to the significant reduction of the HP1-bound state without vanishing H3K2me3 in PCH.

The variability of the H3K9me2 signal for G1 and G2 phase

The actual change of the Aurora B expression, shown for differentiated cell line as $CD4^+$ T cells (Song et al., 2007) and activated B cells (Sabbattini et al., 2007), is only 2-3 times enlarged in the G2 phase as compare to the G1 phase. Consequently, in the model the G2 phase was imitated by the double increase of the phosphorylation rate, *kp*. Thus the systems with and without origins were simulated with *kp* equal to 0.01 min^{-1} and 0.02 min^{-1} for G1 and G2 phase correspondingly.

The appearance of bistable response in the system of 100 nucleosomes lacking the origins is better pronounced in the G1 phase characterized by low Aurora B phosphorylation activity (Fig. 3.5.6 B).

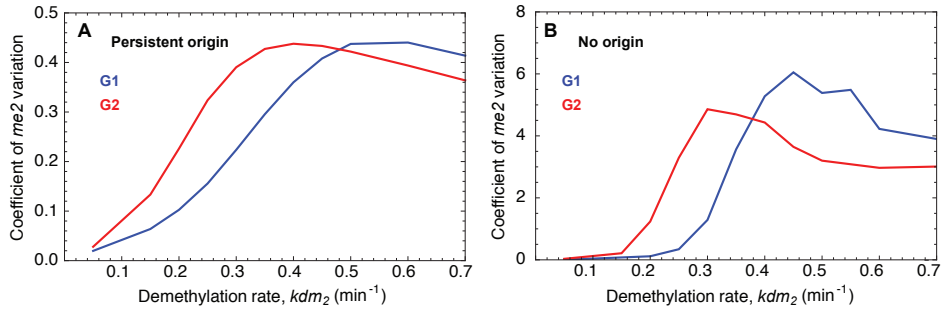

Figure 3.5.6 H3K9me2 variability change with the transition from the G1 to the G2 cell cycle phase. Coefficient of H3K9me2 variation (CV) with respect to the demethylation rate change for the fiber of 100 nucleosomes in G1 phase (blue) and G2 phase (red), with persistent origins (A) and without (B).

This property is reflected in the generally higher variability of the H3K9me2 response to the JMJD2 over-expression for G1 conditions in comparison to the less variable response in G2 phase (Fig. 3.5.6 B blue vs red). However, in the case of origin driven transition from on- to the off-silenced state with increase of the JMJD2 level, the variability does not differ so much between G1 and G2 phases (Fig. 3.5.6 A). Thus, the maximal coefficient of variability for G2 appearing for the lower doses of JMJD2 is relatively equal to the one in the G1 phase for higher doses of JMJD2 (Fig. 3.5.6 A).

In fact, for both scenarios, with and without persistent origin, the H3K9me2 in the G2 phase reached its maximum at two times lower demethylation rates than in G1. That implies higher responsiveness of the foci belonging to G2 phase rather than the G1 phase for low doses of JMJD2 over-expression. Consequently, realizing the PCH as a composition of the origin driven and non-driven isolated chromatin fragments, the G1 related foci of PCH would contribute more into the general foci-foci variability of H3K9me2 signal in the cell population for the high demethylation conditions.

3.6 Stability of the silencing in PCH

3.6.1 Stability of the silent state with the presence of bistability

Higher demethylation rate 0.25-0.3 min^{-1} triggers the on-off flipping of the silenced state signal (Fig 3.1.2 in red) resulting in the appearance of bistability. Under this condition, on-silenced state signal extracted from the complete time track is characterized by well time-correlated noise (Fig. 3.6.2 A, red) in comparison to the uncorrelated stochastic noise in the signal for the low demethylation activity range 0.1-0.2 min^{-1} (Fig. 3.6.2 A, blue and green). Thus noise became time-dependent and being a significant part of the signal is exerted a strong influence on the signal time evolution defining the next moment methylation degree. In this situation, the fluctuations become slower and in absolute terms stronger in amplitude (Fig. 3.6.1 A, red vs. blue) going further for the expected value of stationary methylation degree for on-silenced state, revealing the deterministic tendency to sense the off-silenced state. It signifies that intrinsic noise level in this case is strong enough to enhance the detectability of the weaker off steady state and reduce the stability of the strongest one. Consequently, over all dynamic of the lager time scales allows the flipping on-off behavior of the methyl signal.

Similar effect is reported for other nonlinear systems. The property of such systems whereby a random process optimally enhances the detection of the weak attractors was named stochastic resonance (Deville et al., 2006; Aihara et al., 2008). In other words, the fluctuations in a system under the strict conditions of the demethylation activity allow the stochastic resonance that fundamentally alters the global deterministic bifurcation picture.

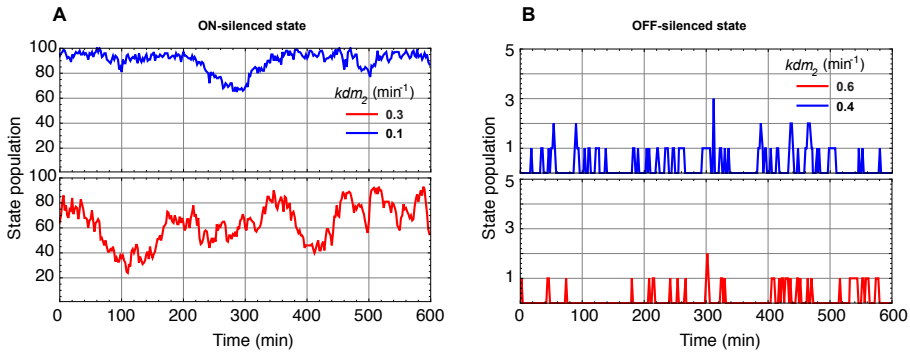

Figure 3.6.1 Continuous-time of the H3K9me2 signal without origin presence. On-silenced state (A) and Off-silenced state (B) time evolution in the steady state situation for the given demethylation rate values.

The difference between the on and off silenced state in terms of the autocorrelation (see Appendix A.3) properties is well-defined. The methylation degree signal for the off-silenced state tends to lose time-correlation with the increase of the demethylation rate (Fig. 3.6.2 B). While the on-silenced state shows better correlation to the higher demethylation activity as discussed above and reduces the correlation with a decrease in the demethylation rate.

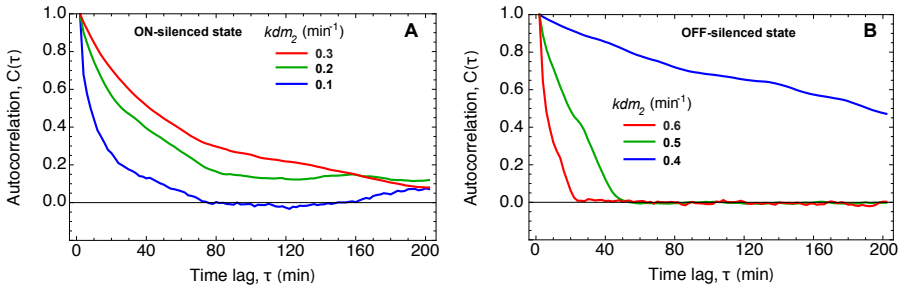

Figure 3.6.2: Autocorrelation of the H3K9me2 signal without origin presence. Autocorrelation of On-silenced state signal (A) and Off-silenced state signal (B) in the steady state for the given demethylation rate values.

Recent study of the epigenetic mechanisms of chromatin regulation in the mouse fibroblasts showed minor difference in methylation levels, H3K9me3, for euchromatin and heterochromatin (Müller-Ott et al., submitted; Fodor et al., 2006; Waterston et al., 2002). According to the experimental results the relative methylation degree were estimated as 43 ± 8 % and 28 ± 5 % for pericentric heterochromatin and euchromatin correspondingly (Müller-Ott et al., submitted). Thus, the proper spatial distinction between the globally silenced and transcriptionaly active regions within the nucleus based only on the static levels of the methylation degree seems unreliable.

Nevertheless, in general methylation level could be more informative with use of live-cell imaging techniques when the time change of the signal can be related to the silencing activity in the chosen spot.

3.6.2 Origin driven stabilization of the silent state

The persistent stimuli originating constant support of the methylation dramatically change the general response course as well as the property of the noise. As stated before the transition from the on- to the off-silenced state was performed in this system in monostable fashion with respect to the increase of the demethylation

activity. In addition this increase must be significantly higher to forces the transition of the fiber from the maximum on-silenced to the maximum off-silenced situation (Fig. 3.4.1, D-F).

The slightly lower autocorrelation of the continuous-time signal (Fig. 3.6.3) for on-silenced state conditions with the presence of the origins exposes the less significant dependency on the history of the signal. Consequently, randomness and stochasticity of the process are better pronounced in this case for the given conditions (Fig. 3.6.4 A).

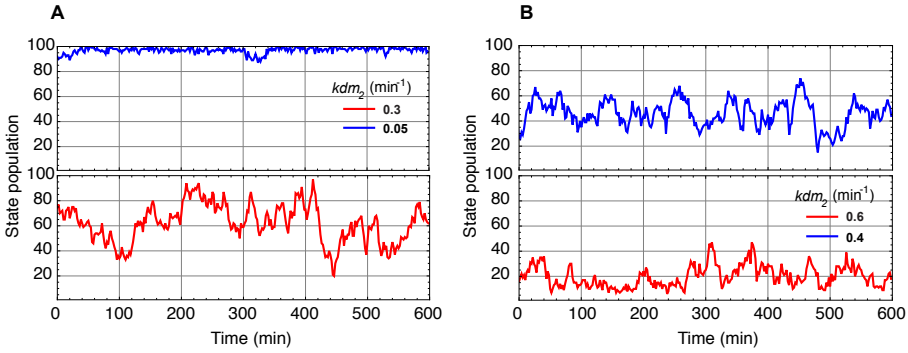

Figure 3.6.3 Continuous-time of the H3K9me2 signal with origin. On-silenced state (A) and Off-silenced state (B) time evolution in the steady state situation for the given demethylation rate values.

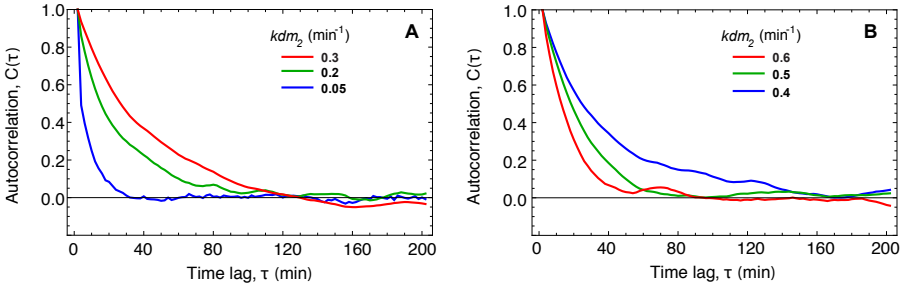

Figure 3.6.4 Autocorrelation of the H3K9me2 signal with origin. Autocorrelation of On-silenced state signal (A) and Off-silenced state signal (B) in the steady state for the given demethylation rate values.

The bistability is hidden by the origins. However, its signature is still reflected on the correlation properties of system outcome (Fig. 3.6.4). Strength of the autocorrelation rises with the enhancement of demethylation for off-silenced signal and decreases for the on-silenced signal as soon as the system crosses the parameter range that favor the bistable switch in the absences of the origins.

Chapter 4

Experimental Data Acquisition and Analysis of the PCH Epigenetic Network Response

The experimental approach for the quantification of H3K9me3 response on the doses of exogenous JMJD2 histone demethylase activity in the PCH foci is presented in the current chapter. The rescue responses of single cells to the increasing doses of JMJD2 are analyzed. The epigenetic variability of methylation degree in the single PCH foci is analyzed as a function of the JMJD2 dose-response course. Moreover, the influence of cell cycle progression on the response of PCH epigenetic network is studied. The qualitative stochastic model predictions for epigenetic mark propagation in PCH (presented in Chapter 3) are compared to the experimental results. The conclusions about the most relevant scenario of H3K9me3 propagation mechanism in PCH are made.

4.1 Acknowledgment

The wet lab experimental procedure of NIH 3T3 cells line transient transfection with Jmjd2c-GFP vector was done by Dr. Qin Zhang in collaboration with Dr. Katharina Müller-Ott from Research Group Genome Organization & Function in Heidelberg as well as the 2D immunofluorescence confocal imaging routine. The stable cell line with Tet-Off system driven Jmjd2b-GFP gene expression was established by Dr. Qin Zhang. The author together with Dr. Qin Zhang conducted confocal microscope setting adjustment and 3D tally scan imaging routine. The scenarios for image processing and quantification were developed and applied to 2D confocal images by the author. Furthermore, advanced 3D segmentation based on developed scenarios was done by Simone Eck, collaborative partner from Research Group Biomedical

Computer Vision in Heidelberg. The author of this thesis carried out the statistical data analysis for 2D and 3D resolution experiments. The fluorescence microscopy work was conducted in the DKFZ Microscopy Core Facility, and Nikon Imaging Center at the University of Heidelberg. The study in its entirety was supported by the EpiSys project within the BMBF SysTec program.

4.2 Experimental evidence for the hidden bistability in the MEF

The idea about indiscriminate activity of histone demethylase JMJD2 towards chromatin has come into view through the experiments of Jeong et al. who published their results in 2011 (Jeong et al., 2011). Authors reported about the extent of H3K9me3 demethylation in the NIH 3T3 cells with the transient expression of JMJD2A-GFP. For instance, no differing effects were detected for low and high GFP levels in the individual cells. In addition, over all transfected cell populations, the groups of cells with different phenotypes that correspond to different H3K9me3 dilution in PCH foci can be distinguished. Three groups were characterized as severe, moderate and weak efficiency of demethylation response All three groups are observed from the lowest to the highest GFP level exploring the full range of JMJD2A overexpression. Therefore, the author of the present dissertation made the suggestion that this type of experiment was the easiest way for quantifying the variable response in the PCH foci at the single cell level. This gives a measure of heterogeneity in the system that can help to verify the presence of bistability. Consequently, the experiment with the Jmjd2c-GFP transient transfection of NIH 3T3 cell was done and combined with a following quantification procedure. Moreover, the supervisor of the present dissertation expanded the idea. The quantification of this variability in a JMJD2 dosage dependent manner and in connection to varying dosage directions was proposed. Therefore, the experiment with the monoclonal cells populations with the stable incorporation of the Tet-off Jmjd2c-GFP vector was performed.

4.3 The experimental and quantification procedure of H3K9me3 response reconstitution

4.3.1 Imaging procedure in 2D

The images were obtained by confocal laser scanning microscopy using fluorescence-tagged antibodies. For confocal imaging, a Leica TCS SP5 microscope equipped with a HCX PL APO lambda blue 63x/1.4 NA oil immersion objective was used. Jmjd2c-GFP transfected cell culture were fixed and immunostained with primary anti-H3K9me3 and subsequent visualization was done with a secondary goat anti-rabbit/mouse Alexa 568 antibody (Invitrogen, Molecular Probes). Finally, the cells were mounted with ProLong Gold (Invitrogen) containing 4',6-diamidino-2'-phenylindole (DAPI) for the staining of chromatin/DNA.

For each GFP, DAPI and Alexa 568 signals in the separate channels, only one middle plane optical section was scanned. As a result, three 512×512 pixels, 8 bits, gray scale images (zoom factor one in TIFF format without compression) were obtained. These experimental data were used to extract quantitative information on H3K9me3 enrichment in the PCH foci for each nucleus that showed a detectable level of Jmjd2c-GFP construct expression.

4.3.2 Image segmentation and quantification in 3D

2D confocal images of JMJD2C overexpressing cells and WT control cells were segmented using a binary - nuclear and PCH foci masks to consequently yield the per-nucleus expression of Jmjd2c-GFP and H3K9me3 enrichment in PCH foci.
The present data acquisition procedure can be subdivided into three major steps, which consist of (1) determination of the nuclear boundaries, (2) determination of the PCH foci boundaries and (3) extraction of quantitative information. At each of these steps different image-processing operations are applied, e.g. median filtering, histogram equalization, thresholding, watershed transformation.

To extract quantitative information on the Jmjd2c-GFP expression level from each nucleus, a nuclear mask is generated. The nuclear mask workflow (Fig 4.2.1) is constructed to find the area occupied by the nuclei in the image precisely.

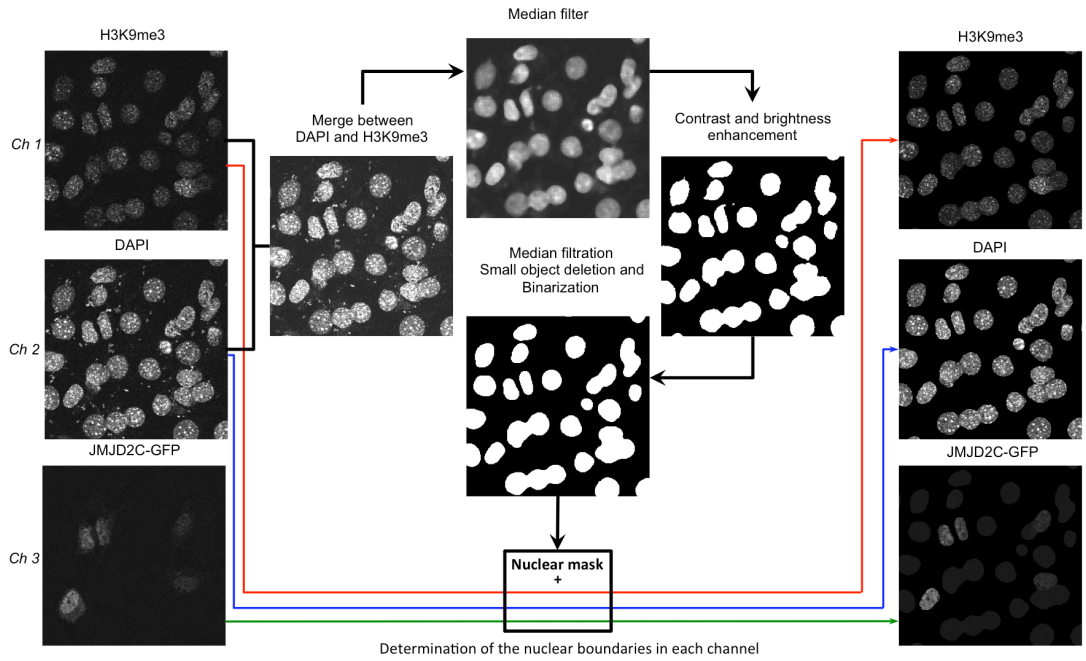

Figure 4.2.1 Nuclear mask pipeline for transiently transfected with Jmjd2c-GFP NIH 3T3 fibroblast cells.

For this purpose only the raw images of DAPI and H3K9me3 signals are used. Each pixel representing the intensity values of the DAPI image are added to the H3K9me3 image to maximize the signal of the nuclear compartment in context with present experiment staining. After the median filter processing, the histogram of this resulting image was equalized. Next, median filter with the same structural elements was applied. To smoothen the border of the mask and remove small elements, the author applied morphological opening procedure that was followed by binarization operation. The final binary image represents the mask in which nuclei area is marked by the foreground pixels. The nuclear mask application to the channel images resulted in the exclusion of the signals originated from cytoplasm and in out cellular space. After all, the thresholding of the GFP channel normalized for the nuclear mask allowed to distinguish between the classes of nuclei with auto fluorescence, that were seen in the same channel, and the class of Jmjd2c-GFP construct expressing nuclei. In the subsequent steps, only a second class of nuclei will be used for data extraction. As a result, the correspondent JMJD2 nuclear mask is generated and applied to each channel image (Fig 4.2.2).

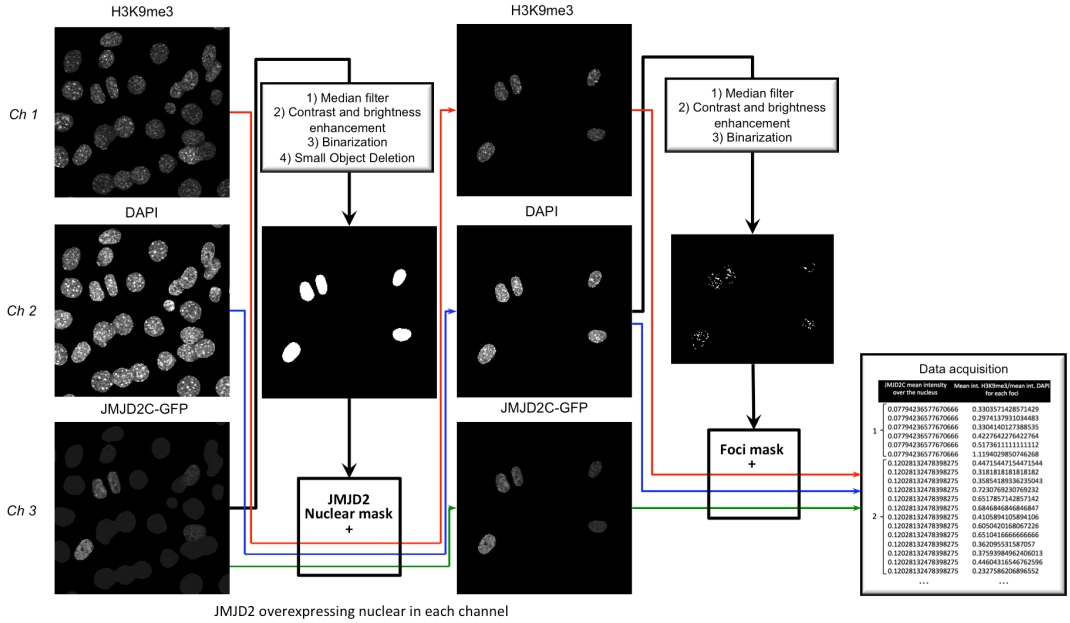

Figure 4.2.2 PCH foci mask pipeline for transiently transfected with Jmjd2c-GFP NIH 3T3 fibroblast cells and data extraction.

The PCH foci mask is constructed by smoothing the nuclear DAPI image with contrast and brightness adjustment and median filtering followed by binarization operation. According to this mask, the pixels belonging to the individual PCH foci within the nucleus are defined. The mean intensity signal over the pixels within each focus was recoded for the DAPI and H3K9me3 channels and theirs ratios were calculated. This ratio characterized the H3K9me3 enrichment in foci of PCH for each nucleus that showed a detectable level of Jmjd2c-GFP expression. The Jmjd2c-GFP and correspondent foci H3K9me3 enrichments were recorded into the text file (Fig 4.2.2).

All image segmentation and quantification pipelines were implemented with `Mathematica 9.0` package (Wolfram Research, Inc.. 2013) using the Image Processing Toolbox (available upon request).

4.3.3 Experiment with controlled doses of JMJD2B overexpression

In the experiment of JMJD2B dose response in 3D resolution, the MEF cells were transfected with Tet-off driven 1-424 Jmjd2b-GFP truncated construct. This N-terminal half of JMJD2B was found to be fully functional, since it is sufficient for abrogating chromosomal H3K9me3 *in vivo* and this fragment becomes enriched at PCH in a Suv39h-dependent manner in spite of the absence of PHD Zn-finger and

Tudor domains (Fodor et al., 2006). The clone with stable GFP expression was selected and used for the monoclonal cell culture establishment. During the experiment, five conditional samples were generated from one monoclonal population. Two of them represent the static H3K9me3 response for the stepwise increase of Jmjd2b-GFP overexpression from the ectopic JMJD2B expression level. Three others represent backward dose response on suppression of Jmjd2b-GFP expression from the maximal level of Jmjd2b-GFP overexpression. Therefore, first two samples are treated for at least 32 hours with 3 µg/ml and 0.4 ng/ml of doxycycline (DOX), demonstrating ectopic and overexpressed JMJD2B level respectively. Three others samples were resting initially for 32 hours without DOX archiving at the maximal Jmjd2b-GFP overexpression level. For two of them the additional expression of exogenous JMJD2B protein was inhibited to different levels by adding 0.4 ng/ml of DOX to one sample and 3µg/ml of DOX to the other. Resulting Jmjd2b-GFP overexpression was lowered up to different steady state levels in correspondence with the given DOX doses.

4.3.4 Imaging procedure in 3D

Five monoclonal samples were fixed and immunostained according to the protocol used in the previous experiment with transient transfection. For confocal imaging, a Leica TCS SP5 microscope equipped with a HCX PL APO lambda blue 63x/1.4 NA oil immersion objective was used. Immunofluorescence signals were collected for DAPI, H3K9me3 and GFP in 3D with 2.5 zooming factor. Multi-channel scanning was performed in 41 z-stacks with 0.25 µm axial resolution. Resulting 16 bits z-stacks images with the lateral resolution 512×512 pixels were conducted from 500 different positions for each sample in each channel by use of the Scan Field function of Leica software. One unified scanning parameter set (laser intensities, gain, offset) was used for all the samples. This optimal parameter set was adjusted to all samples simultaneously allowing direct comparison of extracted quantities among the five experimental conditions.

4.3.5 Image segmentation and quantification in 3D

Advanced 3D segmentation method (Eck et al., 2012) was adapted for the quantitative data acquisition based on the 2D segmentation procedure discussed above. Consequently, the individual foci H3K9me3 and DAPI signal were quantified

together with JMJD2B overexpression level and total DAPI signal per individual nuclei. Total 3D DAPI signal, meaning the total DNA content of the particular nuclei permitted a threshold-based discrimination between G1 and G2 cell phase nuclei.

4.4 Results

4.4.1 H3K9me3 enrichment as a function of JMJD2 activity

The heterogeneous course of H3K9me3 reduction in PCH foci is revealed under the both B and C isoforms of JMJD2 histone demethylase overexpression (Fig 4.4.1 and Fig 4.4.2). The large variability in the degree of methylation among individual PCH foci was found for JMJD2C and JMJD2B overexpressing nuclei. The maximal variability range was detected for the nuclei with lowest JMJD2 overexpression level (Fig. 4.4.1 D). Selecting the group of nuclei with high, intermediate and low JMJD2C overexpression, the correspondent PDF distributions were generated (Fig. 4.4.1 A-B). For all of these three groups, no well-distinguishable metastable response was discovered. However, the shift of the distribution peaked in response to the increasing demethylation activity, characterized by a large deviation around the mean value of H3K9me3 signal (Fig 4.4.1 C). The low JMJD2C overexpressing group of nuclei had the highest variability range of methylation in the PCH foci (Fig 4.4.1 C in blue) as compare to the wild-type (WT) group (Fig 4.4.1 C in red), endogenous expression, and groups with the intermediate and high levels (Fig 4.4.1 C in green and magenta).

Furthermore, the results of experiment with the Tet-off system, that allowed the controlled varying of demethylation activity levels, sheds the light on the details of the H3K9me3 stability in PCH.

First of all, in spite of the large divergence of GFP signals among nuclei of each conditional sample, high JMJD2B overexpressing samples (Fig. 4.4.2 B,D-E) separately revealed the negative correlation between increasing demethylation level and H3K9me3 foci enrichment. Thus, the Spearman rank correlation coefficient (r_s) for two samples with the intermediate JMJD2B level (Fig. 4.4.2 F in blue and dark red) was equal to -0.33 while the correlation for the low overexpressing samples (Fig. 4.4.2 F in black and green) was not present. The sample with the highest demethylation activity was lowering the influence of the JMJD2B dosage, showing a lower negative correlation coefficient equal to -0.12.

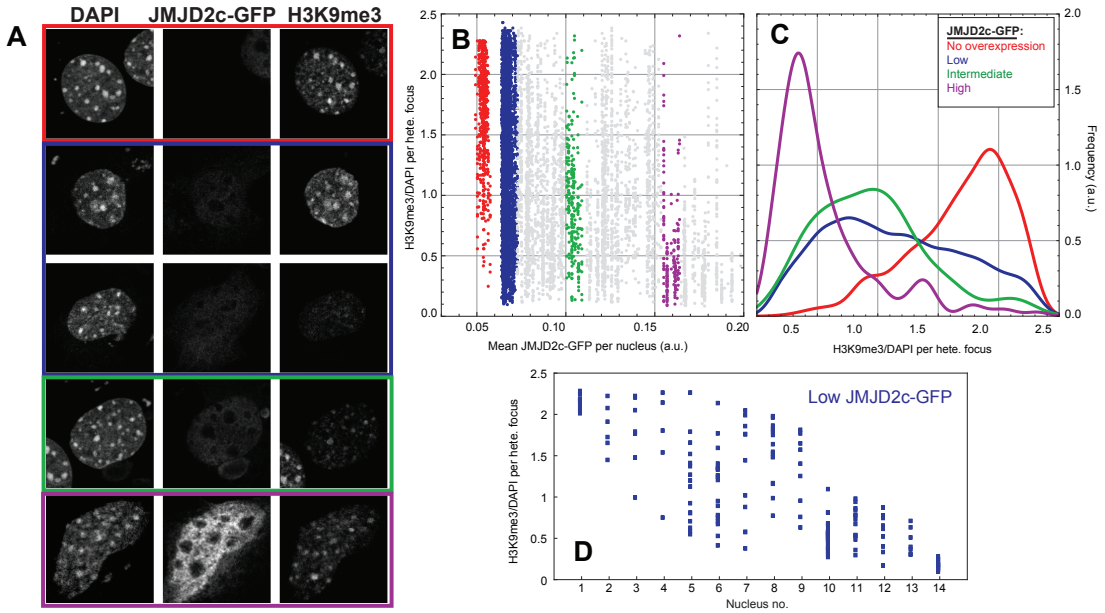

Figure 4.4.1 Transient transfection of NIH 3T3 fibroblast cells with Jmjd2c-GFP. (A) Three channels nuclei images correspondent to the DAPI, GFP and H3K9me3 enrichment (in columns) for the varying transient expression of GFP (in rows) from the low (on the top) to the maximal (on the bottom). (B) Quantified H3K9me3 per PCH foci enrichment as the function of the GFP expression level. (C) Frequency distribution of the foci H3K9me3 enrichment in the groups of non-, low, intermediate and high GFP expression. (D) An example of 14 nuclei in the low GFP expressing range that appear in the heterogeneous response of H3K9me3 enrichment among the individual PCH foci.

Second, the presence of significant noise in the H3K9me3 response of PCH foci to additional doses of demethylase clarified the persistent variability predicted by the model. However, not only the doses of the JMJD2 itself influence the variability range, but also the direction of dose reconstitution. Thus, the suppression of Jmjd2b-GFP expression from its maximum (-DOX+0.4ngDOX) and, on the other hand, induction of Jmjd2b-GFP expression from the minimal level (+0.4ngDOX) both of which resulted in the same steady state exogenous level of demethylase led to different levels of variability in H3K9me3 response (Fig. 4.4.2 F in blue and dark red, respectively). These two distributions agreed on the relatively equal median level, nevertheless, the interquartile range of methylation degree of the induced overexpression is one and a half fold higher than in the situation of Jmjd2b-GFP suppression.

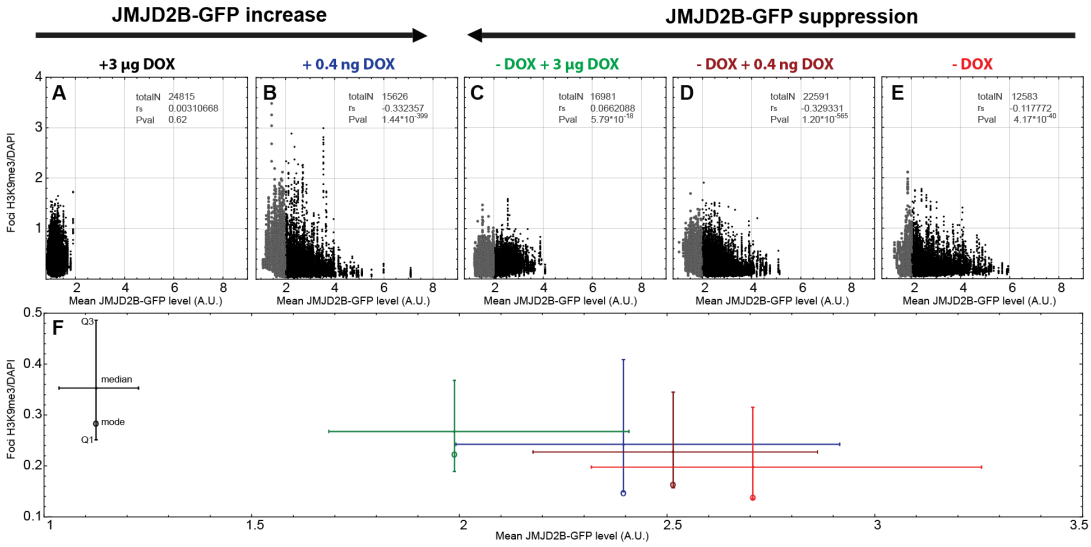

Figure 4.4.2 Tet-off Jmjd2B-GFP monoclonal stable NIH 3T3 cell. (A-E) Five DOX conditional samples represented the induction of GFP expression (B) from the endogenous demethylation level (A) and suppression of the GFP expression (C-D) from the maximal exogenous demethylation level (E). Quantified H3K9me3 per PCH foci enrichment as the function of the GFP expression level for each sample is shown. (F) Statistics on the distribution of H3K9me3 enrichment per PCH foci and the GFP expression for each sample are shown in the correspondent color. The line crosses represent the coordinate of the distribution mean, the error bars are the interquartile ranges and the modes of the foci H3K9me3 enrichment distribution are depicted by the dots.

Moreover, to compare the course of responses in Jmjd2b-GFP suppression and induction experiment, correspondent samples were grouped together. Finally, data were discretized by 5 equally sized bins of Jmjd2b-GFP expression levels using the equal width interval discretization method in each group. Accordingly, the mean H3K9me3 enrichment over all PCH foci within a particular bin and corresponding CV were collected (Fig. 4.4.3). The much-enlarged variability was assigned for increasing demethylation course. For this course of the intermediate JMJD2B overexpression level, the maximal CV value goes two fold higher than in the backward course at the correspondent JMJD2B level. However, for the maximal and minimal JMJD2B overexpression levels in both groups, CV does not vary - appearing at the same low variability levels indicating determined response without siqnificant perturbations. In terms of mean PCH foci, H3K9me3 signal suppression and increased JMJD2B courses are different. Thus, decrease of the demethylation activity from the maximal JMJD2 overexpression case statistically does not reconstitute high enough H3K9me3 as seen in the lowest JMJD2B-GFP bin of the backward course, although increasing demethylation activity originating from the minimal JMJD2B overexpressing case resulted in a significant reduction of the

H3K9me3 enrichment. As such, the level of H3K9me3 drops by three fold (Fig. 4.4.3).

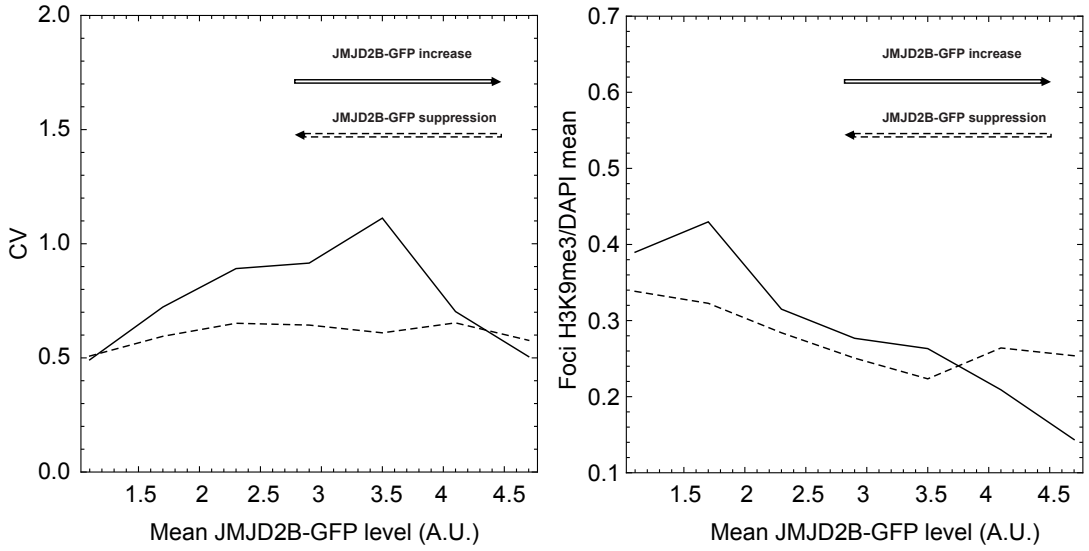

Figure 4.4.3 Directional Jmjd2B-GFP dose alteration. Jmjd2b-GFP suppression (dashed line) and induction (solid line) samples grouped and discretized by 5 equally sized bins of Jmjd2b-GFP expression level using the equal width interval discretization method. The coefficient of variation (CV) and the mean per PCH foci H3K9me3 enrichment for each group in the correspondent bin are shown on the left and right hand side correspondingly.

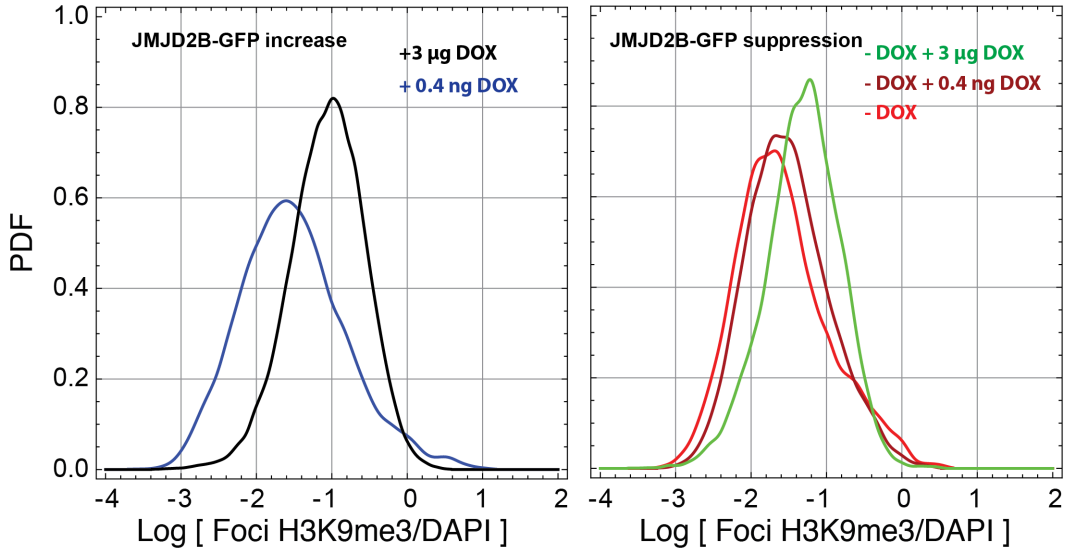

Figure 4.4.4 Jmjd2b-GFP suppression and induction H3K9me3 course response. The induction of GFP expression leading to the reduction of methylation degree is reflected in the shift of PDF distribution from right (black) to the left (blue). The suppression of GFP expression from its maximal level leading to the step wise increase of methylation degree (from red to green).

Consequently, the erasing and recovering of H3K9me3 in PCH foci controlled by JMJD2B (Fig 4.4.4) happened in two different non-overlapping ways, implying the absence of a monostable response.

4.4.2 Cell cycle control of the H3K9me3 propagation

Analysis of mathematical model predictions has confirmed the important influence of Aurora B kinase on the H3K9me3 propagation property as a function of the cell cycle progression. The prediction mainly reflects the global decrease of H3K9me3 enrichment in PCH foci that is an impact of high level kinetic activity in the G2 cell phase. The variability responses for the demethylation activity as a function of JMJD2 expression in G1 and G2 cell phases were characterized for two different scenarios of H3K9me3 propagation - the spontaneous and the origin driven one. Therefore, the 3D experiment allowing the proper distinction between G1 and G2 phase nuclei helps to decide which of these two scenarios is most probable in the definition of mechanisms of H3K9me3 propagation. To this aim, the nuclei in each conditional sample were divided into two groups according to sum of signals collected over the whole nuclear space. These two fractions of the nuclei represent the low and high DNA content that specify the G1 and G2 phases nuclei respectively (Fig 4.4.5).

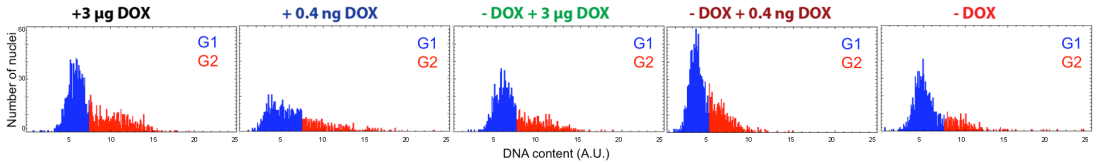

Figure 4.4.5 G1 and G2 cell cycle phases distinction. The nuclei split into G1 and G2 phases based on the total DAPI signal collected over the entire nuclear space representing the total DNA content for each conditional sample.

In the next step, the PDF distributions of per PCH foci H3K9me3 enrichment in G1 and G2 groups were compared for each of the DOX conditions carried out in the experiment. The split of these two fractions was discovered for the low (Fig 4.4.6 A,C) and intermediate (Fig 4.4.6 B) Jmjd2b-GFP overexpressing conditions. However, G1 and G2 phases certainly do not differ in terms of the H3K9me3 signature in PCH for the higher demethylation activity levels represented by two samples with the initially enlarged Jmjd2b-GFP overexpression level (Fig 4.4.6 D, E).

Obviously, the explanation for this is that maximal reduction of the H3K9me3 at the extremely high levels of demethylation function does not allow the actual methylation variation with the course of cell cycle progression.

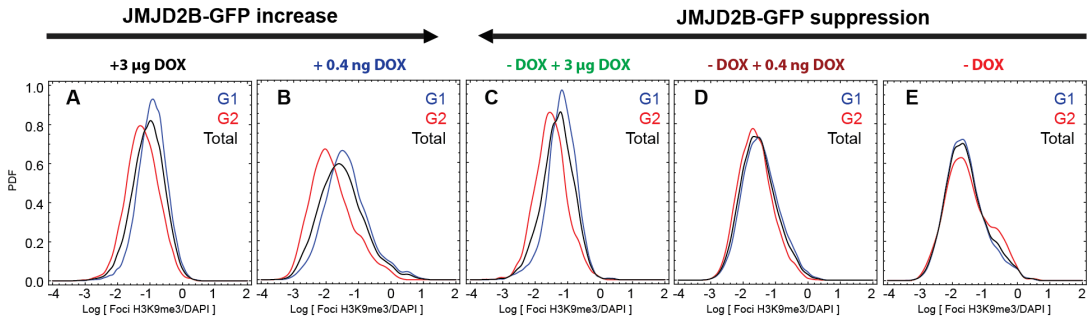

Figure 4.4.6 H3K9me3 enrichment as the function of the cell cycle progression. PDF distributions of the PCH foci H3K9me3 enrichment are compared in G1 and G2 cell phases for each conditional sample.

Furthermore, for comparison of the G1 and G2 H3K9me3 PCH enrichment in response to the dosage of JMJD2B overexpression, the conditional samples were groped together for G1 and G2 nuclei fractions separately. Two resulting data sets were discretized by 5 equally sized bins of Jmjd2b-GFP expression levels using the equal width interval discretization method. The mean and standard deviation were inspected within each bin (Fig 4.4.7 A) as well as the correspondent CV value (Fig 4.4.7 B).

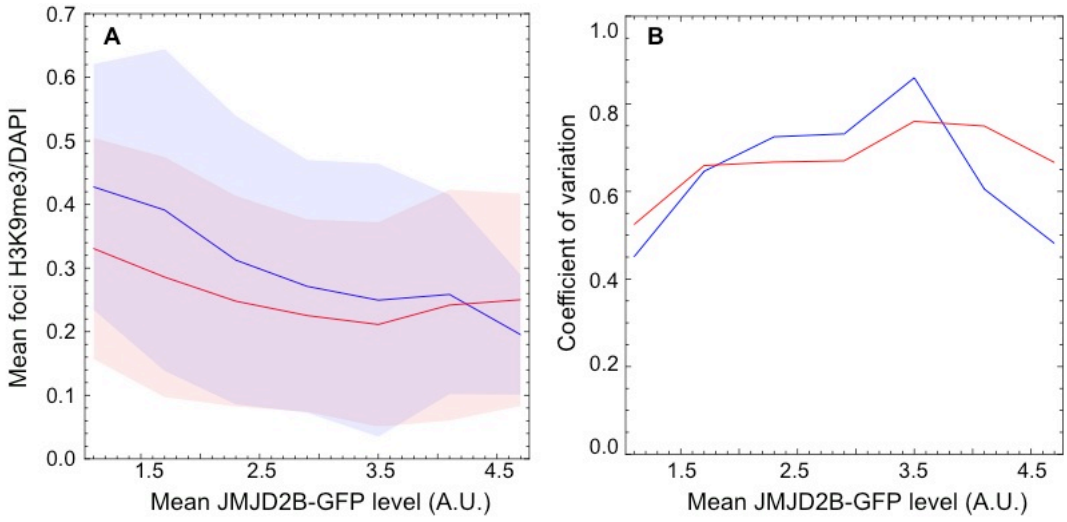

Figure 4.4.7 Response of methylation signal in PCH and its variability on the JMJD2 overexpression doses. Samples grouped together in accordance to the cell cycle phase and discretized by 5 equally sized bins of Jmjd2b-GFP expression level using the equal width interval discretization method. (A) Mean of methylation degree as the function of GFP expression shown in the solid lines for the G1 (in blue) and G2 (in red) cell phases. The

standard deviation is depicted in light blue and light red for the G1 and the G2 respectively. (B) Coefficient of variation as the function of the GFP expression for each bin in the G1 and G2 phase separately and depicted in blue and red correspondently.

As expected, the mean PCH methylation signal in the G1 fraction of the nuclei was dominating the signal response in G2 cell phase till the maximally possible Jmjd2b-GFP overexpression level was reached where the levels are equal. In addition to it, G1 fraction showed higher standard deviation that resulted in higher PCH H3K9me3 variability degree (Fig 4.4.7 B) in the middle range of Jmjd2b-GFP overexpression. Nevertheless, the variability range does not go beyond one for all conditions in both the groups that were considered as being low-variance. Therefore, the experimental results were rather comparable to the origin-driven modeling response prediction that allows a small fluctuation in the intermediate extra demethylation activity range without showing high steepness in transition course.

Chapter 5

Discussion

The robust mechanism of maintaining epigeneticaly silenced state in PCH is particularly important for the control of chromosomal stability and prevention of perturbed chromosome interactions, breakages and missegregation (Pagani et al., 2001). This thesis investigates the properties of PCH epigenetic system by a multidisciplinary approach, starting from mathematical modeling in the deterministic terms continuing with the stochastic system simulations and ending up with experimental proof of the theoretical predictions based on the data analysis of single cell resolution measurements.

A molecular system of silencing propagation in PCH epigenetic network is constructed and translated into a mathematical model. The network represented by the set of the initially essential posttranslational modifications of histone H3 is found to be crucial in maintenance of PCH integrity and its phenomenological functionality. The interplay between the silencing modification, H3K9 methylation, and opposite modifications of transcriptional activity, H3K9 and H3K14 acetylation, assumes the synergistic and antagonistic feedback loops. The loops are explained by the progressive recruitment of modification associated enzymes that bind to the correspondent modified histone tail propagating the same modification for the nucleosome in close proximity to the place of recruitment. Thus, the contribution of chromatin associated components like the HP1 protein, Suv39h methyltransferase and the GCN5 acetyltransferase are considered. The binding of all these enzymes is very rapid events in comparison to the spontaneous chemical transitions in between the histone modifications. Therefore, reduction of dimensionality is

introduced by quasi steady state approximation for all recruitment processes in the system. Nevertheless, the system of the nucleosomal ensemble where the epigenetic state crosstalk of each nucleosome is interconnected with the state of others by nonlinear feedback loops can give rise to rich bifurcation behavior leading to metastable switches.

5.1 Deterministic bistability of silencing in the PCH and its function

Indeed, the bistable switch between H3 methyl-enriched and H3 low-methyl chromatin fragment represented by the linear assembly of 10, 30, 60 and 100 nucleosomes are found by us in the deterministically defined system. The presence and simultaneous stability of two controversial heterochromatic states, off- and on-silenced, are assumed within the fixed conditional parameter space representing the demethylation activity term. Therefore, the bistable response can be interpreted as the function of H3K9 specific histone demethylase JMJD2, the hyper activity of which results in the long-term inheritance of PCH epigenetic state and, on the other hand, a limited range of overexpression can generate the hyper sensitive epigenetic switch.

A few original theoretical studies of the inheritance of the epigenetic state claim that the bistability is the most efficient and most reasonable explanation for the long term memory effect in the epigenetic systems (Dodd et al, 2007; Sedighi et al, 2007). However the nonlocal character of the interaction between the nucleosomes within the chromatin fiber was considered to be essential for the bistable type of response.

On the contrary, the mathematical model presented here determines the bistable response for the system with almost local nucleosomal interaction capacity requiring only nonlinearity in the binding of the HP1-Suv39h complex that feedbacks into the methyl mark propagation.

The hysteresis of system response is utilized by the network as the memory element giving rise to initial condition dependent dynamics. As a result, the spatial methyl mark propagation pattern strictly depends on the initial epigenetic conformation of the chromatin fragment within the bistable parameter space.

The presence of persistent origins of H3 dimethyl mark propagation for the chromatin fragments in PCH was suggested. The origins, certainly, can rescue the

stable silencing conformation of PCH and its reestablishment for the next cell generations after mitosis as well as after the perturbations guided by the cell cycle progression. The modes of silencing propagation from the local origins are varied in accordance with the different regimes facilitated by the bistability for the system. Thus, three scenarios are possible within the bistable regime driven by the JMJD2 activity level. First is the locally limited propagation of the H3K9me2 mark around the introduced origin and the second is unlimited spread of H3K9me2 modification over the entire chromatin fragment. The propagation in the second scenario assuming short-range nucleosomal connectivity can be terminated upon meeting the genomic boundary elements. The transition between these scenarios for varying demethylation level is sudden in correspondence to the bistable switch.

However, the stochastic dynamics would play a leading role here as the random transient silencing appearance over chromatin fragment may give quick support to the main propagation course that is going out of the persistent origin. Therefore, besides the stability analysis of deterministic solutions presented further, the aspects of origin driven H3K9me2 propagation also addressed in the equivalent stochastic model.

5.2 Stochastic effects in the PCH epigenetic network

A number of experimental and theoretical studies have shown that the epigenetic silencing mechanisms can be ultrasensitive and are caused by strong stochastic effects either due to the presence of positive feedback loops in nucleosome modification (Dodd et al, 2008), long-range nucleosomal interactions (Dodd et al, 2007), the cooperativity in recruitment of histone modifiers (Sengupta et al, 2008) or simply due to low concentration.

Indeed, it is a known fact that the concentration of histone modifiers in the cell is relatively low in comparison to the concentration of nucleosomes in PCH. For instance, the measurement of absolute endogenous protein concentrations in PCH of the MEF cells revealed dramatically low, 3.0 ± 1.7 μM, concentration of histone methyltransferase Suv39h1 in comparison to 234 ± 4 μM concentration of the nucleosomes (Müller-Ott et al., submitted). Consequently, even small fluctuations in the molecular number of epigenetic modifiers can significantly impact the general dynamic of the system. Therefore, stochastic simulations were performed to investigate whether intrinsic noise can have an additional effect on the silencing and

activation of the epigenetic system within the bistable regime and how it would change the system dynamics for different nucleosomal numbers and different cell phases with and without persistent silencing origins. Furthermore, an appropriate estimate for the cell-to-cell and foci-foci natural variability in the system is established.

Considering the contribution of the stochastic effects, bistability in the PCH epigenetic system becomes more fragile to the extrinsic fluctuations of the demethylation activity, responding with respect to its own intrinsic fluctuations giving rise to ultrasensitivity.

Due to the intrinsic noise, the stable system observed for a long period of time in this ultrasensitive regime is subjected to the rare event of spontaneous change in chromatin status. Thus, the silencing histone marker H3K9me2 enriched over the whole chromatin fragment within the PCH can be spontaneously removed and suddenly re-established without stimuli. However, the duration of each of the two opposite states on a long term scale is a function of the demethylation activity. There is an exponential decay in the lifetime for on-silenced state and in growth for the off-silenced state with respect to increasing doses of the JMJD2 overexpression. Stabilization of the opposing states duration i.e. the equality of their lifetimes are defined by the strongest bistable condition in the response. For this case, the model of 100 nucleosomal fragment has predicted the duration of each state for at least 65 hours, equivalent to the inheritance for approximately 3 cell cycles in the mouse embryonic fibroblasts cell line (MEF).

The maximal frequency of switching within the bistable response was estimated by rate of 1.15×10^{-2} times per hour. This rate is much higher in comparison to the experimentally observed on-off silencing transition in the *S. pombe* (Grewal et al., 1998) that happened in average 2.5×10^{-4} times per hour.

Remarkably, a perturbing level of JMJD2 is an efficient way of shifting the balance between monomethylated/acetylated, off-silenced, state and the repressive dimethylated, on-silenced, state. For the stochastic system, the bistability is possible only for the strict range of the demethylation rate values. This range, certainly is much shorter than the range predicted with equivalent deterministic system formalization.

Moreover, it has revealed a strong dependency on the number of nucleosomes that comprise individual PCH fragments. Thus, the flux of JMJD2 overexpression level for the bistable response in a system of lager size must be

higher than that for the smaller size system. Of course, the interpretation of the system size i.e. the nucleosomal number for independent chromatin fragments in the model is strictly related to the distribution and enrichment of the genomic boundary elements in PCH that effect the local independency and isolation of the chromatin regions. However, there is not much concrete information available from experiments in mammalian PCH about these elements. Nevertheless, their existence and function are discussed for the euchromatic genomic regions. The first boundary elements organized by identical inverted repeats on DNA have been suggested to mark the borders between adjacent chromatin domains and to act as a barrier against the effects of enhancer and silencer elements from neighbouring regions (Noma et al., 2001). The second, more recently discovered insulator protein CTCF binding sites have emerged as candidates to define the boundary elements punctuating the genome to form higher-order chromatin domains (Shaw et al., 2010; Phillips et al., 2009; Labrador et al., 2002).

There is certain evidence available about the regular content of PCH in mammalian genome. PCH of individual chromosomes has more regular DNA sequence content compared to the rest of the genome. It is represented by the repetitive cassette of the AT-rich major satellites, MaSat, that are enriched in PCH and represent 76% of the all tandem repeats in mouse whole genome assembly (Komissarov et al., 2011; Guenatri et al, 2004). Consequently, model assumption about the homogenous distribution of the boundaries and approximation of the single chromosomal PCH focus by the set of unified and independent chromatin fragments sounds reasonable.

Under this assumption, the degree of variability for H3K9me2 enrichment in PCH is estimated by the variability of the individual chromatin fragment appearing for long simulation times. The degree of variability is estimated by the signal-to-noise ratio and is referred to the coefficient of variation (CV). If CV is higher than one, it signifies high dispersion of the H3K9me2 signal indicating presence of the bistable response.

The changing CV profile with respect to the JMJD2 overexpression level depends on the number of nucleosomes. In accordance with the bistable parameter ranges, the magnification of CV in a system of smaller size requires lower demethylation activity and, contrariwise, large fluxes are required for higher number of nucleosomal fragments.

However, persistent origins of silencing abolish this heterogeneity in the response thereby hiding bistability. Consequently, the variability of H3K9me3 enrichment for fragments of different sizes is lowered due to the homogeneity ranges being less than one. However, on the contrary to the origin lacking case, the response of the lager size system now is more dispersed in terms of H3K9me2 enrichment.

5.3 Variability control in the cell cycle progression

Modeling simulations imitating G2 cell cycle phase by doubling the increase of Aurora B kinetic activity exhibited significant lowering of H3K9me2 heterogeneity in response to the JMJD2 function. However, this effect is observed only for the system lacking the H3K9me2 origins. Thus, the presence of the persistent origins of silencing does not change H3K9me2 dispersion within the G1-G2 phase transition in the single PCH. Nevertheless, for both scenarios, the JMJD2 dependent on-off silencing switching conditions are different for the G1 and G2 phases. As for the origin driven H3K9me3 propagation and unstimulated H3K9me2 establishment, on-off transition in G2 phase happens at lower levels of demethylation activity.

The reason for the different qualitative behavior of H3K9me2 variability is the process of HP1 eviction, which in turn is triggered by the phosphorylation of H3S10 in G2 phase. Without persistent origins that continually support the H3K9me2 and therefore the HP1-Suv39h complex binding, the balance in the system can be much more easily perturbed by variation in kinase levels.

However, experimentally the eviction of HP1 protein from the PCH foci was observed in G2 phase without significant reduction of the H3K9me2. Such an effect is predicted in the simulation experiment for the low doses of Aurora B kinase with the origin driven H3K9me2 propagation program.

Moreover, this program was found to be more effective in the reconstitution of the silencing mark right after replication. In this case, H3K9me2 enrichment was less susceptible to incorporation of the new nucleosomes that are lacking the repressive H3 histone modifications and have high acetylation content that enables relaxed conformation of the histone tail needed for the nucleosome integration into the newly synthesized DNA.

5.4 Experimental test of H3K9me2 response in single PCH

Qualitative comparison of the model predictions with the results of single PCH foci measurement experiment helped to dissect the features of H3K9me2 establishment in the frame of the epigenetic PCH network function in mammals.

First of all, modeling prediction qualitatively agree with experimental observations on the H3K9me2 propagation in PCH foci through cell cycle. Thus, the slight reduction observed for H3K9me2 enrichment in G2 phase relative to the G1 phase is caused by HP1 eviction as a consequence of increased phosphorylation status.

Secondly, variability in H3K9me2 signal is present in the system and can be significant at the single cell level. Nevertheless, this variability cannot be translated into clear hysteresis response that characterizes bistability. Moreover, this variability is slightly higher in G1 phase than in G2. However, both are less than one in terms of CV for all JMJD2 overexpression levels. This observation signifies the influence of origin-driven scenario on H3K9me2 propagational property and its privilege for PCH fragments rather than origin-independent process. Consequently the bistable response can be hidden by the origins as predicted by the model, only showing the relatively high fluctuations in PCH foci H3K9me2 enrichment level.

Bibliography

Allis CD, Jenuwein T, Reinberg D. 2007. Epigenetics. *Cold Spring Harbor Laboratory Press*, *New York*.

Angel A, Song J, Dean C, Howard M. A Polycomb-based switch underlying quantitativeepigenetic memory. *Nature*. 2011 Jul 24;476(7358):105-8.

Bannister AJ, Kouzarides T. Reversing histone methylation. *Nature*. 2005 Aug 25;436(7054):1103-6.

Barski A, Cuddapah S, Cui K, Roh TY, Schones DE, Wang Z, Wei G, Chepelev I, Zhao K. High-resolution profiling of histone methylations in the human genome. *Cell*. 2007 May 18;129(4):823-37.

Baubec T, Ivánek R, Lienert F, Schübeler D. Methylation-dependent and -independent genomic targeting principles of the MBD protein family. *Cell*. 2013 Apr 11;153(2):480-92.

Becker NB, Rosa A, Everaers R. The radial distribution function of worm-like chains. *Eur Phys J E Soft Matter*. 2010 May;32(1):53-69.

Bender S, Tang Y, Lindroth AM, Hovestadt V, Jones DT, Kool M, Zapatka M, Northcott PA, Sturm D, Wang W, Radlwimmer B, Højfeldt JW, Truffaux N, Castel D, Schubert S, Ryzhova M, Seker-Cin H, Gronych J, Johann PD, Stark S, Meyer J, Milde T, Schuhmann M, Ebinger M, Monoranu CM, Ponnuswami A, Chen S, Jones C, Witt O, Collins VP, von Deimling A, Jabado N, Puget S, Grill J, Helin K, Korshunov A, Lichter P, Monje M, Plass C, Cho YJ, Pfister SM. Reduced H3K27me3 and DNA Hypomethylation Are Major Drivers of Gene Expression in K27M Mutant Pediatric High-Grade Gliomas. *Cancer Cell*. 2013 Nov 11;24(5):660-72.

Brümmer A, Salazar C, Zinzalla V, Alberghina L, Höfer T. Mathematical modelling of DNA replication reveals a trade-off between coherence of origin activation and robustness against rereplication. *PLoS Comput Biol.* 2010 May 13;6(5):e1000783.

Bulut-Karslioglu A, Perrera V, Scaranaro M, de la Rosa-Velazquez IA, van de Nobelen S, Shukeir N, Popow J, Gerle B, Opravil S, Pagani M, Meidhof S, Brabletz T, Manke T, Lachner M, Jenuwein T. A transcription factor-based mechanism for mouse heterochromatin formation. *Nat Struct Mol Biol*. 2012 Oct;19(10):1023-30.

Cheung P, Tanner KG, Cheung WL, Sassone-Corsi P, Denu JM, Allis CD. Synergistic coupling of histone H3 phosphorylation and acetylation in response to epidermal growth factor stimulation. *Mol Cell*. 2000 Jun;5(6):905-15.

Chin HG, Patnaik D, Estève PO, Jacobsen SE, Pradhan S. Catalytic properties and kinetic mechanism of human recombinant Lys-9 histone H3 methyltransferase SUV39H1: participation of the chromodomain in enzymatic catalysis. *Biochemistry*. 2006 Mar 14;45(10):3272-84.

Chouliaras L, Rutten BP, Kenis G, Peerbooms O, Visser PJ, Verhey F, van Os J, Steinbusch HW, van den Hove DL. Epigenetic regulation in the pathophysiology of Alzheimer's disease. *Prog Neurobiol*. 2010 Apr;90(4):498-510.

Couture JF, Collazo E, Ortiz-Tello PA, Brunzelle JS, Trievel RC. Specificity and mechanism of JMJD2A, a trimethyllysine-specific histone demethylase. *Nat Struct Mol Biol.* 2007 Aug;14(8):689-95.

Covault J, Chalkley R. The identification of distinct populations of acetylated histone. *J Biol Chem*. 1980 Oct 10;255(19):9110-6.

David-Rus D, Mukhopadhyay S, Lebowitz JL, Sengupta AM. Inheritance of epigenetic chromatin silencing. *J Theor Biol*. 2009 May 7;258(1):112-20.

Dodd IB, Micheelsen MA, Sneppen K, Thon G. Theoretical analysis of epigenetic cell memory by nucleosome modification. *Cell*. 2007 May 18;129(4):813-22.

Dorer DR, Henikoff S. Expansions of transgene repeats cause heterochromatin formation and gene silencing in Drosophila. *Cell*. 1994 Jul 1;77(7):993-1002.

Duan Q, Chen H, Costa M, Dai W. Phosphorylation of H3S10 blocks the access of H3K9 by specific antibodies and histone methyltransferase. Implication in regulating chromatin dynamics and epigenetic inheritance during mitosis. *J Biol Chem*. 2008 Nov 28;283(48):33585-90.

Eck S, Rohr K, Müller-Ott K, Rippe K, and Wörz S. Combined Model-Based and Region-Adaptive 3D Segmentation and 3D Colocalization Analysis of Heterochromatin Foci. *In Proc. Workshop Bildverarbeitung für die Medizin 2012 (BVM'12)*. Berlin. Germany. 9-14.

Fischle W, Wang Y, Allis CD. Binary switches and modification cassettes in histone biology and beyond. *Nature*. 2003 Oct 2;425(6957):475-9.

Fischle W, Tseng BS, Dormann HL, Ueberheide BM, Garcia BA, Shabanowitz J, Hunt DF, Funabiki H, Allis CD. Regulation of HP1-chromatin binding by histone H3 methylation and phosphorylation. *Nature*. 2005 Dec 22;438(7071):1116-22.

Fischle W. Talk is cheap--cross-talk in establishment, maintenance, and readout of chromatin modifications. *Genes Dev*. 2008 Dec 15;22(24):3375-82.

Fodor BD, Kubicek S, Yonezawa M, O'Sullivan RJ, Sengupta R, Perez-Burgos L, Opravil S, Mechtler K, Schotta G, Jenuwein T. Jmjd2b antagonizes H3K9

trimethylation at pericentric heterochromatin in mammalian cells. *Genes Dev*. 2006 Jun 15;20(12):1557-62.

Gillespie DT. 1976. A General Method for Numerically Simulating the Stochastic Time Evolution of Coupled Chemical Reactions. *Journal of Computational Physics* 22(4):403–434.

Grewal SI, Bonaduce MJ, Klar AJ. Histone deacetylase homologs regulate epigenetic inheritance of transcriptional silencing and chromosome segregation in fission yeast. *Genetics.* 1998 Oct;150(2):563-76.

Grewal SI, Jia S. Heterochromatin revisited. *Nat Rev Genet*. 2007 Jan;8(1):35-46.

Guenatri M, Bailly D, Maison C, Almouzni G. Mouse centric and pericentric satellite repeats form distinct functional heterochromatin. *J Cell Biol*. 2004 Aug 16;166(4):493-505.

Hall IM, Shankaranarayana GD, Noma K, Ayoub N, Cohen A, Grewal SI. Establishment and maintenance of a heterochromatin domain. *Science*. 2002 Sep 27;297(5590):2232-7.

Hathaway NA, Bell O, Hodges C, Miller EL, Neel DS, Crabtree GR. Dynamics and memory of heterochromatin in living cells. *Cell*. 2012 Jun 22;149(7):1447-60.
Hodges C, Crabtree GR. Dynamics of inherently bounded histone modification domains. *Proc Natl Acad Sci U S A*. 2012 Aug 14;109(33):13296-301.

Hoffmann I, Roatsch M, Schmitt ML, Carlino L, Pippel M, Sippl W, Jung M. The role of histone demethylases in cancer therapy. *Mol Oncol*. 2012 Dec;6(6):683-703.

Jeong YS, Cho S, Park JS, Ko Y, Kang YK. Phosphorylation of serine-10 of histone H3 shields modified lysine-9 selectively during mitosis. *Genes Cells*. 2010 Jan 13. [Epub ahead of print]

Jeong YS, Park JS, Ko Y, Kang YK. JHDM3A module as an effector molecule in guide-directed modification of target chromatin. *J Biol Chem*. 2011 Feb 11;286(6):4461-70.

Kantarjian H, Issa JP, Rosenfeld CS, Bennett JM, Albitar M, DiPersio J, Klimek V, Slack J, de Castro C, Ravandi F, Helmer R 3rd, Shen L, Nimer SD, Leavitt R, Raza A, Saba H. Decitabine improves patient outcomes in myelodysplastic syndromes: results of a phase III randomized study. *Cancer*. 2006 Apr 15;106(8):1794-803.

Komissarov AS, Gavrilova EV, Demin SJ, Ishov AM, Podgornaya OI. Tandemly repeated DNA families in the mouse genome. *BMC Genomics*. 2011 Oct 28;12:531.

Kubicek M. 1976. Dependence of solution of nonlinear systems on a parameter. *ACM Trans. Math. Software*. 2(1):98-107.

Kubicek S, Jenuwein T. A crack in histone lysine methylation. *Cell*. 2004 Dec 29;119(7):903-6.

Kuznetsov YK. 2001. Elements of applied bifurcation theory. *Applied Mathematical Sciences*. 112:506-511.

Labrador M, Corces VG. Setting the boundaries of chromatin domains and nuclear organization. *Cell*. 2002 Oct 18;111(2):151-4.

Lehrman G, Hogue IB, Palmer S, Jennings C, Spina CA, Wiegand A, Landay AL, Coombs RW, Richman DD, Mellors JW, Coffin JM, Bosch RJ, Margolis DM. Depletion of latent HIV-1 infection in vivo: a proof-of-concept study. *Lancet*. 2005 Aug 13-19;366(9485):549-55.

Lengronne A, Pasero P, Bensimon A, Schwob E. Monitoring S phase progression globally and locally using BrdU incorporation in TK(+) yeast strains. *Nucleic Acids Res*. 2001 Apr 1;29(7):1433-42.

Mateescu B, England P, Halgand F, Yaniv M, Muchardt C. Tethering of HP1 proteins to chromatin is relieved by phosphoacetylation of histone H3. *EMBO Rep*. 2004 May;5(5):490-6.

Micheelsen MA, Mitarai N, Sneppen K, Dodd IB. Theory for the stability and regulation of epigenetic landscapes. *Phys Biol*. 2010; 7(2): 026010.

Mittelmann, H.D. 1987. Continuation methods for parameter-dependent boundary value problems. *IMA Pleprint Series # 346.*

Müller KP, Erdel F, Caudron-Herger M, Marth C, Fodor BD, Richter M, Scaranaro M, Beaudouin J, Wachsmuth M, Rippe K. Multiscale analysis of dynamics and interactions of heterochromatin protein 1 by fluorescence fluctuation microscopy. *Biophys J.* 2009; 97(11): 2876-85.

Müller-Ott K, Erdel F, Matveeva A, Mallm J-P, Rademacher A, Hahn M, Marth C, Zhang Q, Kaltofen S, Schotta G, Höfer T, Rippe K. Specificity, propagation and epigenetic memory of pericentric heterochromatin in mouse fibroblasts. (Submitted)

Nakayama J, Rice JC, Strahl BD, Allis CD, Grewal SI. Role of histone H3 lysine 9 methylation in epigenetic control of heterochromatin assembly. *Science*. 2001 Apr 6;292(5514):110-3.

Nicolis G, Prigogine I. 1989. Exploring Complexity. *R. Piper GmbH & Co. KG Verlag*, *Munich*.

Noma K, Allis CD, Grewal SI. Transitions in distinct histone H3 methylation patterns at the heterochromatin domain boundaries. *Science*. 2001 Aug 10;293(5532):1150-5.

Oki Y, Issa JP. Review: recent clinical trials in epigenetic therapy. *Rev Recent Clin Trials*. 2006 May;1(2):169-82.

Patnaik D, Chin HG, Estève PO, Benner J, Jacobsen SE, Pradhan S. Substrate specificity and kinetic mechanism of mammalian G9a histone H3 methyltransferase. *J Biol Chem*. 2004 Dec 17;279(51):53248-58.

Peleg S, Sananbenesi F, Zovoilis A, Burkhardt S, Bahari-Javan S, Agis-Balboa RC, Cota P, Wittnam JL, Gogol-Doering A, Opitz L, Salinas-Riester G, Dettenhofer M,

Kang H, Farinelli L, Chen W, Fischer A. Altered histone acetylation is associated with age-dependent memory impairment in mice. *Science*. 2010 May 7;328(5979):753-6.

Peters AH, O'Carroll D, Scherthan H, Mechtler K, Sauer S, Schöfer C, Weipoltshammer K, Pagani M, Lachner M, Kohlmaier A, Opravil S, Doyle M, Sibilia M, Jenuwein T. Loss of the Suv39h histone methyltransferases impairs mammalian heterochromatin and genome stability. *Cell*. 2001 Nov 2;107(3):323-37.

Postepska-Igielska A, Krunic D, Schmitt N, Greulich-Bode KM, Boukamp P, Grummt I. The chromatin remodelling complex NoRC safeguards genome stability by heterochromatin formation at telomeres and centromeres. *EMBO Rep*. 2013 Aug;14(8):704-10.

Phillips JE, Corces VG. CTCF: master weaver of the genome. *Cell*. 2009 Jun 26;137(7):1194-211.

Pujadas E, Feinberg AP. Regulated noise in the epigenetic landscape of development and disease. *Cell*. 2012 Mar 16;148(6):1123-31.

Raval A, Tanner SM, Byrd JC, Angerman EB, Perko JD, Chen SS, Hackanson B, Grever MR, Lucas DM, Matkovic JJ, Lin TS, Kipps TJ, Murray F, Weisenburger D, Sanger W, Lynch J, Watson P, Jansen M, Yoshinaga Y, Rosenquist R, de Jong PJ, Coggill P, Beck S, Lynch H, de la Chapelle A, Plass C. Downregulation of death-associated protein kinase 1 (DAPK1) in chronic lymphocytic leukemia. *Cell*. 2007 Jun 1;129(5):879-90.

Rea S, Eisenhaber F, O'Carroll D, Strahl BD, Sun ZW, Schmid M, Opravil S, Mechtler K, Ponting CP, Allis CD, Jenuwein T. Regulation of chromatin structure by site-specific histone H3 methyltransferases. *Nature*. 2000 Aug 10;406(6796):593-9.

Rosa A, Becker NB, Everaers R. Looping probabilities in model interphase chromosomes. *Biophys J*. 2010 Jun 2;98(11):2410-9.

Ryu, H., Barrup, M., Kowall, N.W., McKee, A.C., 2008. P3-260: epigenetic modification in a monozygotic twin with Alzheimer's disease. *Alzheimer's Demen*. 4, T598–T1598.

Ruthenburg AJ, Li H, Patel DJ, Allis CD. Multivalent engagement of chromatin modifications by linked binding modules. *Nat Rev Mol Cell Biol.* 2007; 8: 983-94.

Sabbattini P, Canzonetta C, Sjoberg M, Nikic S, Georgiou A, Kemball-Cook G, Auner HW, Dillon N. A novel role for the Aurora B kinase in epigenetic marking of silent chromatin in differentiated postmitotic cells. *EMBO J*. 2007 Nov14;26(22):4657-69.

Schmitz KM, Mayer C, Postepska A, Grummt I. Interaction of noncoding RNA with the rDNA promoter mediates recruitment of DNMT3b and silencing of rRNA genes. *Genes Dev*. 2010 Oct 15;24(20):2264-9.

Schotta G, Ebert A, Krauss V, Fischer A, Hoffmann J, Rea S, Jenuwein T, Dorn R, Reuter G. Central role of Drosophila SU(VAR)3-9 in histone H3-K9 methylation and

heterochromatic gene silencing. *EMBO J*. 2002 Mar 1;21(5):1121-31.

Schotta G, Lachner M, Sarma K, Ebert A, Sengupta R, Reuter G, Reinberg D, Jenuwein T. A silencing pathway to induce H3-K9 and H4-K20 trimethylation at constitutive heterochromatin. *Genes Dev*. 2004 Jun 1;18(11):1251-62.

Schreiber SL, Bernstein BE. Signaling network model of chromatin. *Cell*. 2002 Dec 13;111(6):771-8.

Sedighi M, Sengupta AM. Epigenetic chromatin silencing: bistability and front propagation. *Phys Biol*. 2007 Nov 7;4(4):246-55.

Shaw A, Olivares-Chauvet P, Maya-Mendoza A, Jackson DA. S-phase progression in mammalian cells: modelling the influence of nuclear organization. *Chromosome Res*. 2010 Jan;18(1):163-78.

Sims JK, Wade PA. Mi-2/NuRD complex function is required for normal S phase progression and assembly of pericentric heterochromatin. *Mol Biol Cell*. 2011 Sep;22(17):3094-102.

Slee RB, Steiner CM, Herbert BS, Vance GH, Hickey RJ, Schwarz T, Christan S, Radovich M, Schneider BP, Schindelhauer D, Grimes BR. Cancer-associated alteration of pericentromeric heterochromatin may contribute to chromosome instability. *Oncogene*. 2012 Jul 5;31(27):3244-53.

Sneppen K, Dodd IB. A simple histone code opens many paths to epigenetics. *PLoS Comput Biol*. 2012;8(8):e1002643.

Song J, Salek-Ardakani S, So T, Croft M. The kinases aurora B and mTOR regulate the G1-S cell cycle progression of T lymphocytes. *Nat Immunol*. 2007 Jan;8(1):64-73.

Sun JM, Chen HY, Davie JR. Effect of estradiol on histone acetylation dynamics in human breast cancer cells. *J Biol Chem*. 2001 Dec 28;276(52):49435-42.

Sun JM, Spencer VA, Chen HY, Li L, Davie JR. Measurement of histone acetyltransferase and histone deacetylase activities and kinetics of histone acetylation. *Methods*. 2003 Sep;31(1):12-23.

Thatcher KN, LaSalle JM. Dynamic changes in Histone H3 lysine 9 acetylation localization patterns during neuronal maturation require MeCP2. *Epigenetics*. 2006; 1(1):24-31.

Varier RA, Timmers HT. Histone lysine methylation and demethylation pathways in cancer. *Biochim Biophys Acta*. 2011 Jan;1815(1):75-89.

Wachsmuth M, Caudron-Herger M, Rippe K. Genome organization: balancing stability and plasticity. *Biochim Biophys Acta*. 2008 Nov;1783(11):2061-79.

Waterborg JH. Dynamics of histone acetylation in Saccharomyces cerevisiae. *Biochemistry*. 2001 Feb 27;40(8):2599-605.

Waterston, R.H., Lindblad-Toh, K., Birney, E., Rogers, J., Abril, J.F., Agarwal, P.,

Agarwala, R., Ainscough, R., Alexandersson, M., An, P.*, et al.* (2002). Initial sequencing and comparative analysis of the mouse genome. *Nature 420*, 520-562.

Whetstine JR, Nottke A, Lan F, Huarte M, Smolikov S, Chen Z, Spooner E, Li E, Zhang G, Colaiacovo M, Shi Y. Reversal of histone lysine trimethylation by the JMJD2 family of histone demethylases. *Cell*. 2006 May 5;125(3):467-81.

William H.; Teukolsky, Saul A.; Vetterling, William T.; Flannery, Brian P. (2007). *Numerical Recipes: The Art of Scientific Computing* (3rd ed.). New York: Cambridge University Press.

Wilson JR. Targeting the JMJD2A histone lysine demethylase. Nat Struct Mol Biol. 2007 Aug;14(8):682-4.

Wolfram Research, Inc.. 2013. Mathematica Version 9.0. *Wolfram Research, Inc., Champaign, Illinois.*

Yamamoto K, Sonoda M. Self-interaction of heterochromatin protein 1 is required for direct binding to histone methyltransferase, SUV39H1. *Biochem Biophys Res Commun*. 2003 Feb 7;301(2):287-92.

Yang H, Lee SM, Gao B, Zhang J, Fang D. The histone deacetylase Sirtuin 1 deacetylates IRF1 and programs dendritic cells to control Th17 differentiation during autoimmune inflammation. *J Biol Chem*. 2013 Nov 8. [Epub ahead of print]

Young LC, Hendzel MJ. The oncogenic potential of Jumonji D2 (JMJD2/KDM4) histone demethylase overexpression. *Biochem Cell Biol*. 2013 Dec;91(6):369-77.

Zee BM, Levin RS, Xu B, LeRoy G, Wingreen NS, Garcia BA. In vivo residue-specific histone methylation dynamics. *J Biol Chem*. 2010 Jan 29;285(5):3341-50.

Appendix A

A.1 Stochastic simulations

The deterministic model based on mass action kinetics was converted into the corresponding stochastic model following the chemical master equation formalism. Monte-Carlo simulations by using the Gillespie stochastic simulation algorithm were performed with implementation in C++ language. The comparing samples are outcomes of the long time simulations of the system in the parameters defined steady state. The stochastic simulation algorithm were run over 7-24 hours in the real time to reconstruct the variables time evolution over the 10^6 min for different demethylation rate values for the fixed set of other and for differing phosphorylation rate value with the fixed set of others. The output for long time steady state runs recorded with the 2 min time-step interval.

The dynamic for the short time observations, for example for the replication test simulation experiment, output is given for every minute.

In the particular cases of the bistable switching dynamics, for demethylation rates 0.25 and 0.275 min^{-1}, the simulation runs were longer, over 3×10^6 min.

Analysis of the stochastic system dynamic was done with the assumption of the ergodicity of the process for all considered conditions. Consequently, the averaging among the numbers of sample realizations of the process at the particular time point was replaced by the time averaging over sufficiently long time domain for single realization of the process. Thus, simulations for particular parameter set were run only once.

A.2 Spearman rank-order correlation coefficient

The Spearman's rank-order correlation coefficient used as the measure of a monotonic relationship between two continuous variables me2 and hp1.

This non-parametrical statistical method found to be more reliable in this study since it does not rest upon an assumption of normality of a distribution of the variables and it is robust to outliers. The statistic calculated according to the formula:

$$r_s = \frac{\sum_{t=1}^{T}\left(R_t - \overline{R}\right)\left(S_t - \overline{S}\right)}{\sqrt{\sum_{t=1}^{T}\left(R_t - \overline{R}\right)^2}\sqrt{\sum_{t=1}^{T}\left(S_t - \overline{S}\right)^2}}$$

R_t and S_t here are the ranks of *me2(t)* and *hp1(t)* among the *me2* and *hp1* of the other time observations correspondingly. If some of the variables over the sample have identical values, the midrank assign for this particular ties meaning the ranks of this values, as they would be slightly different (William H et al., 2007).

The test performed on the large enough variable sample size to assume the significance of any small difference in the correlation for range of tested phosphorylation conditions.

A.3 Autocorrelation

To examine the stability and memory of the on- and off-silenced state population the normalized autocorrelation function for different parameter values were calculated using the following definition

$$C(\tau) = \frac{\sum_{t=1}^{T-\tau}\left(me2(t) - \langle me2\rangle\right)\left(me2(t+\tau) - \langle me2\rangle\right)}{\sum_{t=1}^{T}\left(me2(t) - \langle me2\rangle\right)^2}$$

where *me2* is the total number of the nucleosomes within the considered region having the H3K9me2 histone modification. There by *me2* mathematically express as

$$me2(t) = \sum_{i=1}^{N} \left(Yd_i(t) + Yh_i(t) + Ym_i(t) + Yr_i(t) \right)$$

Due to the stochastic treatment of the system the *me2* is not static and constantly fluctuates characterized by different amplitude and random noise component depending on the explored parameter regime.

A.4 Abbreviations

Abbreviation	Explanation
CpG	Cytosine and Guanine separated by phosphate
CV	Coefficient of variation
DAPI	4',6-diamidino-2-phenylindole
DNA	Deoxyribonucleic acid
DOX	Doxycycline
GCN5	General control of amino acid synthesis protein 5
GFP	Green fluorescent protein
G1 phase	Growth 1 phase of the cell cycle
G2 phase	Pre-mitotic phase of the cell cycle
JMJD2	JmjC domain-containing histone demethylation protein 2
HP1	Heterochromatin protein 1
MEF	Mouse embryonic fibroblasts
ODE	Ordinary differential equation
PCH	Pericentric heterochromatin
SSA	Stochastic simulation algorithm
Suv39h	Suppressor of variegation 3-9 homolog
S phase	Synthesis phase of the cell cycle
WT	Wild-type phenotype

Acknowledgement

First of all, I would like to express my gratitude to my advisors, Prof. Dr. Thomas Höfer and PD Dr. Karsten Rippe for their guidance, encouragement and support during the entire course of my PhD study. I am obliged to them for the confidence they have shown in me and for the patience they have exercised during entire course of work.

I am thankful to the Helmholtz International Graduate School for Cancer Research at the DKFZ that in the most efficient way supports the progress of their students and provide the indispensable care of students concerns.

I thank all my colleagues and collaborators I was pleased to communicate with during the work. All of them are very open minded and intelligent people.

My especial warmest regards go to Anneke Brümmer, Sandip Kar, Florian Lamprecht and Michael Floßdorf for their direct and indirect help during my work. I really appreciate their entire interest in scientific tasks of my project, advices and fruitful discussions.

My beloved office mates, Melanie, Tim and Erika, we had a lots of fun during these years. Brainstorming, window fights, Xmas eggs and numbers of outdoor activities made my stay with you unforgettable. Thank you for your support and patience as well.

I thank my collaboration partners Katharina Müller-Ott, Fabian Erdel, Qin Zhang and Simon Eck. Besides that, I am truly thankful to Diana Haendly and Michael Nemetz whose professional assistance in administration and IT support cannot be overestimated.

Special thanks go to Vasantika Singh, Carsten Maus, Nils Becker, Michael Floßdorf and Tim Heinemann for critical reading of this thesis as well as to Olga Kuzminykh and Anne Weiser for help with German translation.

Last but not the least regards go to my friends and to my family for their love and long continuing support extended to me.

List of Publications

A. Matveeva, K. Kozlov and M. Samsonova (2006). Methodology for Building of Complex Workflows with PROSTAK package and iSIMBioS. *Proceedings of the 5th International Conference on Bioinformatics of Genome Regulation and Structure* (*BGRS'2006*), July 16-22, 2006, Novosibirsk, Russia. 2:204-208.
http://www.bionet.nsc.ru/meeting/bgrs_proceedings/papers/2006/BGRS_2006_V2_041.pdf

A. Matveeva, K. Kozlov, M.Samsonova (2006). Extraction of quantitative gene expression data from the images of gene expression patterns with ProStack and iSIMBioS. *Proc. of the 4rd TICSP Workshop on Computational Systems Biology* (*WCSB'2006*), Tampere, Finland, 12-13 June, 2006, 65-68.
http://www.cs.tut.fi/~wcsb06/proceedings.pdf

Matveeva A.D., Ionides J.M.C., Reinitz J., Samsonova M.G (2009). Modeling the expression of the *Drosophila even-skipped* gene. *«The Herald of Vavilov Society for Geneticists and Breeding Scientists»/«Russian Journal of Genetics: Applied Research»*.13(1):194-200.
http://www.bionet.nsc.ru/vogis/pict_pdf/2009/Моделирование%20механизмов%20регуляции%20экспрессии%20гена%20even-skipped%20у%20дрозофилы.pdf

Müller-Ott K, Erdel F, Matveeva A, Mallm J-P, Rademacher A, Hahn M, Marth C, Zhang Q, Kaltofen S, Schotta G, Höfer T, Rippe K. Specificity, propagation and epigenetic memory of pericentric heterochromatin in mouse fibroblasts. *Cell* (Submitted)

Zhang Q, Eck S, Müller-Ott K, Matveeva A, Claudino N, Wörz S, Rohr K, Rippe K, Höfer T. Heterochromatic histone methylation is reversible without memory. (Manuscript in preparation)

Heidelberg, 13 January 2014

Anna Matveeva